Smart Water for Enhanced Oil Recovery from Seawater and Produced Water by Membranes

by

Remya Ravindran Nair

Thesis submitted in fulfilment of
the requirements for the degree of
PHILOSOPHIAE DOCTOR
(PhD)

Faculty of Science and Technology
Department of Chemistry, Bioscience and Environmental Engineering
2019

University of Stavanger
NO-4036 Stavanger
NORWAY
www.uis.no

ISBN: 978-82-7644-828-3
ISSN: 1890-1387
PhD: Thesis UiS No. 442

Acknowledgements

I would like to address my utmost gratitude to my main supervisor Professor Torleiv Bilstad for his support and guidance throughout this research. Professor Torleiv Bilstad is a great inspiration and I would like to thank him for giving me the opportunity to present my work at several national and international conferences.

I am deeply grateful to Dr. Skule Strand for his advice and guidance as my co-supervisor. The friendly, supportive, long technical discussions with Dr. Skule have been inspiring. I highly appreciate my former colleague Evgenia Protasova for constructive reviewing of my papers and assisting in the lab and for creating such a wonderful working atmosphere.

Special thanks to the National IOR Centre of Norway for the financial support of my Ph.D. project. Special mention to Professors Merete Vadla Madland and Aksel Hiorth for proper guidance. It has been a great experience working with the Centre. I am also grateful to emeritus Professor Aud Berggraf Sæbø for lessons on presentations.

I also appreciate the time, effort and commitment of all the people at the faculty. Special thanks to Liv Margaret Aksland for her advice and timely supply of my research equipment, Lyudmyla Nilson for using her lab and equipment during experiments, Kåre Bredeli Jørgensen for his help with the IR. I would also like to thank Reidar Inge Korsnes for guiding me with the IC experiments. Special mention to John Grønli, Jan Magne Nygård and Tor Gulliksen from the Mechanical Engineering. Thanks to Terje Jåsund at Statsbygg for always arranging transportation of seawater from Mekjarvik. The administrative support from the faculty is also highly appreciated.

Many Ph.D. students at the University have helped with my experiments. A special thanks to Mona Wetrus Minde for helping me with SEM

analysis. I am also thankful to the master and bachelor students for their assistance in the lab.

I want to express my deepest gratitude to my parents and sister for all their support and encouragement.

Lastly, I want to express my sincere gratitude to my husband, Anil for moral support and my kids, Hemant and Nandita for their love and patience through all these years.

Remya Ravindran Nair

Summary

Sustainable use of scarce water resources and stringent environmental regulations are currently moving the focus towards environmentally friendly and cost-effective injection methods in the offshore oil industry. Water injection is used for most oil reservoirs as pressure support and improved displacement of oil. Most water-based enhanced oil recovery (EOR) techniques consist of chemical injection into reservoirs resulting in hazardous flow back of chemicals and produced water (PW). Smart water injection is an alternative and simultaneously represents a sustainable environmental and economic EOR flooding technique. The optimized ionic composition of injection water improves the initial wetting towards more water-wet conditions, which improves displacement efficiency due to increased capillary forces.

Smart water improves oil recovery by wettability alteration in both carbonate and sandstone reservoirs. Seawater is the main injection brine offshore and when enriched in divalent ions such as SO_4^{2-} and Ca^{2+} and depleted in Na^+ and Cl^- is considered smart water in carbonates. Injection brine with salinity below 5,000 mg/L and low in divalent cations are considered suitable as smart water in sandstone reservoirs.

Nanofiltration membranes (NF) are efficient in performing partial desalination of seawater and PW at low feed pressures resulting in high flux and low power consumption. The main focus of this research was to determine appropriate technical conditions and limitations of NF membranes for producing smart water from seawater and PW.

Special focus was on exploring NF membrane performance in terms of flux and rejection under varying feed compositions, pressures, pH and recoveries of polyamide and sulfonated polyethersulfone membranes. Both permeate and retentate streams from NF membranes are used for producing smart water. The divalent ion rich retentate could be used in carbonate reservoirs, whereas the permeate with low divalent ion

concentrations is optimal for sandstone reservoirs with seawater as membrane feed.

Produced water re-injection (PWRI) as smart water was evaluated as an alternative to PW discharge in terms of environmental and economic advantages. One of the main concerns in membrane treatment of PW is the presence of organics that cause membrane fouling. De-oiling of synthetic PW by media filtration upstream NF membranes eliminated fouling during short-term membrane experiments.

Additionally, the presence of barium and strontium ions in PW cause scaling if mixed with seawater. Membrane removal of Ba^{2+} and Sr^{2+} was optimized by increasing the concentration of scaling ions in the feed which resulted in efficient removal of Ba^{2+} and Sr^{2+} during NF experiments. However, the main challenge in reusing PW as smart water is low flux through NF membranes.

Experiments with altering pH of seawater were performed within pH limitations of the membrane materials to determine the effect of pH on membrane performance. A comparison between pH tolerance on polyamide and sulfonated polyethersulfone membranes were conducted during the experiments. A significant change in ion rejection was observed even with small changes in pH.

Another limitation with NF membrane separation with PW is the high total dissolved solids (TDS) in PW yielding high osmotic and operating pressures. Dilution of PW with NF permeate with seawater as feed reduces TDS.

Artificial neural network (ANN) was used to predict ion rejection based on multiple variable experimental data for feed pH, pressure and flux. An ANN structure was designed that were in close agreement between ANN predictions and experimental data, exceeding 95 % agreement for the tested membranes.

Based on experimental data, a predictive model was developed to quantify individual ion rejection by polyamide membranes using

Spiegler-Kedem model based on non-equilibrium thermodynamics and steric hindrance pore model. These models using rejection and flux values from six commercially available membranes determined the membrane transport parameters that included reflection coefficient and solute permeability. Membrane characterization was also accomplished by determining the effective pore radius of each membrane based on steric hindrance pore model for individual ions present in seawater. Experimental data were implemented for modeling the rejection characteristics of polyamide NF membranes with pure water permeabilities suitable for smart water production. Equations were formulated from plots of pure water permeability versus reflection coefficient and solute permeability, which enable end users to choose suitable NF membranes without performing extensive membrane experiments.

Power consumption analysis of membrane operations was evaluated for smart water production in carbonates and sandstones using both seawater and PW as membrane feed. Power consumed per cubic meter of smart water produced for carbonates was 0.7 kWh/m^3 and 5.2 kWh/m^3 for sandstones using seawater as feed. A power consumption analysis using PW as feed was 0.88 kWh/m^3 for carbonate reservoirs. For sandstone reservoirs, the power required for smart water production was 13.99 kWh/m^3.

List of Articles

Paper I

Membrane Performance Analysis for Smart Water Production for Enhanced Oil Recovery in Carbonate and Sandstone Reservoirs

Remya R. Nair, Evgenia Protasova, Skule Strand and Torleiv Bilstad
Energy & Fuels, 2018, 32 (4), pp 4988-4995
DOI: 10.1021/acs.energyfuels.8b00447

Paper II

Evaluation of Nanofiltration Membrane Process for Smart Water Production in Carbonate Reservoirs from Deoiled Produced Water and Seawater

Remya R. Nair, Evgenia Protasova, Skule Strand and Torleiv Bilstad
SPE Productions and Operations (In press)

Paper III

Effect of pH on Produced Water Treatment Using Nanofiltration Membranes: Artificial Neural Network for Performance Assessment and Steric Hindrance Pore Model for Flux Variation Evaluation

Remya R. Nair, Evgenia Protasova, Skule Strand and Torleiv Bilstad
Desalination and Water Treatment (In press)

Paper IV

Implementation of Spiegler - Kedem and Steric Hindrance Pore Models for Analyzing Nanofiltration Membrane Performance for Smart Water Production

Remya R. Nair, Evgenia Protasova, Skule Strand and Torleiv Bilstad
Membranes, 2018, 8 (3), 78

DOI:org/10.3390/membranes8030078

Conference Presentations and Proceedings

1. "Produced Water Treatment with Membranes for Enhanced Oil Recovery in Carbonate and Sandstone Reservoirs", 19th European Symposium on Improved Oil Recovery, Stavanger, Norway from 24-27th April 2017, DOI:10.3997/2214-4609.201700296.
2. "Reuse of Produced Water by Membranes for Enhanced Oil Recovery", SPE Annual Technical Conference and Exhibition, Dubai, September 26-28, 2016, ISBN 978-1-61399-463-4. DOI: 10.2118/181588-MS.
3. "Applicability and Costs of Nanofiltration for Produced Water Reinjection for EOR", Industrial and Hazardous Waste Management, organized by Technical University of Crete, September 27-30, 2016, extended abstract is published (ISSN 2241-3138. ISBN: 978-960-8475-24-3. p. 265-266).
4. "Oily Waste Regulations and Best Available Technologies for Sustainable Development", Industrial and Hazardous Waste Management, organized by Technical University of Crete, September 27-30, 2016, (ISSN 2241-3138. ISBN: 978-960-8475-24-3. p. 357-358).
5. "Re-injection of Produced Water for Enhanced Oil Recovery by Membranes", European Desalination Society, Desalination for the Environment: Clean Water and Energy, Rome, Italy, May 22-26, 2016.
6. "Evaluation of NF Membrane Characteristics and Ionic Selection from Produced Water for IOR", AWWA/AMTA Membrane Technology Conference, San Antonio, Texas, USA, February 1-5, 2016.
7. "Evaluation of NF Membrane Characteristics and Ionic Selection from Seawater for IOR", AWWA/AMTA Membrane Technology Conference, San Antonio, Texas, USA, February 1-5, 2016.

8. "Ionic Selection from Seawater using Membranes for IOR", 2nd International Conference on Desalination using Membrane Technology, July 2015, Singapore.
9. "Improved Oil Production by Membranes", 26th Drilling-Oil-Gas AGH 2015 Conference, June 2015, Poland, – Paper published, (AGH Drilling Oil Gas 2015; Volume 32 (1) p. 221-231. ISSN 2299-4157, dx.doi.org/10.7494/drill.2015.32.1.221
10. "Produced Water Treatment with Membranes for Enhanced Oil Recovery in Carbonate and Sandstone Reservoirs", NFiP (Petroleum Research School of Norway), Stavanger Oil Museum, November 2017
11. "Cost Effective Smart Water Production for Enhanced Oil Recovery by Membranes", NORWEP (Norwegian energy partners), Energy seminar: Efficiency in the oil industry, Norwegian Energy Partners, 6 April 2017, Jakarta, Indonesia.
12. "Smart Water Production from Seawater and Produced Water by Membranes", 6th annual November conference for Norwegian / Brazilian Energy Research, 12-13th November 2018, Rio de Janeiro, Brazil.

Poster Presentations

1. Modification of Seawater by Membranes for Enhanced Oil Recovery", European Desalination Society, Desalination for the Environment: Clean Water and Energy, Rome, Italy, May 22-26, 2016.
2. 'Smart Water for EOR by Membranes' at The National IOR Centre Annual Conference, Stavanger, Norway, April 26-27, 2016.
3. *"*Ionic Selection from Seawater for IOR*"*, IDA World Congress 2015 Technical Program, San Diego, California, August 30, 2015 – September 4, 2015.

4. “Ionic Selection from Produced Water using NF Membranes for IOR” as co-author, 2nd International Conference on Desalination using Membrane Technology, July 2015, Singapore.

Abbreviations and Symbols

ANN	Artificial Neural Network
A	Membrane Area or Feed Channel Cross-section
a	Membrane Width
$A_k/\Delta x$	Ratio of Membrane Porosity to Membrane Thickness
b	Channel Spacer Height
CoBR	Crude Oil-Brine-Rock
CP	Concentration Polarization
C_f	Feed Concentration
C_p	Permeate Concentration
C_c	Retentate Concentration
C_m	Concentration at the Membrane Surface
D	Hydraulic Diameter
EDS	Energy Dispersive X-Ray spectroscopy
EOR	Enhanced Oil Recovery
E_{oil}	Hydrocarbon Removal Efficiency
FW	Formation Water
h_{ch}	Channel Height
IR	Infrared
J_v, J_s	Solvent and solute flux, respectively
k	Mass Transfer Coefficient
L_p	Pure Water Permeability
LS	Low Salinity
LSE	Low Salinity Effect
MF	Microfiltration
MWCO	Molecular Weight Cut-off
MSE	Mean Square Error
NF	Nanofiltration
NTU	Nephelometric Turbidity Unit
OOIP	Original Oil in Place

PV	Pore Volume
PW	Produced Water
PWRI	Produced Water Reinjection
P_s	Solute Permeability Coefficient
Δp	Pressure Difference
PV	Pore Volume
Q_f	Feed Flow Rate
Q_p	Permeate Flow Rate
Q_r	Retentate Flow Rate
RO	Reverse Osmosis
R_{obs}	Observed Rejection
r_p	Pore Radius
S_D	Steric Hindrance Factor for Diffusion
S_F	Steric Hindrance Factor for Filtration Flow
SHP	Steric Hindrance Pore Model
SI	Spontaneous Imbibition
SK	Spiegler-Kedem Model
t	Filtration Time
TDS	Total Dissolved Solids
TFC	Thin Film Composite
UF	Ultrafiltration
v	Permeate Volume
VF	Viscous Flooding
w_{ch}	Channel Width
η	Efficiency of the pump
μ	Feed Viscosity or dynamic viscosity
π_F	Feed Osmotic Pressure
$\Delta\pi$	Osmotic Pressure Difference
σ	Reflection Coefficient
υ	Cross-flow Velocity
ρ	Density of Feed Water
Ø	Flow Channel Porosity
ν	Kinematic Viscosity

Table of Contents

List of Figures

List of Tables

1 Introduction

Global energy requirements will rise 30 % and the demand for oil will reach 105 million barrels/day by 2040 [1]. Environmentally friendly and cost-effective recovery mechanisms are preferred to mitigate the demand-supply balance. A range of approaches has been developed over the years to meet this increasing energy demand. Most oil reservoirs implement waterflooding and water-based EOR. Ionic modification of seawater and PW by membranes is such an appropriate energy-efficient method for hydrocarbon recovery.

1.1 Oil Recovery Methods

In classic reservoir engineering, oil recovery is classified as primary, secondary and tertiary processes [2].

Primary recovery results from natural pressures in reservoirs transporting oil to the well surface [3]. Typical recoveries for primary production are 5-20 % of the original oil in place (OOIP). Secondary recovery methods are applied when reservoir pressures decrease during production. Water or gas is injected to retain reservoir pressure and sustain the flow of hydrocarbons towards the production wells. Water forces oil through the reservoir rocks towards the production wells. Seawater is readily available offshore in large quantities and with its incompressible nature requires less energy compared to gas injection. Secondary recovery is pursued until injected fluid appears in considerable amount in the production wells making oil production uneconomical. Primary and secondary recoveries from reservoirs produce 20 - 50 % of OOIP depending on the properties of oil and reservoirs [2].

Tertiary recovery is also referred to as enhanced oil recovery (EOR) and is implemented following primary and secondary recoveries. EOR

includes techniques for improving oil displacement leading to further increase in hydrocarbon production.

EOR methods are classified into four different categories relating to the mechanisms of oil displacement as shown in Table 1.

Table 1. EOR classifications [2]

Thermal EOR processes	Steam flooding Hot waterflooding In-situ combustion Cyclic steam stimulation
Chemical EOR processes	Surfactant flooding Polymer flooding Alkaline flooding Solvent flooding Micellar
Gas EOR processes	Hydrocarbon injection CO_2 flooding Nitrogen flooding Flue gas injection Water - Alternating - Gas (WAG)
Emerging EOR processes	Smart water Low salinity waterflooding Carbonated waterflooding Microbial EOR Foam

EOR methods recover 50 – 80 % of OOIP [2, 3]. In modern reservoir management, pressure maintenances are mostly achieved through water injection and it is generally accepted that EOR should be implemented as early as possible for optimizing the EOR effect.

1.2 EOR by Smart Water

Chemicals added for EOR methods is a major concern in the oil and gas industry due to its environmental impact. The traditional water injection method uses many chemicals for altering the wettability in the reservoir for displacing more oil. ¨Smart Water¨ injection is a comparatively new EOR method that improves oil recovery by wettability alteration in both carbonate and sandstone reservoirs with minimum use of chemicals. This method emphasizes selectively retaining the favorable inorganic ions in seawater for wettability alteration and minimizing the less favorable ions. EOR by smart water is both cost-effective and environmentally friendly compared with alternative methods in Table 1. Recent extensive studies and experiments have confirmed that initial wetting equilibrium in reservoirs between pore surface minerals, crude oil and formation water (FW) could be changed by injecting brines with different ion compositions compared with FW. Smart water facilitates wettability alteration towards more water-wet conditions. Increased positive capillary forces improve the microscopic sweep efficiency in heterogeneous pore systems, which increase oil recovery. Both field observations and laboratory studies confirm significant EOR potentials using smart water.

Wettability is defined as the *¨tendency of one fluid to spread on or to adhere to a solid surface in the presence of other immiscible fluids*¨ [4]. Reservoir mineralogy has a fundamental property which regulates the type of interactions controlling adsorption of polar organic compounds in crude oil. Carbonate and sandstone reservoirs differ as the carbonate surface charge is positive whereas sandstones are negatively charged due to the presence of minerals such as clays, quartz, feldspar, and silicate [5].

Injected brine composition is of utmost importance in a wettability alteration process. Ion composition, pH and salinity of the brines are the determining factors [6]. An injected brine with an ion composition

different from FW could be capable of modifying the chemical equilibrium between mineral - FW - crude oil [7].

1.3 Smart Water Production from PW

PW is the largest wastewater stream from oil production and is a mixture of FW, injected water, production chemicals, and crude oil. The content is mainly hydrocarbons, inorganic salts, metals and naturally occurring radioactive materials [8]. Salinity of PW varies between 1000 and 250,000 mg/L [9].

Generally, treatment of PW involves removal of organics such as dissolved and emulsified oil components, dissolved inorganic ions, and particulates such as sand and clay. PW is treated by physical and chemical means before discharging to the environment. Numerous treatment technologies are used to reduce oil in water before discharge where the maximum allowed concentration is 40 mg/L of oil in water in several countries [10]. The official threshold for oil in water discharges in Norway is 30 mg/L [11]. Treatment technologies are selected based on PW chemistry, available space, cost, discharge, and reuse options.

Reuse of PW as smart water by modifying the ionic composition with membranes is a new approach. A number of pre-treatment steps upstream of membrane treatment are required to prevent membrane fouling. Pre-treatment involves de-oiling, disinfection to avoid biofouling, and suspended solids removal to avoid membrane pore blockage.

1.4 Smart Water Production by Membranes

Membranes are defined as selective barriers that permit passage of certain components while retaining others in a feed [12]. Membrane desalination processes were investigated for producing injection water with required smart water ionic composition. Most onshore oil fields use surface or aquifer water for pressure maintenance and oil displacement.

NF and reverse osmosis (RO) membranes are two pressure-driven membrane desalination technologies of interest offshore for smart water production.

During cross flow membrane operations, the feed stream is split into retentate (reject) and permeate [13]. The retentate from an NF membrane with seawater as feed becomes enriched in divalent ions and meet criteria for smart water in carbonate reservoirs. The NF permeate, depleted in divalent ions and enriched in monovalent ions, may be used as smart water in sandstone reservoirs. A schematic of an NF membrane process is shown in Figure 1.

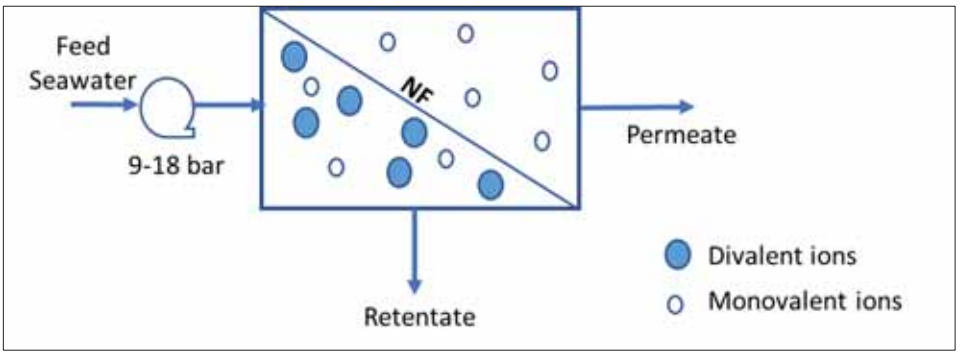

Figure 1. Schematic of smart water production from seawater using NF membranes

NF membranes are easy to operate and are without phase change during operation. Membrane systems are readily combined with supplemental separation processes. Another potential advantage of the NF membrane is that performance changes with temperature, pH and feed concentrations [14]. Membrane-based technologies are more suitable for offshore applications due to relatively compact footprint as well as low weight and power requirements compared to alternative desalination technologies [15].

NF and RO membrane desalination processes are widely used both onshore and offshore for desalination and sulfate removal for scale prevention.

- Marathon Oil Co.UK Ltd. developed together with FilmTec, a thin film composite membrane (TFC) for sulfate removal with a capacity of 40,000 barrels per day on South Brae platform and was installed in November 1988. GE Power and Water reported in 2015 that there are over 80 sulfate removal membrane units globally [16].
- Major seawater desalination plants for potable water production include 330,000 m^3/day in Ashkelon, Israel and a 136,000 m^3/day Tuas in Singapore [17].

2 Objectives and Scope

In this thesis, ¨Smart Water¨ is defined as a brine with an ionic composition different from the formation water, that disturbs the established equilibrium in the reservoir by wettability alteration. There is no specific ionic composition for smart water since the required composition of injected brine mainly depends on individual reservoir properties. Smart water replaces a number of water-based chemicals added during EOR making the process environment-friendly.

Production of smart water from seawater and produced water by membranes is not fully developed and involves a number of technical and operational challenges. This research investigates various opportunities for the feasibility of producing smart water and to decrease the knowledge gap by implementing membrane technology in industrial scale-up.

The main objective of this research was to evaluate the potential of using RO and NF membranes for producing smart water by using seawater and de-oiled synthetic PW as membrane feed. Experiments were performed with NF and RO membranes to provide new insights into the application of membranes in the industry.

The **first hypothesis** is that membranes are practically feasible for smart water production from seawater and de-oiled produced water for both carbonate and sandstone reservoirs, from an environmental point of view.

The **second hypothesis** is that NF membranes can handle PW with traces of oil and varying pH during smart water production.

The **third hypothesis** is that empirical correlations can be developed to predict the performance of a membrane with a minimum number of variables within a given range of conditions.

The **fourth hypothesis** is, from an economic point of view, membranes are practicable for smart water production from seawater and de-oiled produced water for both carbonate and sandstone reservoirs.

All the assumptions have been addressed in the research papers presented in this thesis.

Paper I evaluate the production of smart water from seawater for carbonate and sandstone reservoirs, which address the first hypothesis. Seawater was spiked with divalent ions to determine the effect of increased concentrations of SO_4^{2-}, Ca^{2+}, and Mg^{2+} on flux and ion rejection. The results were explained with reference to NF separation mechanisms. The energy consumed by major desalination technologies was also compared. It was concluded that the use of membranes was optimal for the production of smart water in both reservoirs. The power consumed for producing 1 m^3/h of smart water from seawater using membranes for both reservoirs were evaluated.

Paper II evaluates the possibility of reusing de-oiled PW as smart water in carbonate reservoirs. Research on PWRI as smart water is an innovative idea and experiments with de-oiled PW were performed to determine membrane separation efficiencies and addresses the second hypothesis. Main challenges that can occur while reusing PW includes high TDS of PW, varying range of pH of PW depending on the reservoir properties, presence of scaling ions such as barium and strontium, the effect of traces of oil in PW and compatibility of treated PW with reservoir properties.

De-oiling of synthetic PW was performed using a media filtration unit. Rejection of Ba^{2+} and Sr^{2+} were also determined during the experiments. The NF permeate with PW as feed was subjected to equilibration experiments to analyse whether the permeate is compatible with chalk. The effect of high TDS in PW was negated by dilution with low TDS water. Power consumed for different water sources used to produce smart water from PW was calculated and addresses the fourth hypothesis.

In **Paper III**, the effect of pH on NF membrane performance was discussed. At neutral pH, most NF membranes are negatively charged. Hence, electrostatic interactions between charged solutes and membrane play a role in ion rejection and this interaction depends on feed pH. During reuse of PW as smart water, pH of PW is one of the main concerns that affect NF membrane performance and addresses the second hypothesis.

Experiments were performed on three commercially available NF membranes with varying feed pH values from 2.5 to 10.2. The corresponding ion rejections and flux were measured. Spiegler - Kedem and steric hindrance pore models were used to determine the variations in pore size with pH. The experimental results were also used for predicting ion rejections at a given pressure, flux and pH using a feed-forward back propagation artificial neural network (ANN).

An ANN was designed with pH, flux and pressure as inputs to the model to quantitatively predict ion rejection. There are many mathematical models based on various ion transport mechanisms for evaluation of NF membrane performance. However, these models are mathematically complex and require a detailed knowledge of membrane characterization and performance. The extensive experimental data collected by changing the key parameters have shown interdependency and provides an opportunity for using the ANN tool for predicting the performance of membranes. Even though this approach is a 'black box' concept and heavily depends on the quality and quantity of data with constraints in experimental data collection, it is a simple approach considering the difficulty in modeling the various mechanisms with multivariables. These results can be implemented in industrial scale-up when PW and other saline brines with different pH are used.

The selection of the most appropriate membrane for a particular smart water composition is of high importance. Thus, experiments were performed with eight commercially available membranes and the results are discussed in **Paper IV,** addressing the third hypothesis. Using the

experimentally obtained values of flux and rejection, membrane transport parameters such as reflection coefficient and solute permeability in the Spiegler–Kedem model were estimated for NF membranes. Correlations were developed for the membrane transport parameters in relation to the pure water permeability. The pure water permeability is dependent on the structural parameters of a membrane. In addition, steric hindrance pore model was used for estimating the pore radius, which is one of the main structural parameters.

Thus, the developed correlations can be used for selecting porous polyamide membranes with high feed ionic concentrations for smart water production. The suggested ten correlations are useful to predict the rejection, reflection coefficient and solute permeability of individual ions when pure water permeability of a specific membrane was known.

The fourth hypothesis is validated by calculating the power consumed by membranes during the smart water production process. The results are discussed in **Paper I** and **Paper II**.

3 Literature Review

Initial reservoir wetting is controlled by polar acidic and basic organic components present in crude oil. These components can be quantified by acid or base number analysis. The unit of measurement is mg KOH/g for both cases. In acid number analysis, the measurement unit represents the amount of KOH required to neutralize the acidic components in one gram of oil. For basic number measurement, the unit represents the equivalent concentration of basic organic material present in one gram of crude oil.

These acidic materials are generally represented by the carboxylic functional group, -COOH and naphthenic acids where the basic material are typically nitrogen in aromatic molecules and is represented by R_3N:.

Acid and basic material present at the oil-water interface undergoes fast proton exchange reaction that is affected by the pH of the aqueous media and is presented in Equation 1 and Equation 2.

$$R_3NH^+ \rightleftarrows H^+ + R_3N: \quad (1)$$

$$RCOOH \rightleftarrows H^+ + RCOO^- \quad (2)$$

Acid material control initial wetting in carbonates and have alkaline pH due to $CaCO_3$ dissolution, and positively charged mineral surfaces interact with negatively charged acidic components.

3.1 Smart Water

Smart water has an ion composition and salinity different from FW and can alter the established equilibrium between crude oil, FW and pore surface minerals thereby modifying the wetting properties of reservoirs [18]. Smart water is easily implementable, environment-friendly and cost-effective compared to other water-based chemical EOR methods. Optimized smart water compositions have to be evaluated for individual

reservoirs depending on initial wetting, FW composition and reservoir temperature.

3.1.1 Smart Water in Sandstone Reservoirs

Injection water with salinities less than 5,000 mg/L is defined as smart water in sandstones [19]. Mineral surfaces in sandstone reservoirs are generally negatively charged [5]. The wettability in sandstones can change from strongly water-wet to strongly oil-wet. Silica or clay minerals contribute with a large surface area with permanent localized negative charges. Clays undergo CoBR interactions through cation exchange processes and it is confirmed that they have an affinity for crude oil components. It has been suggested that low salinity effect (LSE) in sandstones is controlled by desorption of the polar compounds from the silicate surfaces [20], and is pH dependent. The degree of oil wetness is related to the affinity of polar components at a certain pH, temperature and brine salinity [20].

Figure 2 shows the effect of low salinity brine on sandstone cores at 60 °C confirming that increased oil recovery was observed during low salinity waterflooding.

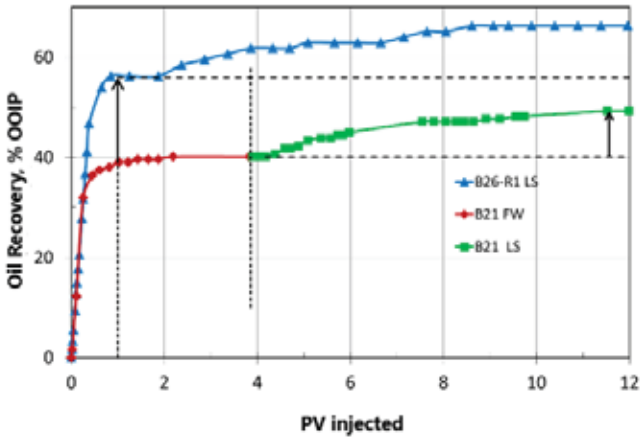

Figure 2. Oil recovery tests on sandstone cores at 60 °C by secondary and tertiary LS injection [21, 22]

The core was initially injected with FW resulting in 40 % OOIP. This was followed by LS brine injection resulting in an OOIP increase to 50 %. However, when the core was injected with LS brine from start resulted in a plateau of 60 - 65 % OOIP by less PV injection.

LSE reported by Tang and Morrow [23] indicated that oil recovery in sandstones increased during spontaneous imbibition (SI) and waterflooding with low salinity water. However, several authors have argued to the existence of different thresholds of salinity that aids in positive salinity effects [24, 25]. It was argued that the presence of divalent ions in low salinity brines have mixed results [26]. Austad et al. [19, 20] suggested that the presence of divalent ions in low salinity brines is not advantageous as it may hinder the rise in pH which is essential to obtain LSE. However, recent research shows that EOR effects with 25,000 mg/L NaCl are possible [27].

Figure 3 presents an explanation for smart water effect in sandstones according to Austad et al. [20]. Figure 3 explains how the acidic and basic components adsorbed onto the clay minerals are desorbed from the clay surface by an in-situ pH increase.

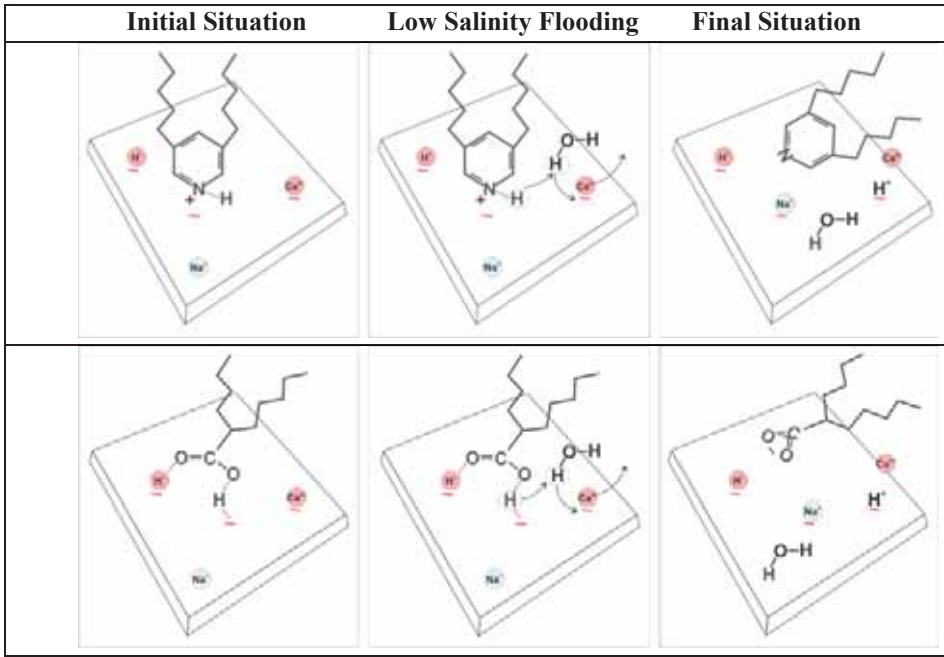

Figure 3. Smart water mechanisms with LSE on sandstone reservoirs [20]

Clays have permanent negative charges and behave as the main wetting mineral in sandstone reservoirs. Equilibrium established with formation water is disturbed when low salinity brine is injected into the reservoir. This results in desorption of Ca^{2+} from the surface to establish a new equilibrium which creates negative charges on the clay surfaces. This negative charge is balanced by adsorption of H^+ at the negative site located on the clay surface. The adsorbed H^+ creates a local pH rise and is the basis for desorption of organic components from clay. Equation 3 explains the reaction.

$$Clay - Ca^{2+} + H_2O \rightarrow Clay - H+ + Ca^{2+}\ OH^- + heat \qquad (3)$$

Presence of divalent ions can reduce the rise in pH by precipitation of hydroxides as shown in Equation 4 and Equation 5 and resulting in reducing possible LSE in sandstones.

$$Mg^{2+}{}_{(aq)} + 2OH^-{}_{(aq)} \rightleftarrows Mg\ (OH)_{2\ (s)} \qquad (4)$$

$$Ca^{2+}_{(aq)} + 2OH^{-}_{(aq)} \rightleftarrows Ca(OH)_{2(s)} \quad (5)$$

3.1.2 Smart Water in Carbonate Reservoirs

The mechanisms by which modified brines or smart water change the wettability of carbonate reservoirs are explained in Figure 4. The initial wetting in carbonates is controlled by negatively charged acidic polar components adsorbed to positive sites at the mineral surface. The wettability alterations are promoted by desorption of acids from the mineral surface.

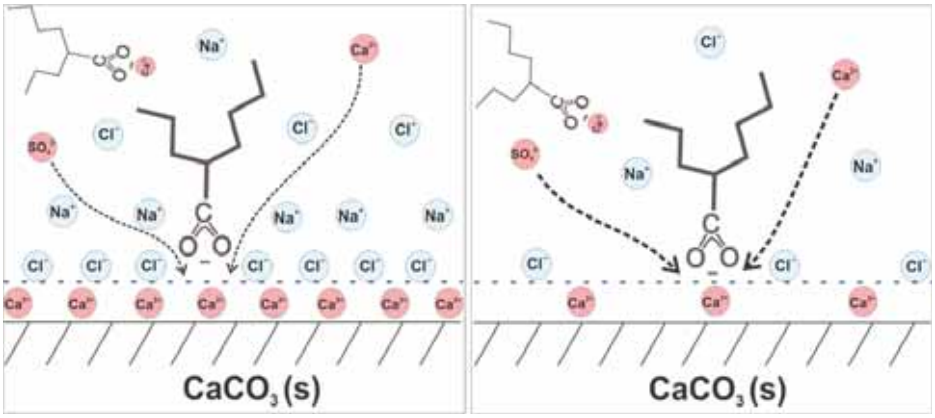

a) b)

Figure 4. Schematic of mechanisms for wettability alteration in carbonates a) Mechanisms when monovalent ions are present b) Mechanisms with increased Ca^{2+} and SO_4^{2-} and decreased Na^{+} and Cl^{-} concentrations [28].

The wettability alterations are triggered by chemical adsorption of SO_4^{2-} and Ca^{2+} [19] present in seawater. Hence, seawater can act as smart water in carbonates and shift the wettability from mixed-wet to water-wet state.

Injection of fluids with salinities between 6,000 and 28,000 mg/L is suitable for carbonate reservoirs. Smart water enriched in sulfate and divalent cations but depleted in monovalent ions are desired in

carbonates. Smart water should be enriched with 2 - 4 × SO_4^{2-} and 1 - 2 × Ca^{2+} concentrations compared to seawater for EOR [18, 19, 29].

Figure 5 shows increased oil recovery when seawater was injected into a carbonate core.

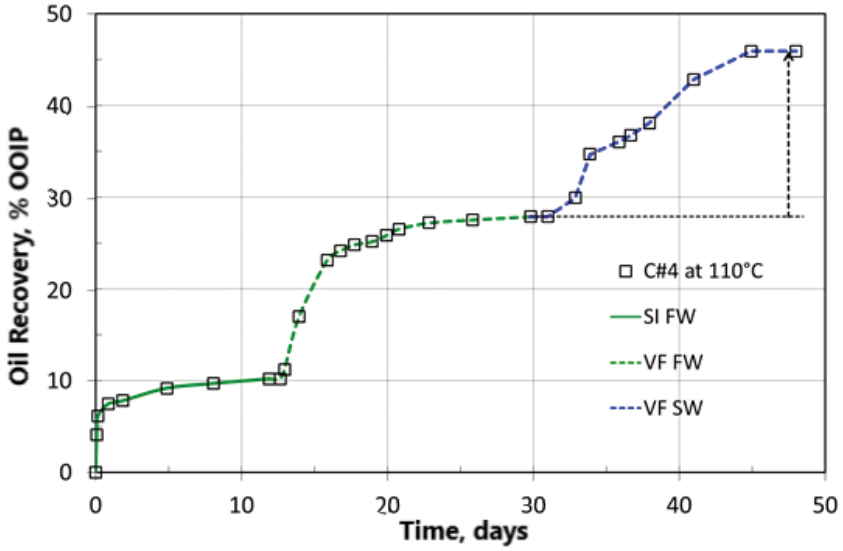

Figure 5. Effect of smart water on carbonate core at 110 °C [19]

The core is subjected to spontaneous imbibition with FW for 12 days resulting in 10 % OOIP confirming initial mixed wetting (Figure 5). Viscous flooding (VF) of the core with FW after SI increased the recovery to 28 %. Switching to seawater after 30 days resulted in an increase to 45 % OOIP. Figure 5 confirms the positive impact of seawater or smart water injection in carbonate reservoirs.

The established chemical equilibrium of a carbonate system is disrupted when a brine with a different ion composition is injected. Negatively charged SO_4^{2-} interacts with positively charged carbonate surface, lowering the surface charge. Due to less electrostatic repulsion, more Ca^{2+} approach the surface and displaces the carboxylic material from the mineral surface. This symbiotic SO_4^{2-} - Ca^{2+} interaction initiates desorption of active polar organic components from the carbonate

surface, resulting in wettability alteration [19, 30]. At temperatures above 90 °C, in the absence of Mg^{2+} in the brine, $CaSO_4$ anhydrite precipitation occurs, decreasing the concentration of active ions. If Mg^{2+} is present in the brine, the ion stabilizes SO_4^{2-} by forming an ion pair between Mg^{2+} and SO_4^{2-}.

Strand et al. [18] and Zhang et al. [30] described the effect of varying sulfate and calcium concentrations in a brine based on seawater and concluded that the oil recovery increased as SO_4^{2-} and Ca^{2+} concentrations in the imbibing fluid increased. The results are presented in Figure 6 and Figure 7.

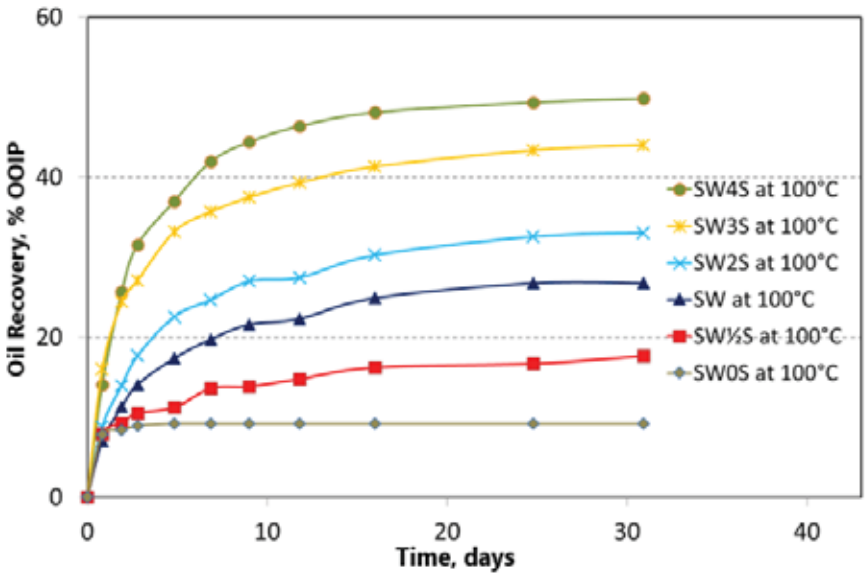

Figure 6. Spontaneous imbibition of brines with varying SO_4^{2-} concentrations into fractional intermediate wetted chalk cores [30]

SO_4^{2-} acts as a catalyst for wettability alteration as presented in Figure 6. The figure demonstrates that brine with no sulfate had the least oil recovery and the recovery increased with increasing SO_4^{2-} concentrations. The result confirms that seawater act as smart water in carbonates [30].

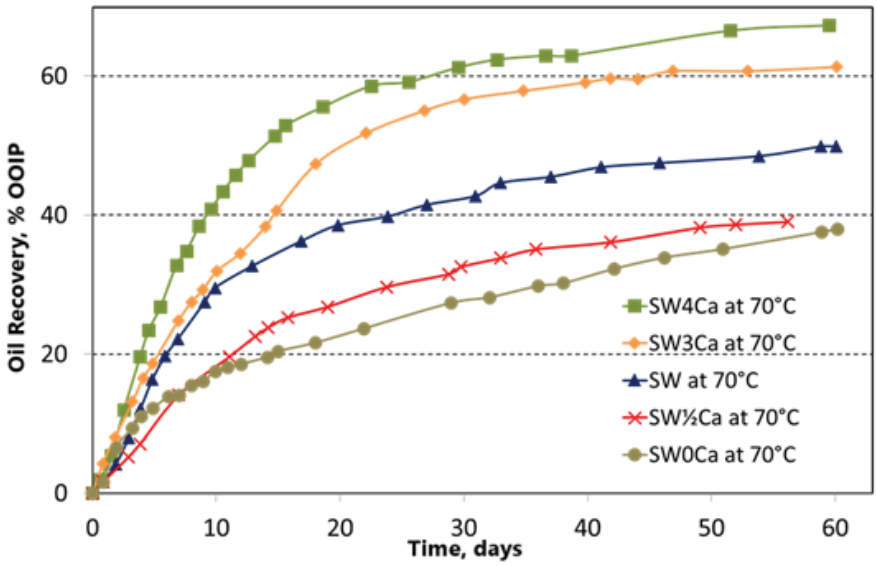

Figure 7. Spontaneous imbibition of brines with varying Ca^{2+} concentrations into chalk cores at 70 °C [30]

Increased wettability alteration with increased calcium concentration occurs as confirmed in Figure 7. Mineral dissolution could not explain the EOR effect due to the common ion effect. Increased Ca^{2+} concentrations reduce $CaCO_3$ dissolution.

Figure 8 shows the oil recovery effect when modified seawater with only divalent SO_4^{2-} and NaCl were used [31].

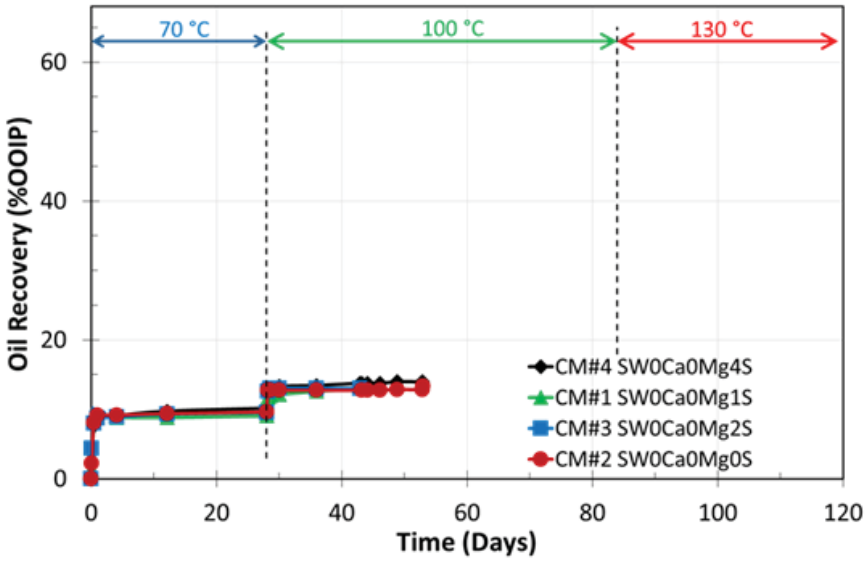

Figure 8. SI experiments with modified seawater containing only SO_4^{2-} and NaCl (without Ca^{2+} and Mg^{2+}) [31]

Figure 8 demonstrated that modified seawater with only sulfate is not smart water even though sulfate could change the mineral surface charge. Presence of Ca^{2+} and Mg^{2+} in the brine is required for wettability alteration and further oil displacement.

Smart water EOR is temperature dependent. EOR brines at high temperature should have only reduced NaCl concentration or low salinity without any increase in SO_4^{2-}/ Ca^{2+} since an increase in these ions will result in precipitation. At low reservoir temperature, low NaCl concentration and increased SO_4^{2-}/ Ca^{2+} concentration will improve the efficiency compared to seawater.

The results confirm that seawater can act as an EOR fluid in chalk reservoirs [19]. However, seawater could be made even smarter and result in a further increase in oil recovery. Figure 9 shows the impact of modified brines when spontaneously imbibed into the chalk core [32].

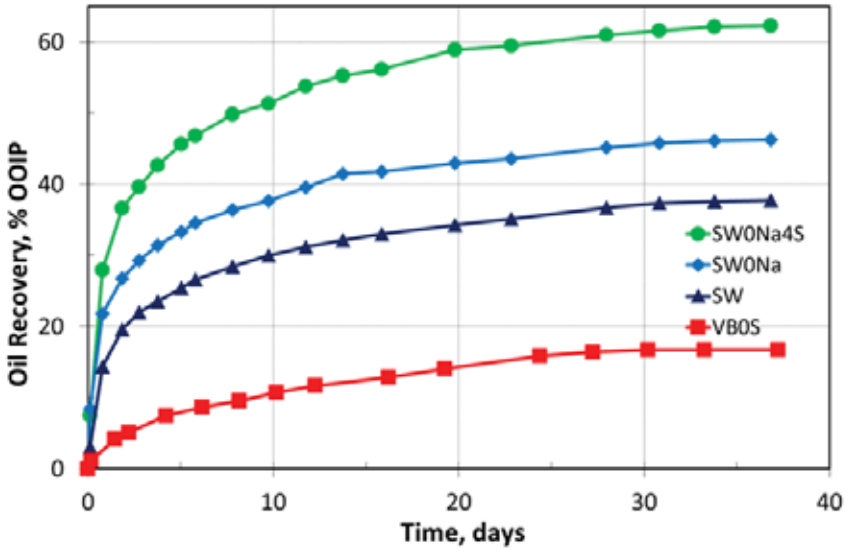

Figure 9. Spontaneous imbibition of brines into oil saturated chalk cores at 90 °C with VB (FW), seawater (SW), and modified seawater (SW0NaCl, and SW0NaCl- 4 × SO_4^{2-}) [32]

FW gave an ultimate recovery of 18 %, seawater behaved as a smart water and improved the oil recovery to 38 %. Seawater depleted in Na (SW0Na) resulted in a maximum oil recovery of 47 % of OOIP, and further spiked four times with sulfate (SW0Na4S), the oil recovery increased to 62 % OOIP. Hence, the imbibition rate was improved when NaCl was removed and when sulfate concentration was increased. This behavior is in line with the mechanism explaining the increased concentration of active ions in the double layer at the chalk surface. The results confirm that wettability alteration in carbonate reservoirs is sensitive to the ionic composition and concentration of ions in the injected brine.

3.2 Membrane Technology

Membrane desalination processes are designed based on the ability of semipermeable membranes to selectively separate or minimize the

passage of certain ions. Microfiltration (MF), ultrafiltration (UF), NF and RO are pressure-driven membrane processes and is classified according to pore sizes. MF membranes have pores in the range 0.1-10 μm with operating pressure 0.1-2 bar. UF membranes have pores from 1-100 nm with operating pressures 1-10 bar [13]. Removal of substances by MF and UF is based on sieving mechanisms. UF rejects colloids, viruses, and macromolecules from solution but allows the passage of dissolved ionic species. The separation based on sieving in UF depends on molecular weight cut-off (MWCO) of solutes [12]. The cut-off value is defined as the molecular weight of the solute where 90 % is rejected by the membrane [33].

NF and RO membranes are both pressure-driven and diffusion-controlled membrane processes and are mainly used when small organic molecules such as glucose or low molecular weight solutes such as inorganic salt separation are required. For NF membranes, the pore size ranges from 0.1 to 1 nm whereas RO membranes are considered non-porous [13]. The operating pressure of NF membranes is 3-20 bar whereas for RO the operating pressure varies from 10 to 100 bar depending on the osmotic pressure of feed solutions. The main difference between RO and NF is based on selectivity. RO membranes work on the solution-diffusion mechanism and reject all ions including monovalent ions with only water molecules passing through the membrane. NF rejects divalent ions and allows passage of monovalent ions. Thus, due to a change in pore size, the operating pressure for all membranes varies significantly and increases with a decrease in pore size.

NF membranes are mostly TFC consisting of active polyamide or polysulfone layer deposited on a microporous polysulfone layer supported by a reinforcing fabric. Membrane separation is solely by the active layer.

Membrane performance is evaluated by determining rejection, flux, and recovery.

3.2.1 Rejection

Rejection measurements are performed to determine the separation characteristics of membranes. Observed rejection R_{obs} is calculated using Equation 6.

$$R_{obs} = 1 - \frac{C_p}{C_f} \quad (6)$$

where C_p is the solute concentration in the permeate, C_f is the solute concentration in the feed.

3.2.2 Flux

Flux J_v is defined as volume flowing through a membrane per unit area and time and is generally presented as L m^{-2} h^{-1} [13]. Flux is calculated using Equation 7.

$$J_v = \frac{V}{t \times A} \quad (7)$$

where V is permeate volume during time t and A is membrane area.

For a semipermeable membrane, the flux is also defined as in Equation 8.

$$J_v = L_p(\Delta P - \Pi_F) \quad (8)$$

where L_p is water permeability, ΔP is pressure and Π_F is the osmotic pressure of the feed. The plot of pressure against pure water flux Jv results in a straight line if no membrane fouling occurs. The slope of the line corresponds to the pure water permeability of the membrane.

The pure water permeability is also expressed by the Hagen-Poiseuille equation and is defined by Equation 9.

$$L_P = r_p^2(\frac{A_k}{\Delta x})/8\mu \quad (9)$$

where r_p is pore radius, $A_k/\Delta x$ is the ratio of membrane porosity to membrane thickness and μ is the feed viscosity.

3.2.3 Permeate Recovery

Permeate recovery is an important parameter in the design and operation of membranes. Recovery is the fraction of feed flowing through the membrane and defined by Equation 10.

$$Recovery\ (\%) = {}^{Q_p}\!/_{Q_f} \times 100 \qquad (10)$$

where Q_p and Q_f are the permeate and feed flow rates, respectively.

3.3 Factors Affecting NF Membrane Performance

The main factors influencing the performance of NF membranes are:

1. Feed - Solids retention and water flux through NF membranes are strongly dependant on the concentration of feed. The higher the feed concentration the lower will be the ion retention and flux. This is a typical characteristic of charged membranes [34].
2. Pressure - Flux increases linearly with operating pressure provided no membrane fouling occurs.
3. pH - Numerous studies have focussed on the effect of pH on separation of ions with NF membranes [35, 36]. NF membranes normally contain functional groups that are strongly pH dependent that protonate or deprotonate with changing pH. At low pH, a high proton concentration is present in the solution leading to protonation of the functional group, resulting in positive membrane charge below the membrane isoelectric point [36]. At high pH, the proton concentration is low and leads to deprotonation of the functional group resulting in negative membrane charge. Thus, the feed pH can change the nature of the membrane surface charge [37] and pore size and thus affect the membrane separation efficiency.
4. Temperature - Feed viscosity decreases with increasing temperature and reduces membrane resistance resulting in higher water flux and solute passage through the membrane. An increase

in temperature also reduces concentration polarization (CP) due to reduced viscosity. Hence, total resistance to filtration decreases reducing necessary transmembrane pressure at a constant flux [38].

5. Membrane - Variations in membrane performance occur depending on membrane material. A wide range of polymers is used for manufacturing membranes that include cellulose acetate, polyamide, and sulfonated polyethersulfone. The hydrophilic or hydrophobic properties of membrane materials affect performance. Hydrophilic membranes made from polyamide and cellulose acetate are less prone to fouling in comparison to more hydrophobic membranes such as polyethersulfone. Polyethersulfone, however, has a wider pH tolerance [12].
6. Turbulence - Spiral wound membranes operate in turbulent flow [12]. Turbulence has a large effect on flux through membranes. Turbulent flow reduces formation of a gel layer or concentration polarization near the membrane surface. The turbulence in the system is calculated by measuring cross-flow velocity. The velocity in feed channel is calculated by dividing the volumetric flow rate by cross-sectional area.
   The cross-flow velocity (υ) in ms^{-1} is calculated by Equation 11 [39].

$$\upsilon = \frac{Q_f}{A} = \frac{Q_f}{W_{ch} \times h_{ch} \times \emptyset} \qquad (11)$$

   where Q_f is feed flow rate in Lh^{-1}, A is feed channel cross-section which is the product of channel width w_{ch}, channel height h_{ch} and flow channel porosity ($\emptyset$).
   Porosity of a material is a measure of voids. For spiral-wound membranes, feed channel porosity is measured as the ratio of void volume over total spacer volume and varies between 0 and 1 [39].

For flow velocity calculations in this research, the porosity is assumed to be 0.89.
Reynolds number *Re* is calculated to determine whether the flow is in laminar or turbulent regions and is calculated by Equation 12.

$$Re = \frac{\rho v D}{\mu} \quad (12)$$

where ρ is the density of feed water in kg m^{-3}, v is the kinematic viscosity in $m^2\ s^{-1}$, μ is the dynamic viscosity in Ns m^{-2}, D is the hydraulic diameter (m) calculated by Equation 13.

$$D = \frac{2ab}{a+b} \quad (13)$$

where a is membrane width and b is channel spacer height (m).

3.4 Separation Mechanisms

Nanoscale pores and charged membrane surfaces make the partitioning and transport mechanisms in NF complex. Separation in NF is based on sieving or steric hindrance, Donnan or electrostatic effects and dielectric exclusion [40, 41].

Removal of uncharged solutes is mainly due to steric or size exclusion in which shape and solute size are predominant factors. Solutes with a larger size than membrane pores are rejected due to sieving. Smaller solutes pass through the membrane [42].

The Donnan effect results from the charged nature of membranes where most NF membranes are negatively charged at neutral pH. Solutes with the same charge as the membrane, co-ions, are repelled while counter-ions are attracted to the membrane [43]. Due to the Donnan effect, the distribution of charged ions between the membrane and solution is affected by interactions between ions in solution and membrane surface charge. Hence, high retention of SO_4^{2-} occurs while the retention of Na^+

is low. However, the separation mechanism is dependent on feed pH since the membrane surface charge can vary due to dissociation of functional groups on membrane surface with changing pH [44, 45].

Dielectric exclusion occurs due to the difference between interfaces of solution and membrane with different dielectric constants [46, 47].

Hydration energy of ions also plays a role in ion separation. Ions with higher hydration energy are more efficiently retained. More energy is required to remove ions with high hydration energy compared with ions having low hydration energy [48, 49].

3.5 Kedem - Katchalsky Permeability Equations

Transfer of solutes through a charged membrane is described using the principles of nonequilibrium thermodynamics. In a two-component system consisting of a solute and water with two fluxes J_v and J_s, respectively, is related by three membrane coefficients [50]

1. The hydraulic permeability L_p
2. The solute permeability P_s
3. The reflection coefficient σ

Kedem and Katchalsky [51] proposed a set of equations to define the volume flux J_v and the solute flux J_s and membrane coefficients in Equation 14 and Equation 15.

$$J_V = L_p(\Delta P - \sigma\Delta\pi) \tag{14}$$

$$J_s = P_s\Delta C_s + (1-\sigma)J_v\, C_m \tag{15}$$

where $\Delta C_s = C_m - C_p$, with C_m the solute concentration at the membrane surface. ΔP the pressure difference and $\Delta\pi$ the osmotic pressure difference across the membrane.

3.6 Spiegler - Kedem Model

An important aspect of membrane modeling involves characterizing membranes in terms of parameters that allow the membrane to be defined by simplified mathematical models. The Spiegler - Kedem Model (SK) [50] is based on principles of irreversible thermodynamics and is used to determine the transport parameters of NF membranes. This model considers a membrane as a black box [52] with no insight into the structure and morphology of the membrane [53]. The relation between observed rejection R_{obs} and volume flux J_v with regard to this model is given by Equation 16 and Equation 17.

$$R_{obs} = \sigma \frac{(1-F)}{1-\sigma F} \tag{16}$$

where

$$F = \exp\left(-\frac{1-\sigma}{P_s} J_{v)}\right) \tag{17}$$

and σ is the reflection coefficient and P_s the solute permeability coefficient.

The membrane parameters σ and P_s are determined by fitting the SK model by using flux and rejection values from experiments.

The reflection coefficient σ is a measure of the selectivity of a membrane. If $\sigma = 1$, the membrane is semipermeable whereas if $\sigma = 0$, the membrane is unselective with no ion separation [54].

3.7 Steric Hindrance Pore Model

The first step in membrane characterization involves the estimation of membrane effective pore size. The steric hindrance pore model (SHP) was developed by Nakao et al. [55], and later applied by researchers [34] to predict the separation performance of NF membranes. According to this model, the reflection coefficient σ and the solute permeability P_s obtained from the SK model is linked to the membrane morphological

parameters pore radius r_p and the ratio of membrane porosity to membrane thickness $A_k/\Delta x$.

The membrane parameters σ and P_s are related to the membrane structural parameters according to Equations 18 - 22.

$$\sigma = 1 - S_F \{1 + (^{16}/_{9})q^2\} \quad (18)$$

$$P_s = D.S_D.(^{A_k}/_{\Delta x}) \quad (19)$$

where

$$S_D = (1-q)^2 \quad (20)$$

$$S_F = 2(1-q)^2 - (1-q)^4 \quad (21)$$

and $$q = {}^{r_s}/_{r_p} \quad (22)$$

where S_D and S_F are the steric hindrance factors for diffusion and filtration flow, respectively, D is diffusivity and r_s is the Stokes radius of the solute. Stokes radii and ion diffusivity of solutes are provided in Table 2.

Table 2. Ion Properties [56, 57, 58, 49]

Ions	**Cl^-**	**Na^+**	**SO_4^{2-}**	**Ca^{2+}**	**Mg^{2+}**
Stokes Radius (nm)	0.121	0.184	0.231	0.310	0.348
Ion Diffusivity, D_∞ ($m^2/s \times 10^{-9}$)	2.03	1.33	1.06	0.792	0.706
Hydration free energy (KJ/mol)	-340	-365	-1145	-1592	-1922

3.8 Artificial Neural Network (ANN) Theoretical

ANN's are computational models inspired by structural and functional aspects of biological neural networks. ANN's can effectively create a relation between input and output variables without considering any detailed physical interaction between variables. ANN's are capable of mapping non-linear relationships between inputs and outputs in a system through interconnected groups of artificial neurons. A multi-layer perceptron ANN structure may consist of a single layer or multiple layers of neurons.

Weight coefficients and biases connect the neurons and to generate a neuron output, an activation or transfer function is established on the summation of weights and bias input of neurons in each layer. Each neuron is a computational processor that has a summing junction operator and a transfer function. The transfer function converts the net inputs into an output. Generally used transfer functions for solving regression problems include the log-sigmoid transfer function (logsig), the hyperbolic tangent sigmoid transfer function (tansig), and the linear transfer function (purelin) [59].

Feed-forward backpropagation algorithm was used for data training. The method by which the input neurons and the outputs are connected is known as the architecture of the neural network. The neuron networks are usually grouped into several layers such as input, hidden and output layers. The number of neurons in the input layer corresponds to the number of inputs provided to the neural network and are considered as passive and only transmits the signal to the next layer. Neurons present in the hidden layer are active and take part in signal modification. The number of neurons in the output layer are also active and corresponds to the number of outputs in the network. ANN works through a training process where the network trains the neurons on how to produce an output within the desired accuracy corresponding to an input pattern.

For evaluation of ANN accuracy, the mean square error (MSE) and statistical coefficient of determination R^2 were used after training performance of the network. The MSE is expressed in Equation 23.

$$MSE = \frac{\sum_{i=1}^{n}(t_i - a_i)^2}{n} \quad (23)$$

where t_i is the i-th target value, a_i is the predicted output value and n is the number of samples.

3.9 Membrane Regeneration

Adequate pre-treatment is required to slow down or prevent membrane fouling and to maintain the production capacity of a membrane. According to the guidelines, membranes should be cleaned in any of the following cases; when a 10 % drop in permeate flow is observed, when a 15 % increase in operating pressure is observed for identical flow rate or when the permeate salt content increases by 10 % [60]. The frequency of cleaning influences the operating lifetime of a membrane.

Chemical cleaning is commonly the main requirement of a cleaning procedure and that cleaning should be able to restore membrane flux and be effective against the foulants as well as sustain membrane retention characteristics. Cleaning agents are chosen based on the type of foulants, thermal and chemical properties of the membrane material [13]. Acidic cleaners are used to reduce inorganic foulants whereas alkaline cleaners are used for organic foulants [12].

4 Experiments and Methods

4.1 Membrane Selection

Eight commercially available membranes were chosen for this research. Seawater and synthetic PW were used as membrane feed. *Dow FilmTec* provided FilmTec NF 270 and SR 90 and *Nitto Hydranautics* provided other six membranes. The membranes used for the experiments have a spiral wound configuration and are negatively charged. The main specifications of these membranes provided by the manufactures are given in Table 3.

Table 3. Membrane specifications according to manufacturers [61, 62]

Membranes	**Material**	**Area (m^2)**	**pH range**	**Feed Spacer thickness (mil)**
HYDRACORe10* 2540	Sulfonated polyethersulfone	2.3	2-11	29.9
HYDRACORe50* 2540				29.9
NF 270-2540	Composite polyamide	2.6	3-10	28
SR90 2540				-
ESNA1-LF2-2540		2.3	2-10	31
NANO-SW-2540			3-9	31
LFC3-2540			2-10.6	31
HYDRApro501-2540			2-11	34

* MWCO of HYDRACoRe10 and HYDRACoRe50 are 3000 and 1000 Daltons, respectively.

The maximum operating pressures of all membranes are from 41 to 41.6 bar. All membranes except for HYDRApro 501 has a maximum operating temperature of 45 °C. The operating temperature is pressure dependent for HYDRApro 501 and may be operated at 41 bar and 14 bar at 65 °C and at 90 °C, respectively.

4.2 Membrane Testing

The operating pressures were gradually changed from 9 bar to 18 bar at 25 °C with 25 minutes membrane stabilization between pressure changes. All experiments were performed at the Membrane Lab at the University of Stavanger from 2015 to 2018. A schematic of the membrane set-up for experiments is shown in Figure 10. It consists of one low pressure and a high-pressure pump. It also includes two pre-treatment filters of 5 and 20 μm. The pressure gauge on the retentate stream measures the transmembrane pressure. The pressure vessel had one spiral-wound membrane module.

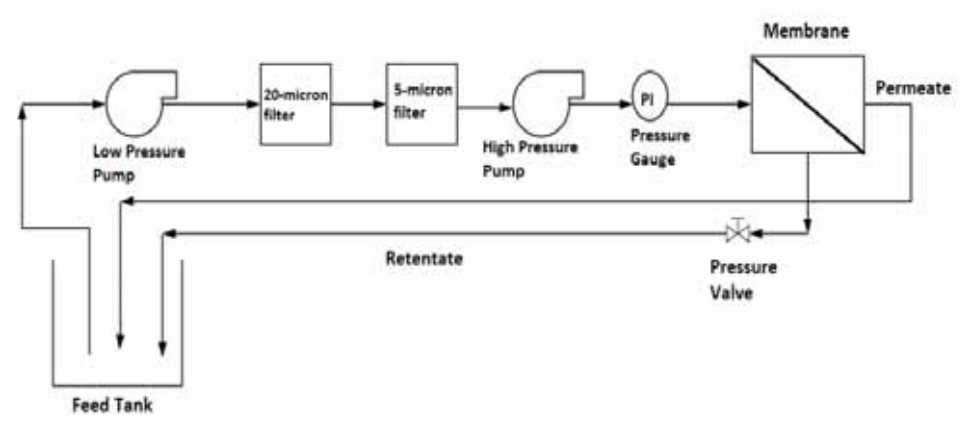

Figure 10. Schematic of the membrane system used for the experiments [63]

Retentate and permeate were recirculated to a feed tank to maintain identical feed concentrations over time. Retentate and permeate samples were collected before recirculation for further analysis.

Equation 24 exemplifies the mass flow through the membrane.

$$Q_f C_f = Q_p C_p + Q_c C_c \quad (24)$$

where Q_f, Q_p, and Q_c are feed, permeate and retentate flow rates, respectively.

C_f, C_p and C_c are feed, permeate and retentate concentrations, respectively.

The permeate and retentate flow rates were manually measured by using a calibrated cylinder and a stopwatch. pH, TDS, conductivity and temperature were recorded for all samples.

Three trials were performed for each experiment and the results in graphs and tables are average values of each trial. Experiments were repeated in case of deviations or error during mass and flow rate balances.

4.3 Chemicals, Analytical Instruments and Feed Compositions

Analytical grade chemicals were used for all experiments. pH was recorded by VWR Phenomenal pH 1100L. TDS and conductivity were measured using a TDS meter VWR collection CO3100N. Individual ion concentrations in the feed, permeate and retentate was determined using ion chromatography (Dionex ICS-5000$^+$ DP). The turbidity of the samples was measured in nephelometric turbidity unit (NTU) using a turbidimeter. At each pressure, temperature, conductivity, salinity, TDS, pH and flow rates of retentate and permeate were determined.

Different feeds were used during the experiments. Filtered normal seawater with a conductivity of 49 mS/cm and pH 8 was normally used.

The ionic composition of PW and seawater are similar, however, with a difference in salinity. For ease of experiments, all synthetic PW experiments were performed with seawater at different concentrations.

- For determining Ba^{2+} and Sr^{2+} rejection discussed in **Paper II**, seawater was used as feed for NF. Permeate without SO_4^{2-} was collected and mixed with $BaCl_2$ and $SrCl_2$.
- In **Paper II**, synthetic PW was produced by mixing Ekofisk oil with seawater at 0.1, 0.2, 0.3, 1, 2- and 3-mL/L oil in seawater at 19,000 rpm using *Polytron PT 300 Mixer* from *Kinematica*.
- During PW pH experiments, discussed in **Paper III**, for reuse of PW as smart water, it was assumed that PW was diluted to seawater concentrations and analytical grade HCl and NaOH were thus added to normal seawater. 12 feed pH values were used; 2.5, 3, 3.5, 4, 4.5, 5, 6, 7, 8.5, 9.2, 9.7 and 10.2. Experiments were also performed with normal seawater at pH 8.

Brine compositions used for experiments and analysed by IC are reported in Table 4.

Table 4. Ion compositions of feed analysed by IC

Ions	**Concentrations, mM**	
	Seawater	**Synthetic PW for Ba^{2+} and Sr^{2+} experiments**
HCO^{3-}	2	0.00
Cl^-	525	352
SO_4^{2-}	24	0.00
Mg^{2+}	51	7.1
Ca^{2+}	9.3	5.67
Na^+	450	396
K^+	10	7
Ba^{2+}	-	1.6
Sr^{2+}	-	1.6
Li^+	-	

4.4 Membrane Cleaning and Preservation

The interval for cleaning of membranes depends on the type of feed. Membranes were routinely cleaned with pure water at 9 bar after each experiment to prevent accumulation of irreversible foulant on the membranes. HCl and NaOH cleaning solutions recirculated for 30 - 45 minutes through the membranes after each set of experiments. The membranes were first washed with HCl diluted with tap water at pH 3 followed by NaOH washing at pH 10 - 11. At the end of each cleaning, the membranes were immediately rinsed with clean water until the permeate conductivity was as pure water. Metabisulfite was used to preserve membranes when not used for more than a week.

4.5 Media Filtration for Oil Removal

As mentioned in **Paper II**, a lab-scale media cylindrical filtration unit of diameter 25 cm and height 120 cm was constructed to remove oil from synthetic PW. The media was powdered activated carbon and anthracite. Anthracite was placed on top followed by activated carbon. Pebbles were placed at the bottom to provide support. Backwashing was performed with a 350 W pump at a maximum flow rate of 2500 L/h. Synthetic PW was used as feed and the effluent was collected and immediately used as NF feed. Three trials were performed for each concentration. The unit was backwashed with tap water after experiments for each concentration. Samples were collected from the influent, effluent and backwashed water in regular intervals to check concentrations of oil in water. The media was replaced when the backwash water contained oil droplets even after prolonged washing.

Hydrocarbon removal efficiency E_{oil} (%) was calculated using Equation 25.

$$E_{Oil} = 1 - {C_{p(oil)}}/{C_{f(oil)}} \times 100 \qquad (25)$$

where $C_{p(oil)}$ and $C_{f(oil)}$ are the oil concentrations in the effluent (permeate) and influent (feed), respectively.

A schematic of the filtration unit is shown in Figure 11.

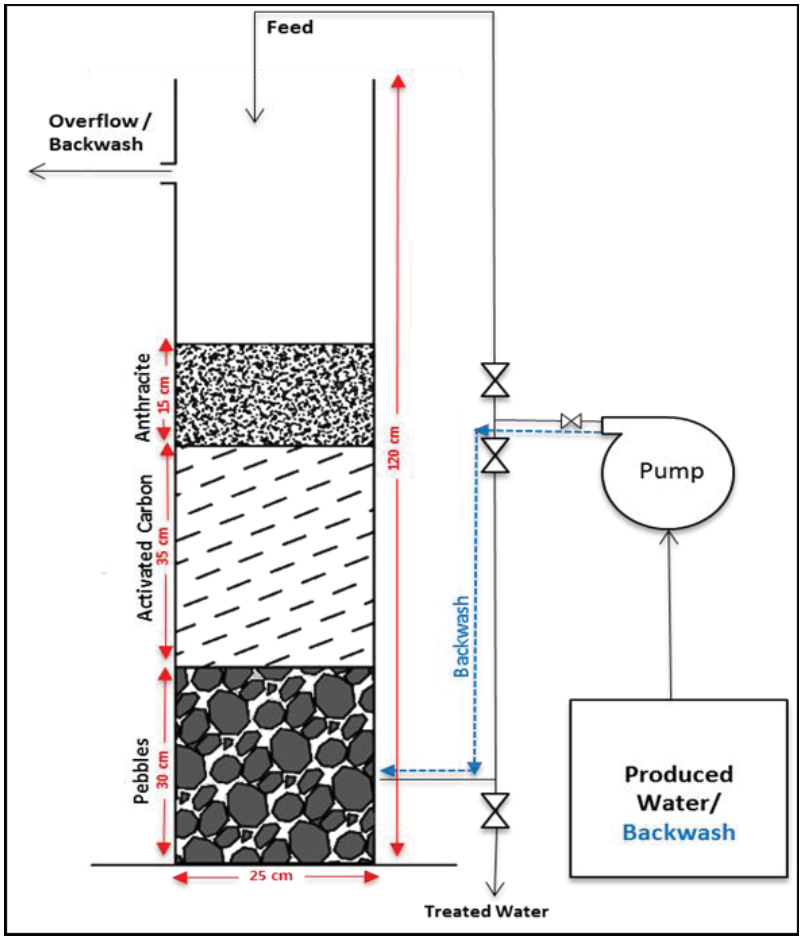

Figure 11. Schematic of the lab-scale media filtration unit

4.6 Infrared (IR) Analysis

Oil in synthetic PW was analysed by IR spectrometer (Agilent Cary 630 FTIR). Extraction of media filter influent, effluent and de-oiled NF feed and permeate were performed immediately using cyclohexane according

to ASTM D7678-17 [64]. IR analysis method and results are described in **Paper II**.

4.7 Scanning Electron Microscopy (SEM)

SEM was used in this research to analyse the membrane surface after one year of operation. The membrane was thoroughly cleaned during this period. However, to analyse the effect of barium and strontium scaling, the membrane was not cleaned for one week. The membrane was then subjected to SEM analysis. While using SEM, the membrane surface must be conductive to produce signals and avoid charging when the electron beam impinges on the membrane surface. Thus, a conductive coating of palladium was applied. However, SEM could only give information on the macroscopic structure of the NF membranes, as the maximum resolution obtained was 200 nm. The analysis was performed at 10 mm working distance with an accelerating voltage of 15 kV and an aperture size of 30 μm.

4.8 Modeling of Membrane Experiments

Modeling based on experiments were performed using Spiegler - Kedem and steric hindrance pore models in **Paper III and Paper IV**. ANN was used during experiments with PW **in Paper III**. Flux, pressure and pH from three NF membranes were used as input and rejection of Cl^-, Na^+, Mg^{2+} and Ca^{2+} were the output.

4.8.1 Models-based on Spiegler - Kedem and SHP models

A predictive model helps users obtain membrane characteristics, predict process performance and aid in improving the process. Beginning with the SK model for filtration through a porous membrane, equations were derived to compute NF reflection coefficient and solute permeability within a particular pure water permeability range and possible rejection for individual ions in seawater. For this purpose, the transport parameters were obtained using a nonlinear least squares method by fitting the

experimentally obtained rejection and flux data to the SK model. The SHP model determined the pore radius of membranes by using the Stokes radius of ions from Table 2.

4.8.2 Data Training by Artificial Neural Network

Rejection of ions was predicted using ANN when feed pH was varied **in Paper III.** A feed-forward back propagation ANN was used that works with a set of input and output data. Feed pH, pressure and flux data were used as input. A number of neurons were altered to design the best ANN structure for predicting ion rejection. The number of hidden neurons was selected after evaluating the neurons performance by calculating the mean square error (MSE). The set of neurons with least MSE was selected for the ANN structure. The training of the ANN model was carried out by using the Levenberg - Marquardt algorithm. For proper network training, and to avoid overfitting, the experimental data were randomly divided into three sets of 70 %, 15 % and 15 % for training, validation, and testing, respectively. A set of 65 samples were provided for each membrane with varying pH and operating pressures. Hence, 45 samples were used for training and 10 each for validation and testing of the proposed ANN design.

5 Results and Discussion

Performance of NF, based on brine composition, concentrations, pressure and pH, was determined by measuring permeability, flux and rejection. Major results obtained during the research are explained in this section.

5.1 Pure Water Permeability

Membrane performance from pure water feed flux and applied pressure was obtained for the membranes prior to testing of seawater and PW. The membranes were washed with tap water until all preservatives were removed. The permeate and retentate were recirculated to the feed tank during washing. The feed tank was replenished with fresh water every two minutes. The washing was continued until the conductivity of the feed water equals the conductivity of tap water. Water flux from eight membranes was recorded. Pure water permeability is used as a baseline to evaluate the cleaning efficiency of membranes.

Pure water permeabilities of individual membranes are presented in Table 5. The experiments were performed at 25 °C.

Table 5. Pure water permeabilities of tested membranes

Membranes	**Pure water permeability ($Lh^{-1} m^{-2} bar^{-1}$)**
HYDRACoRe 10	13.56
ESNA	10.52
NF 270	9.38
HYDRACoRe 50	5.15
SR 90	4.46
NANO-SW	3.27
LFC3	2.85
HYDRApro 501	1.32

Pure water permeability is related to the structural parameters of the membrane according to Hagen Poiseuille as shown in Equation 9. Thus, a membrane with a higher permeability has a larger pore size. According to Table 5, the effective pore size of the membranes is in the descending order HYDRACoRe 10 > ESNA > NF270 > HYDRACoRe 50 > SR 90 > NANO-SW > LFC3 > HYDRApro 501.

5.2 Reynolds Number

Reynolds number was calculated to determine whether the flow was laminar or turbulent. Equations 11, 12 and 13 were applied with seawater as membrane feed with density, kinematic viscosity and dynamic viscosity of seawater at 25 °C used for calculations. The spacer height was obtained from membrane manufacturers.

The Reynolds number was 261. Theoretically, this value is in the laminar region. However, the feed spacers between the membranes act as turbulence promoters and contribute additional turbulence.

5.3 Effect of Applied Pressure on Ion Rejection

Ion rejection from NF membranes with seawater as feed showed high divalent and low monovalent ion rejection. Rejection varied with membrane pore size. Figure 12 shows rejection by NANO-SW membrane, a tight membrane according to the pure water permeability values in Table 5.

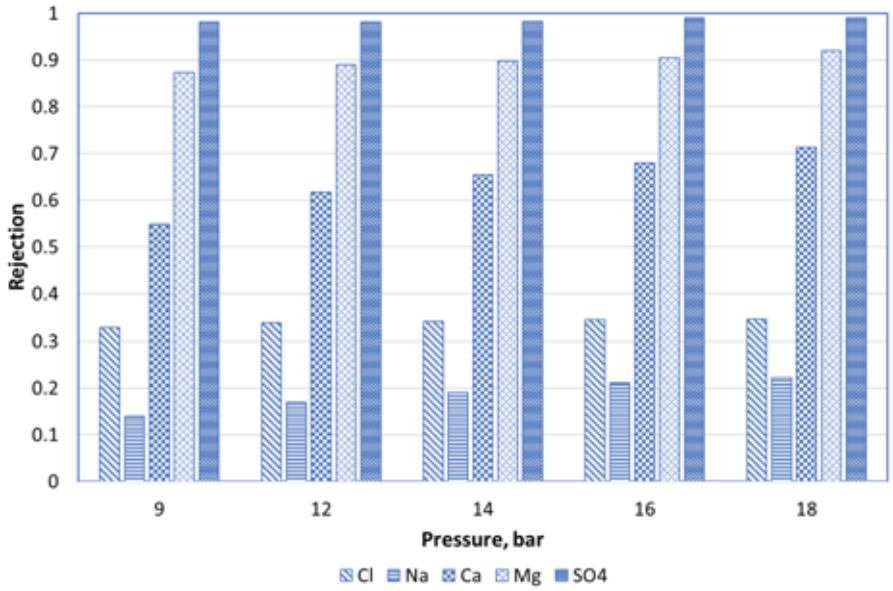

Figure 12. Ion rejection with increasing pressure with NANO-SW

Ion rejection for NANO-SW in Figure 12 shows that rejection increased in the order $Na^+ < Cl^- < Ca^{2+} < Mg^{2+} < SO_4^{2-}$ and is explained by differences in hydration free energy of ions. Na^+ and Cl^- have a hydration free energy of -365 KJ/mol and -340 KJ/mol, respectively. Na^+ is attracted by the membrane and is rejected the least as observed in Figure 12. Ions with lower hydration energies permeate easier through the membrane. However, the effect of negative membrane charge plays a major role in separation. Cl^- will be rejected by the membrane even with a lower hydration energy. Cl^- rejection is higher than Na^+ due to its charge. Hydration free energy of Ca^{2+} (-1592 KJ/mol) is lower than Mg^{2+} (-1922 KJ/mol) and has accordingly the lower rejection of the two. The negatively charged divalent sulfate has the highest rejection by NF membranes. Hydration free energy of SO_4^{2-} is -1145 KJ/mol [49].

Rejections of Cl^- and Na^+ with a change in pressures are demonstrated in Figure 13 and Figure 14, respectively.

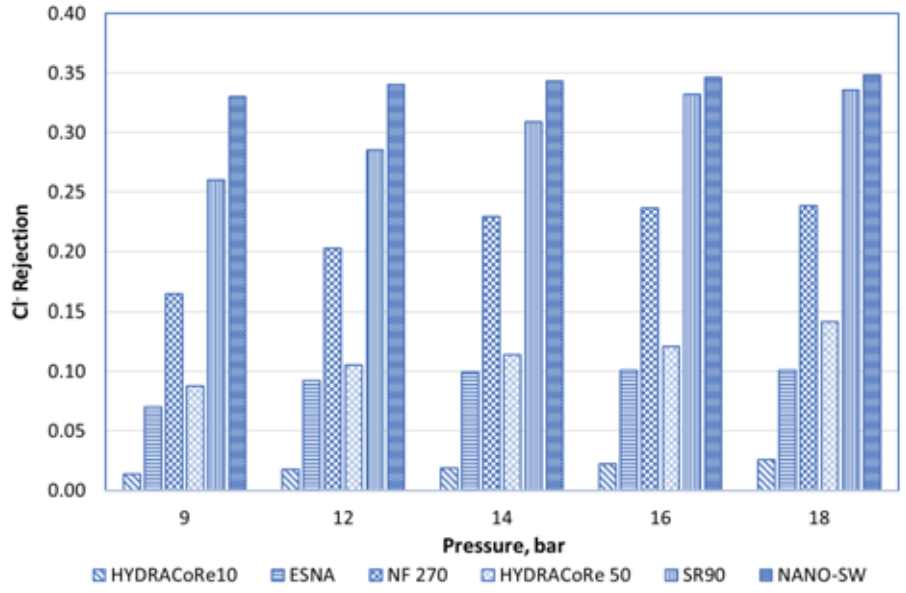

Figure 13. Cl^- rejection for six NF membranes

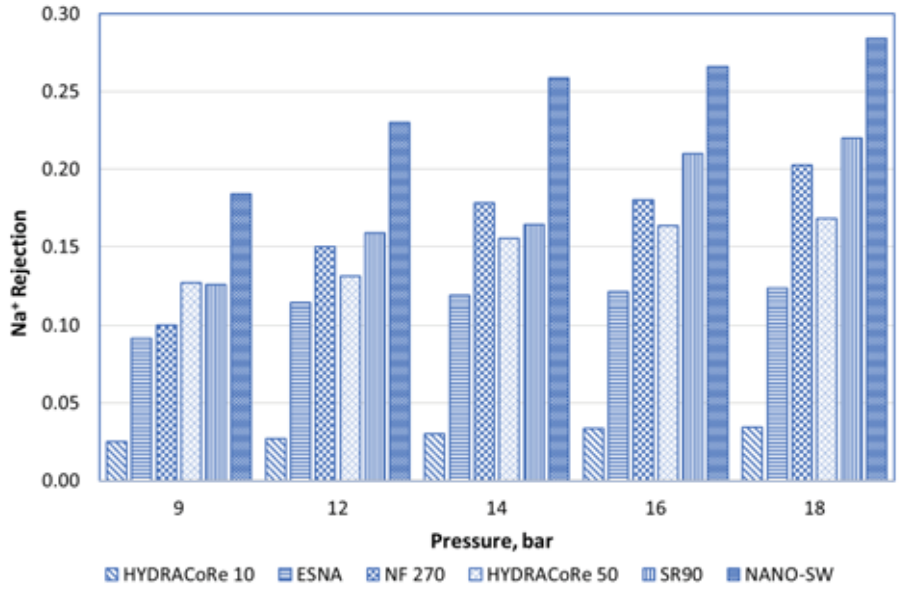

Figure 14. Na^+ rejection for six NF membranes

Figure 13 shows that Cl^- rejection is higher than Na^+ rejection at all pressures except for HYDRACoRe 10 and HYDRACoRe 50. Anions will be rejected more than cations when a negatively charged membrane is used. However, for both HYDRACoRe membranes, the rejection is opposite, perhaps due to a comparatively lower surface charge.

SO_4^{2-} rejection with increasing pressure for six membranes are shown in Figure 15.

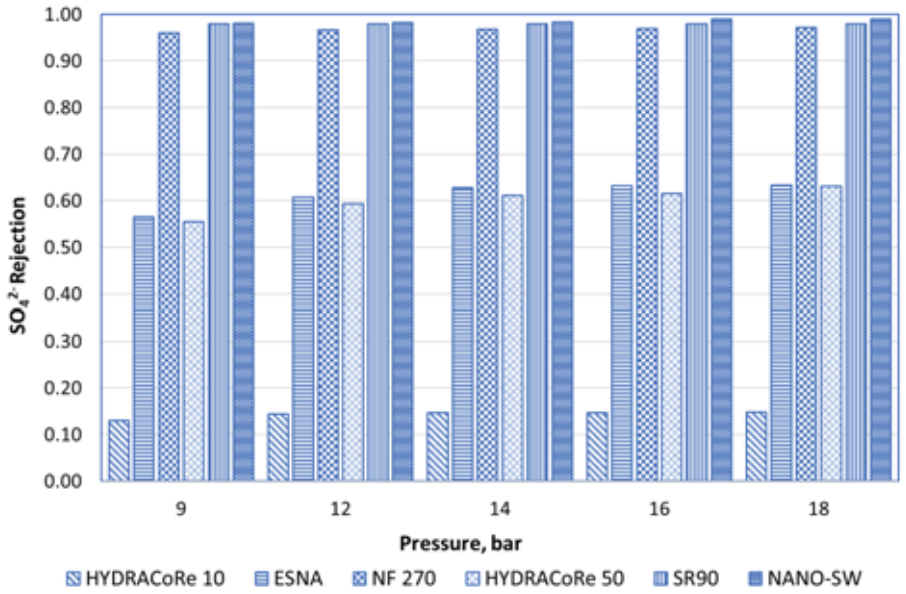

Figure 15. Comparison of SO_4^{2-} rejection with pressure for six membranes

Rejection presented in Figure 15 confirms that NANO-SW, SR 90 and NF 270 are highly negatively charged and have smaller effective pore sizes yielding high divalent anion rejection. ESNA is likewise a negatively charged membrane, however, with larger pore size. Both HYDRACoRe membranes showed lower SO_4^{2-} rejection due to lower surface charge. The overall results show that retention of multivalent ions was higher than the retention of monovalent ions though the tighter membranes also retained monovalent ions. The results are supporting

reported values of Stokes radius and confirms that ions with a relatively larger diffusivity have lower rejection. Ion permeability through NF membranes has strong correlations to their radius of hydration and hydration energy. Mg^{2+} and Ca^{2+} have larger Stokes radius and higher hydration energy as reported in Table 2. These ions hold their hydration shells more strongly, thus are more effectively removed by membranes.

5.4 Effect of Increased Feed Concentration on Ion Rejection

Experiments with seawater spiked with chemicals using NANO-SW were performed to investigate the effects of increased divalent ion concentrations on rejection of ions. Several researchers have reported a decrease in salt retention with increasing feed concentrations [65, 66]. The method and results obtained are discussed in **Paper I**.

Concentrations of SO_4^{2-}, Ca^{2+} and Mg^{2+} were increased individually by addition of Na_2SO_4, $CaCl_2$ and $MgCl_2$ to seawater. Spiking with divalent ions was performed as smart water for carbonates requires high divalent ion concentrations.

SO_4^{2-} was added in doses of 54 mM (dose 1), 76 mM (dose 2) and 95 mM (dose 3) to seawater. Three trials at each dose were performed and samples were collected for IC analysis. Pressures were increased from 8 bar to 16 bar. Membrane stabilization time was 25 minutes for each pressure change. Washing with pure water was performed after each dose. The NANO-SW membrane was rinsed with seawater before another spiking. Figure 16 shows flux behavior with increasing feed concentration, dose 1 to dose 3, by addition of Na_2SO_4 to seawater.

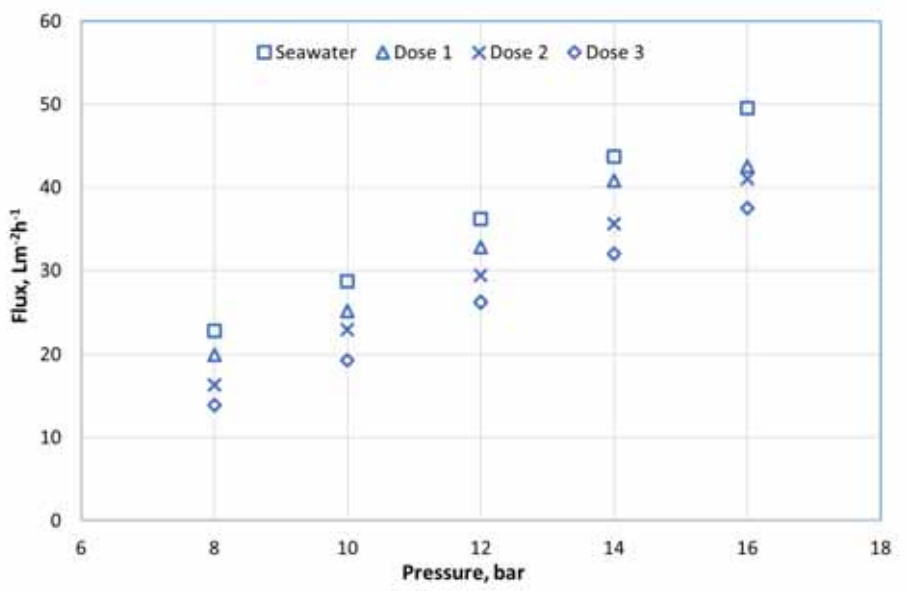

Figure 16. Flux variations with increased SO_4^{2-} concentrations in the feed

The results confirm that volume flux increases linearly with applied pressure and decreases with an increase in feed concentration. This behavior is due to an increasing osmotic pressure difference across the membrane as the ion concentration increases.

Figure 17 shows the effect of increased SO_4^{2-} concentration on Cl^- rejection using NANO-SW.

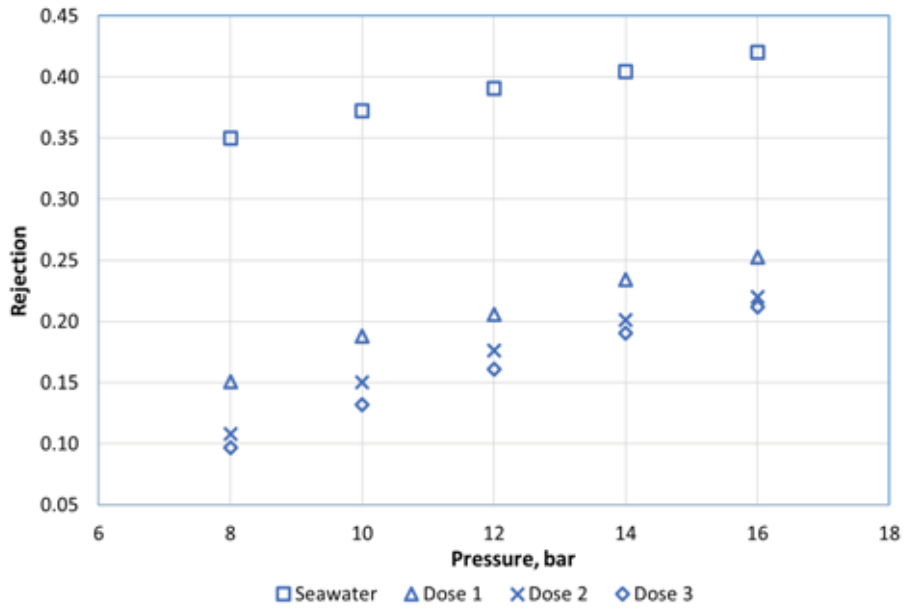

Figure 17. Cl^- rejection with increased SO_4^{2-} concentration

According to Figure 17, with increased SO_4^{2-} concentrations in the feed, retention of Cl^- decreased for a fixed pressure. This variation is explained by electrostatic and steric hindrance effect. At low feed concentrations, membrane charge has a dominant role in ion rejection and the negatively charged membrane rejects Cl^-. When SO_4^{2-} concentration in feed increased, effective membrane charge reduces and the dominant separation mechanism becomes steric hindrance, thus increasing permeation of Cl^-. Similar effects are observed in the literature [66, 67, 68]. Further explanation for the observed decrease in Cl^- rejection is due to the increased concentration of Na^+ added to the solution with SO_4^{2-} as Na_2SO_4. For maintaining electroneutrality, one of the co-ions has to permeate with the counterion. This results in a preferential permeation of Cl^- rather than SO_4^{2-} due to high hydration energy and Stokes radius of SO_4^{2-}.

According to Figure 16 and Figure 17, it will be advantageous to spike divalent ions in the feed rather than to the retentate for producing smart

water in carbonates. This assist in increased permeation of Cl^- with increasing SO_4^{2-}.

5.5 Produced Water Treatment

Oily wastewater contains impurities resulting in membrane fouling and scaling, affecting the filtration process and shortening membrane life. Though the RO membrane provides better water quality, NF membranes are more cost-effective for reuse of PW in the oil and gas industry. However, real and synthetic PW must be evaluated carefully as real PW makes the membrane process less effective due to fouling.

5.5.1 De-oiling of Synthetic PW by Media Filtration Unit

The following experiments performed in **Paper II** and **Paper III** relate to hypothesis 1 and 2 to validate whether PW can be reused as smart water. The main issues related to the treatment of feed water containing traces of oil, the presence of scaling ions, pH of feed water are discussed.

Synthetic PW with oil was filtered through a media filtration unit. The influent and effluent samples were extracted according to ASTM D7678-17 with cyclohexane and the extracted samples were analysed with IR Spectrometer. A detailed description of the method implemented during the experiments, extraction method and IR analysis is described in **Paper II**.

96 - 98 % hydrocarbon removal efficiency was calculated according to Equation 25. A visual comparison of the influent and effluent samples from the media filtration unit before and after extraction with cyclohexane is shown in Figure 18.

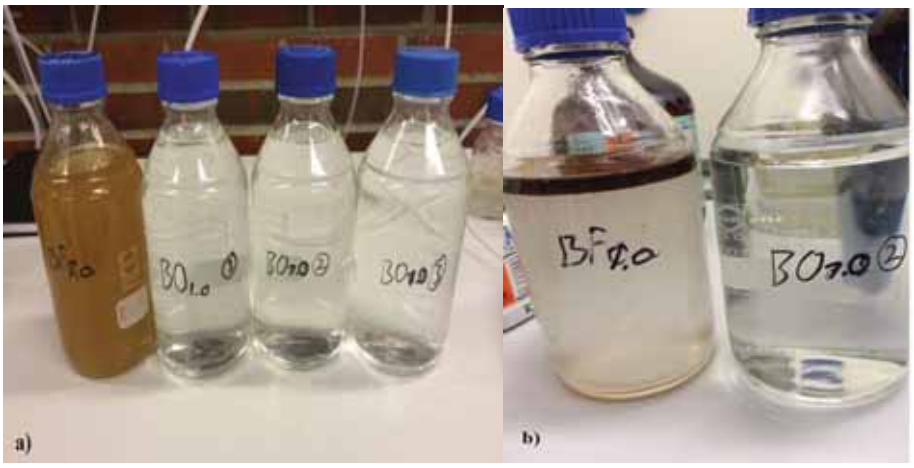

Figure 18. Comparison of influent and effluent samples a) before extraction b) after extraction

5.5.2 Barium and Strontium Removal

Removal of scaling ions such as barium and strontium from de-oiled PW is crucial before reusing as smart water. The treated water is used in smart water production in both carbonate and sandstone reservoirs.

Synthetic PW spiked with Ba^{2+} and Sr^{2+} was treated with NANO - SW at room temperature and is discussed in **Paper II**. The results are shown in Figure 19.

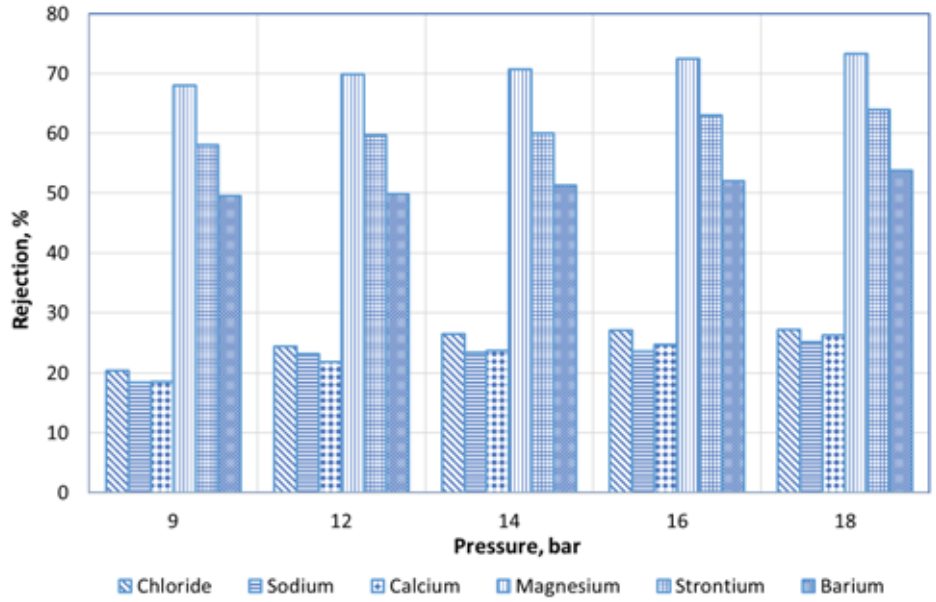

Figure 19. Rejection of Ba^{2+} and Sr^{2+} with NANO-SW

The results show that the membrane rejected 64 % Sr^{2+} and 53 % Ba^{2+}. The hydration free energy of Ba^{2+} is -1273 KJ/mol [69] whereas that of Sr^{2+} is -1395.7 KJ/mol [70] The difference in hydration free energy explains the higher rejection of Sr^{2+} compared to Ba^{2+}. Figure 20 shows flux versus pressure when Ba^{2+} and Sr^{2+} were spiked in the feed. The linear relation confirms that no fouling occurred during the operation.

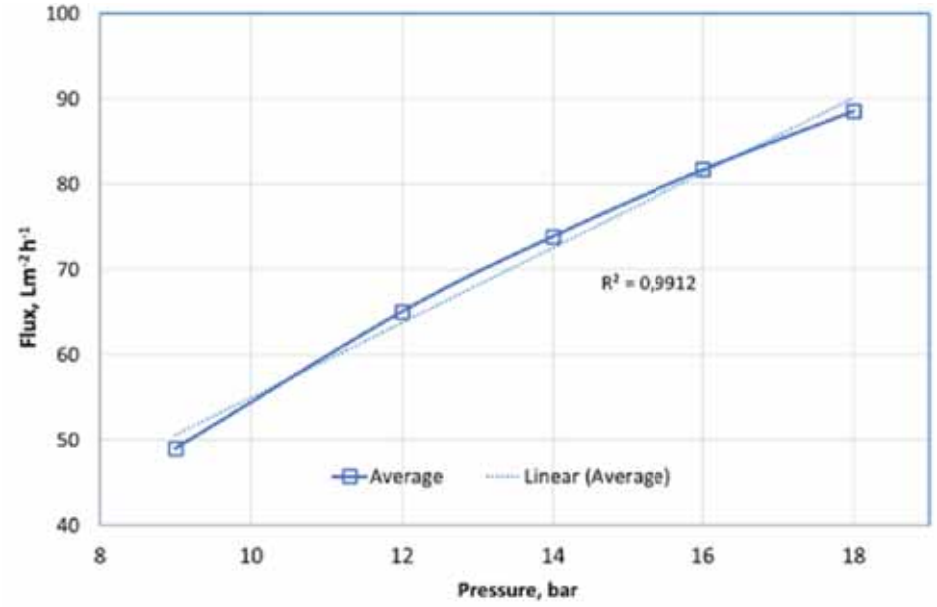

Figure 20. Flux versus pressure with Ba^{2+} and Sr^{2+} in the feed

5.5.3 Importance of Adequate Membrane Cleaning

The polyamide NF membrane (NANO - SW) after operation for a year was analysed using SEM. The SEM experiments were performed after several experiments with synthetic PW containing Ba^{2+} and traces of SO_4^{2-} (6 mg/L) in the feed. No chemical treatment or washing was conducted on the membrane after the experiments in order to analyse the amount of Ba^{2+} precipitation during membrane separation.

The SEM images revealed that ion precipitation occurred and was largely seen on the feed side of the membrane. The SEM images of the membrane are presented in Figure 21.

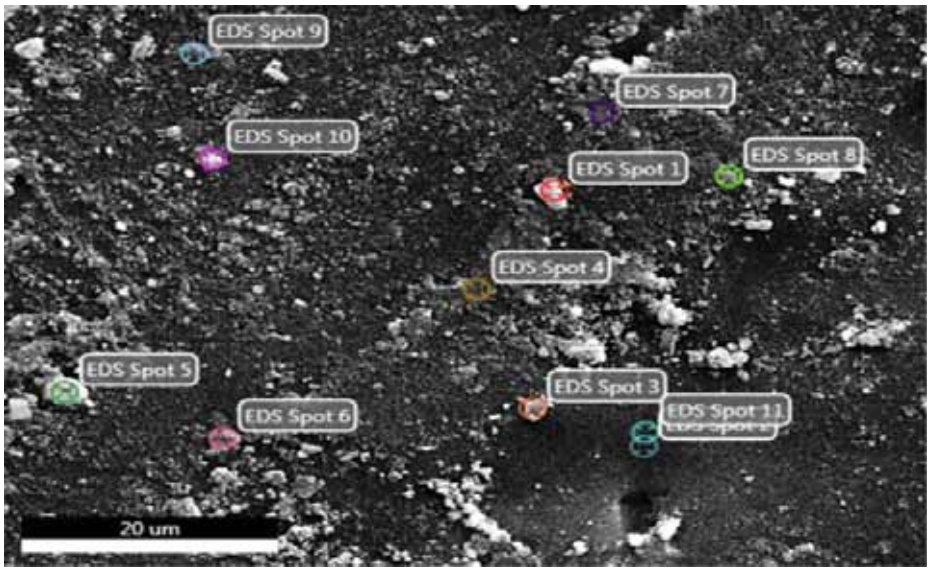

Figure 21. SEM image of NF membrane on the feed side

The energy dispersive X-ray spectroscopy (EDS) resulted in an analysis of the elements present on the surface. EDS analysis of Spot 1 in Figure 21 is presented in Figure 22.

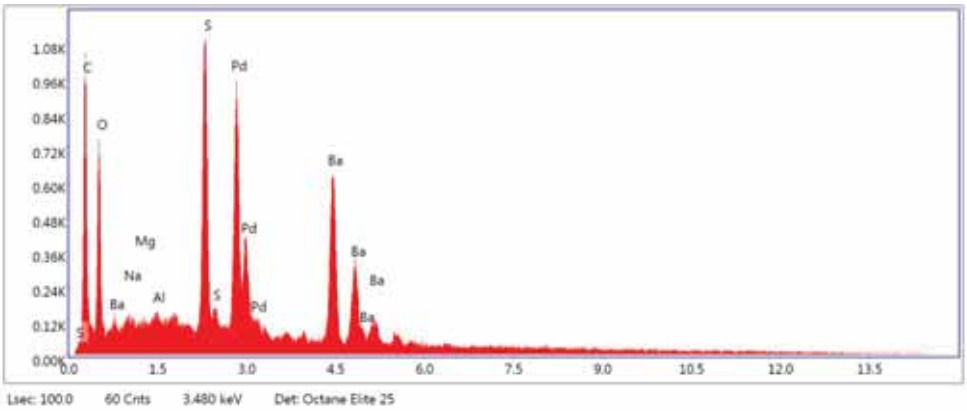

Figure 22. EDS analysis of Spot 1

The SEM-EDS analysis revealed the accumulation of inorganic precipitates on the NF membrane surface. It is evident that Ba^{2+} and

SO_4^{2-} are present on the surface due to high concentration of Ba, S, and O in the spectrum. Figure 23 demonstrates the SEM image on the permeate side of the membrane. Precipitation of ions on the permeate side is less than on the membrane feed side.

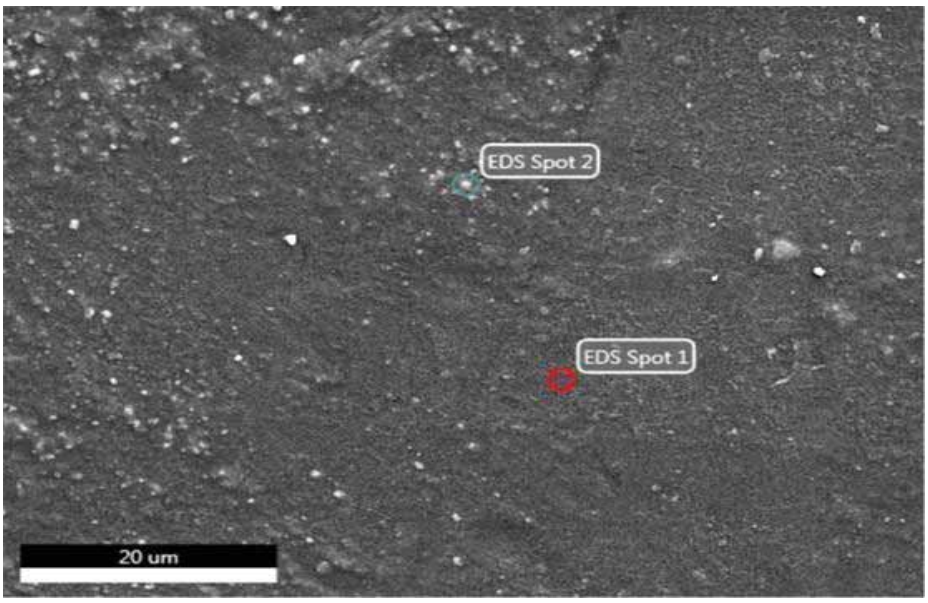

Figure 23. SEM image on the permeate side of the membrane

Analysis of SEM images suggests that proper chemical membrane cleaning is required during treatment of PW with scale causing ions, which could otherwise lead to permanent scaling and membrane production loss.

5.5.4 Effect of Produced Water pH on NF Membrane Performance

Paper III discusses the effect of PW pH on membrane performance. pH of synthetic PW was varied from 2.5 to 10.2 and pressure was increased from 9 to 18 bar. Experiments were performed for three NF membranes; ESNA1- LF2 - 2540, NF 270 - 2540 and HYDRACoRe 50 - 2540. Three trials each were performed at all pH concentrations.

A significant change in flux and rejection was observed with variations in pH. Flux was higher in basic environments. When flux increased with an increase in pH, the rejection of charged ions decreased. Highest flux was observed for ESNA indicating a larger pore size than for HYDRACoRe and NF 270. A change in ion rejection was noticeable between acidic and alkaline environments for divalent ions. A sharp decrease in Mg^{2+} rejection was observed in the basic environment for ESNA and NF 270. It was confirmed that pore size decreased with a decrease in feed pH using SK and SHP models (Equation 16 - Equation 22).

Effect of feed pH on flux with ESNA is shown in Figure 24.

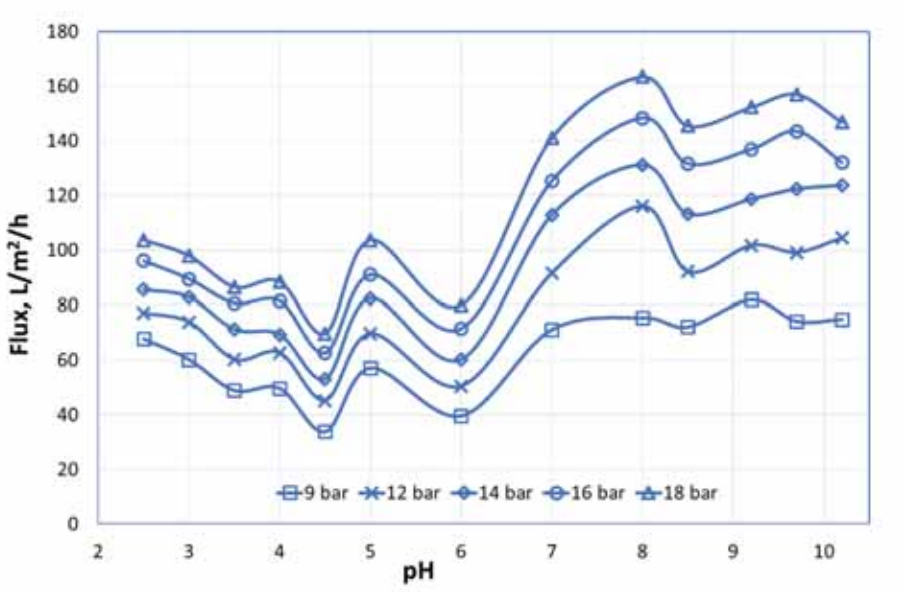

Figure 24. Flux variations with a change in pH with ESNA membrane

According to the Donnan effect, negatively charged membranes attract positively charged ions. NF membrane acquires charges in the presence of an ionic solution due to the association or dissociation of functional groups on the membrane surface that strongly depends on the pH of the solution.

Polyamide NF membranes consist of both carboxyl group (≡ COO^-) and amino groups (≡ NH^{3+}) and exhibit positive and negative surface charges depending on pH. At acidic conditions, protonation of amine occurs (≡NH_2 → ≡NH_3^+) resulting in increased pore size and increasing flux. This explains a slight peak in flux in an acidic environment at pH 5 in Figure 24. At alkaline pH, polyamide membrane matrix appears to be more expanded due to deprotonation of the carboxyl group (≡COOH → ≡COO-) resulting in increased flux [36, 44] as for ESNA and NF 270.

Figure 25 shows Cl^- rejection for NF 270 when feed pH varied from 2.5 to 10.2. A rejection minimum at acidic pH was observed between pH 4 and pH 5 and a maximum Cl^- rejection was observed at pH 3.

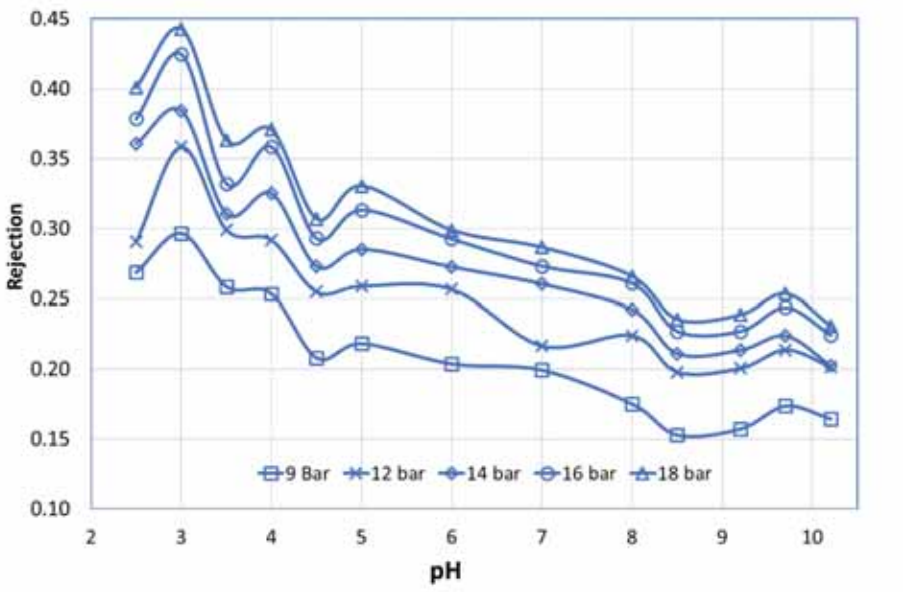

Figure 25. Effect of pH on Cl^- rejection for NF 270

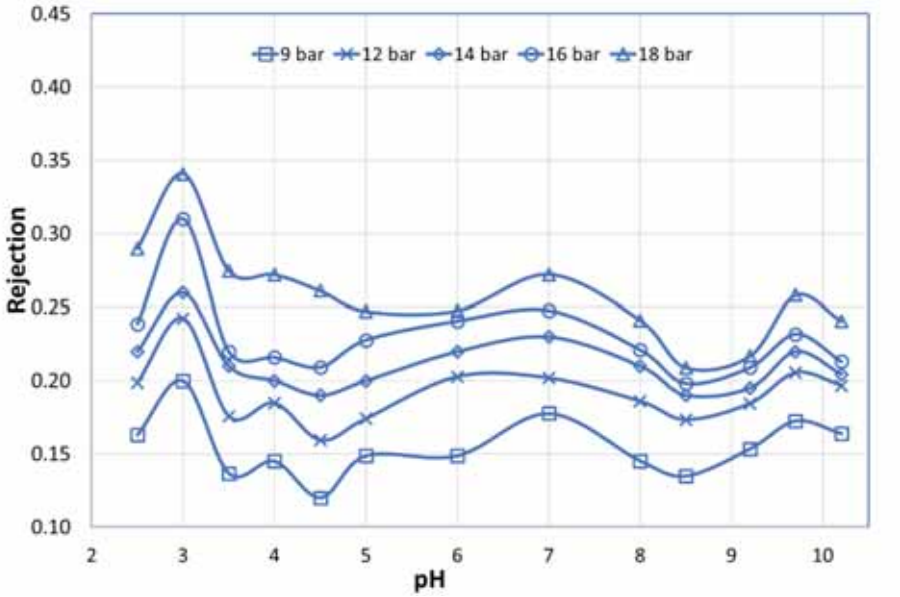

Figure 26. Effect of pH on Na^+ rejection with NF 270

Figure 26 shows Na^+ rejection at varying feed pH. The results show that Na^+ rejection coincides with Cl^- rejection at varying pH. At pH 3, a Na^+ rejection maximum is observed which confirms that monovalent cation is also rejected enabling electroneutrality in solution.

Positive charges of a membrane increase with a decrease in pH below the isoelectric point of the membrane [44] and results in more Na^+ rejected by the membrane. The isoelectric point is the point where rejection of Na^+ and Cl^- is the lowest. The membrane charge is considered positive below the isoelectric point and is negative above the isoelectric point [36, 44, 71]. Since anions and cations do not act independently, Cl^- is also rejected to maintain electroneutrality. Similarly, at pH 9.7, when the membrane is more negatively charged, Cl^- experiences an electrostatic repulsion from the membrane and thus more Cl^- is rejected and explains the peak at pH 9.7 in Figure 25. This results in a subsequent increase in Na^+ rejection to maintain the electroneutrality of the permeate as observed in Figure 26.

Change in pore size with varying pH was determined using SK and SHP model and is presented in Figure 27. The pore size was calculated based on the solute - to - pore size ratio of Mg^{2+} for the three NF membranes.

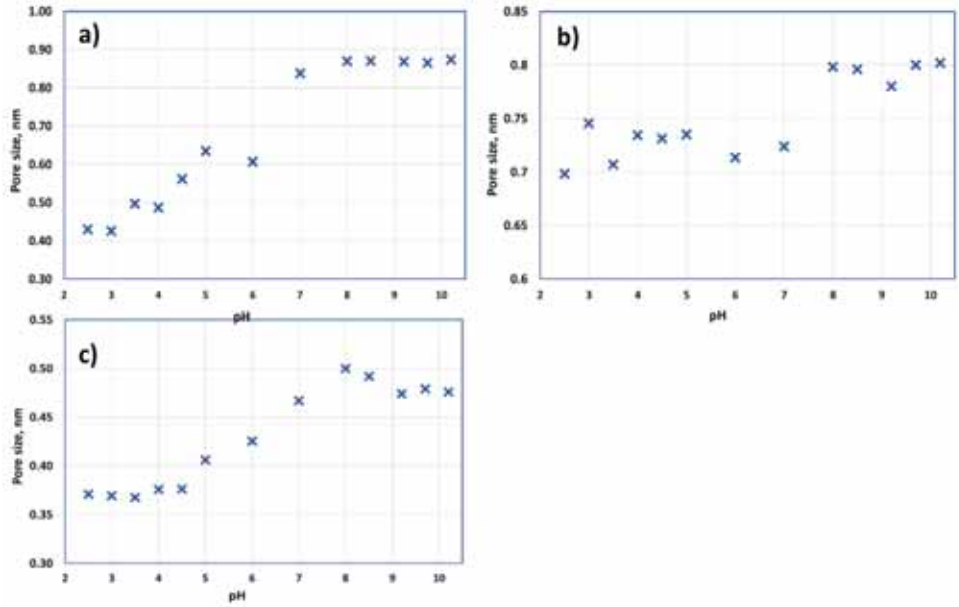

Figure 27. Variations in pore radius r_p with pH on the NF membranes a) ESNA b) HYDRACoRe c) NF 270

Figure 27 shows that the separation performance of membranes varies with membrane material. Variations between acidic and basic pH are more obvious in polyamide membranes since they are more hydrophilic and are prone to ionization and hydration in aqueous solutions. This results in changes on the conformation of polymer chains, especially at different pH. Since the NF membranes have nanoscale pore dimensions, even a small change in pore size would have a clear impact on membrane performance. ESNA and FilmTec NF 270 are hydrophilic polyamide membranes whereas HYDRACoRe membranes are made of hydrophobic polyethersulfone with a high pH tolerance [12]. This explains the relative stable behavior of HYDRACoRe with pH.

5.5.5 Predicting Ion Rejection by Artificial Neural Network

The extensive experimental data collected according to experiments performed in **Paper III**, by changing the pressure and pH have shown interdependency and it provides an opportunity for using the ANN tool for predicting the performance of membranes. After providing the required data, the input values for pressure, pH and flux, the neural network model was created using MATLAB.

A feed-forward back propagation ANN model with a hyperbolic tangent sigmoid transfer function (tansig) was chosen as the most suitable network for predicting ion rejection in this research. ANN approach is data-driven and hence is specific for a particular membrane.

The number of neurons used for the network in this research is seven where the calculated MSE values were the least along with the highest R^2 values. A relatively low mean square error in the range of 0.00011 to 0.00393 for individual ion rejections were calculated.

It was observed that the training of input and output data was well performed with an R^2 value of 0.996 for training. R^2 value for test data is also greater than 0.99 confirming that ANN predicted rejection values and experimental values are in close agreement. These values signify the ability of ANN in predicting major ion rejection (Na^+, Cl^-, Ca^{2+} and Mg^{2+}) if flux, pH and pressure are available. Figure 28 shows the ANN structure used for ion predictions with varying input variables.

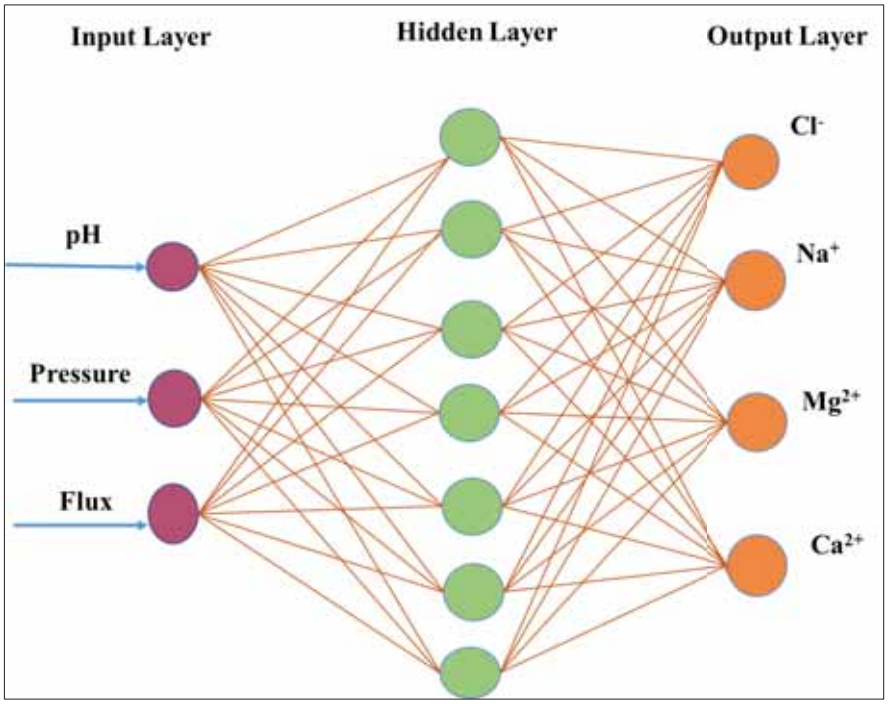

Figure 28. ANN design with 7 neurons to predict ion rejections at varying feed pH

5.6 Spiegler - Kedem Model

Estimation of transport parameters σ and P_s was performed by using the SK model and is presented in **Paper IV**. Equations 16 and 17 were independently fitted to each set of experimentally obtained values for R_{obs} and J_v, corresponding to each major ion in seawater, which did yield the transport coefficients specific for individual ions. The procedure was repeated for six NF membranes. The transport parameter σ confirmed that with an increase in ion rejection, the reflection coefficient increased and with an increase in ion permeability coefficient, P_s increased. Figure 29 shows rejection versus flux for Na^+ with ESNA when the values were fitted using the SK model. The data points present the rejection values from the experiment and the solid line presents the values obtained using

the SK model with the best-fitted σ and P_s values. Figure 29 shows that the theoretical curves are in close agreement with experimental values.

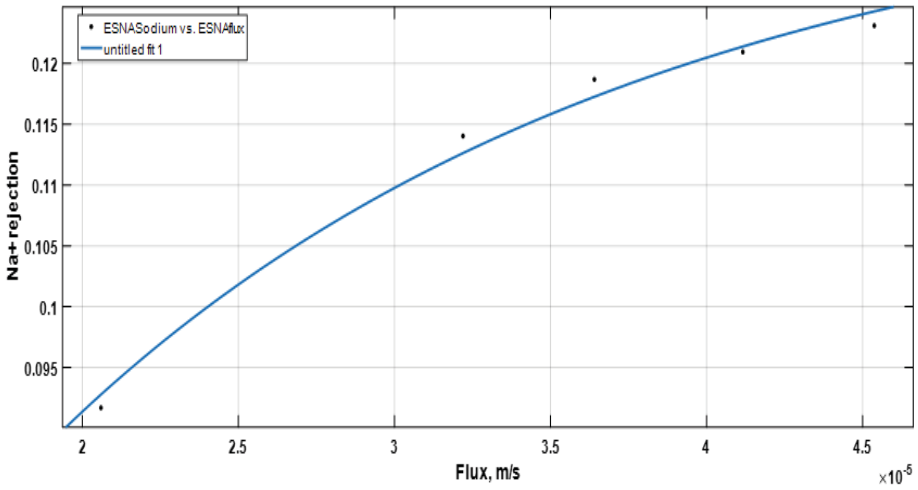

Figure 29. Rejection versus flux for Na^+ for ESNA

5.7 Steric Hindrance Pore Model

Estimation of pore radius for the tested NF membranes is discussed in **Paper IV**. Evaluation of effective pore size r_p of the membranes was determined using steric hindrance pore model. The value of such measurements enables determining the pore size based on a single ion rather than using an uncharged molecule such as glucose for measuring the effective pore radius. This increase proper understanding of real case scenario using membranes for desalination.

Transport parameters for each ion with NF membranes were determined by fitting R_{obs} versus J_v according to the SK model. The estimated σ and P_s values for each ion were substituted in Equations 18 - 22 to determine the pore radius specific to a particular ion and is presented in Table 6. This method assumes that only steric effects cause ion rejection and that ions with Stokes radius larger than the membrane pore size are rejected.

The SK model used to analyse the experimental rejection data versus flux showed a good fitting for all ions investigated.

Table 6. Effective ion pore radius r_p calculated using SK and SHP models for different membranes

Ions	**ESNA**	**NF 270**	**SR 90**	**HYDRACoRe 10**	**HYDRACoRe 50**	**NANO-SW**
	r_p (nm)					
Cl^-	0.41	0.35	0.24	-	0.37	0.24
Na^+	0.63	0.52	0.45	1.42	0.46	0.42
SO_4^{2-}	0.34	0.25	0.24	0.73	0.33	0.24
Ca^{2+}	0.71	0.58	0.39	0.99	0.67	0.37
Mg^{2+}	0.86	0.62	0.41	2.15	0.68	0.40

Negative reflection coefficients were obtained for Cl^- with HYDRACoRe 10. This could be due to negative rejection of Cl^-. However, during experiments with HYDRACoRe10, negative rejections were not observed. This could be mainly due to the fact that the experiments were performed at operating pressures between 9 and 18 bar and negative rejection is generally observed at lower pressures and rejection becomes positive with increasing pressure [72, 73, 74].

The estimated r_p values confirm that the effective pore size was lowest for NANO-SW and HYDRACoRe10 had the largest pore size. Hence, the pore size of the tested membranes was in the sequence HYDRACoRe10 > ESNA > HYDRACoRe 50 > NF 270 > SR 90 > NANO-SW. This order is valid when Cl^-, Ca^{2+} and Mg^{2+} effective pore radius of each ion is compared for six membranes. While comparing the r_p values for Na^+, results were slightly different; HYDRACoRe50 was tighter than NF 270. The r_p values for SO_4^{2-} cannot be compared due to several mechanisms affecting the ion. SO_4^{2-} is a divalent anion and will

be rejected by the negatively charged membrane though the hydration energy of SO_4^{2-} is low (-1145 KJ/mol).

Ten model correlations were developed using results from four polyamide NF membranes as discussed in **Paper IV**, which could determine the rejection, reflection coefficient and solute permeability of individual ions in seawater. The four membranes chosen were ESNA, NF 270, SR 90, and NANO-SW.

The pure water permeability chosen for the model is in the range required for smart water production. The only variables required for this model is the pure water permeability and membrane flux with seawater as feed.

Figure 30 shows the pure water permeability of polyamide membranes versus σ and P_s of chloride for four NF membranes mentioned earlier.

The pure water permeability of polyamide membranes versus σ and P_s for sodium, calcium and magnesium ions for four NF membranes are presented in **Paper IV**.

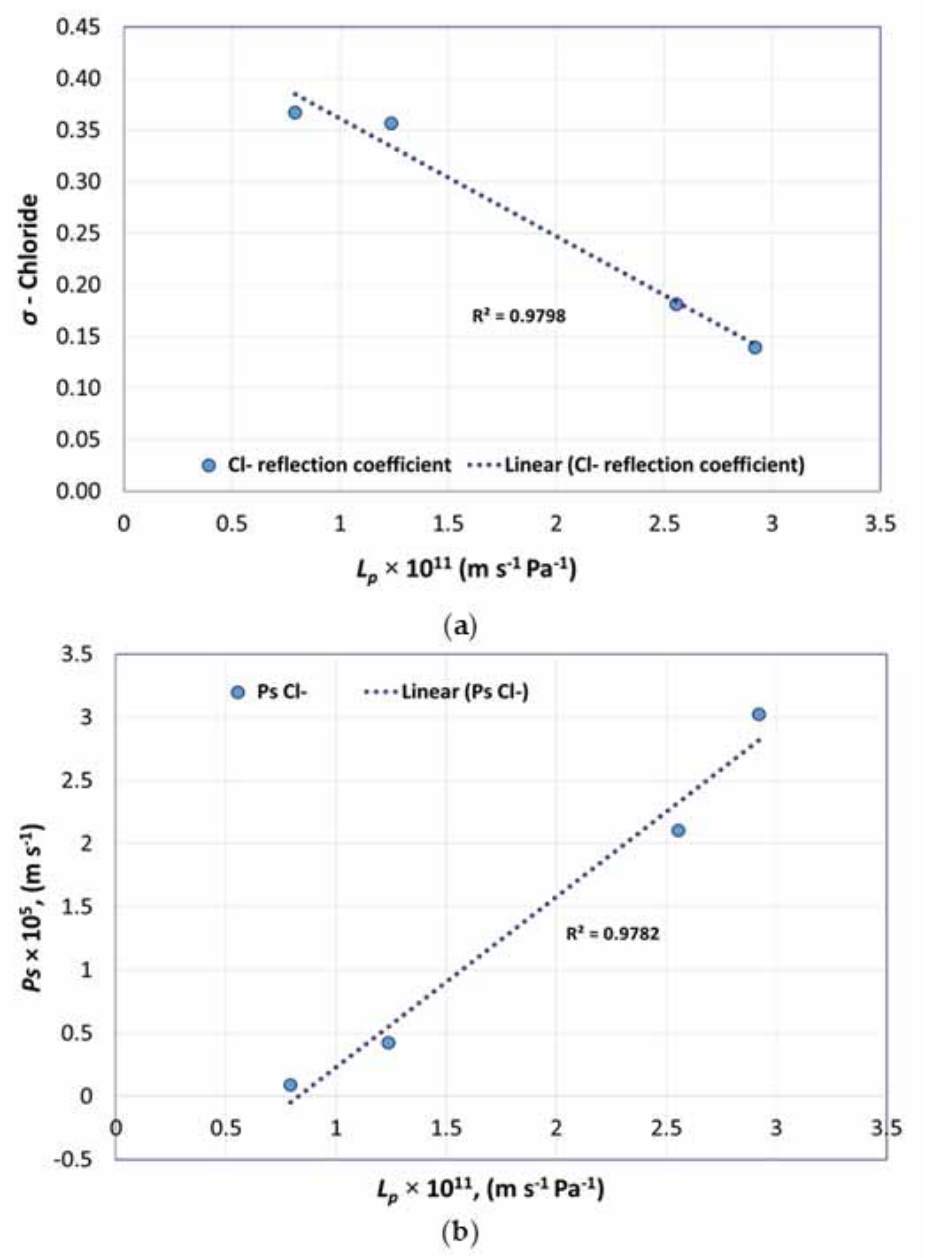

Figure 30. Pure water permeability versus (a) reflection coefficient (b) solute permeability of chloride

Figure 30 (a) shows that with an increase in water permeability, the reflection coefficient of ions decreased whereas Figure 30 (b) shows that the solute permeability increased. This confirms that when the effective membrane pore radius increases, permeability increases, resulting in low ion rejection.

A close correlation between the model and experimental values of σ, P_s, and rejection of ions were obtained. The correlations are valid if the feed is seawater with no change in viscosity and ionic concentration for all four tested polyamide membranes. Equations 26 – 35 determines σ and P_s of each ion with a given pure water permeability L_{p0}.

$$\sigma_{Cl^-} = -1 \times 10^{10} \times L_{p0} + 0.4749 \quad (26)$$

$$\sigma_{Na^+} = -6 \times 10^{9} \times L_{p0} + 0.3318 \quad (27)$$

$$\sigma_{SO_4^{2-}} = -1 \times 10^{10} \times L_{p0} + 1.118 \quad (28)$$

$$\sigma_{Ca^{2+}} = -3 \times 10^{10} \times L_{p0} + 1.1354 \quad (29)$$

$$\sigma_{Mg^{2+}} = -3 \times 10^{10} \times L_{p0} + 1.2559 \quad (30)$$

$$P_{s_{Cl^-}} = 1 \times 10^{11} \times L_{p0} - 1.1144 \quad (31)$$

$$P_{s_{Na^+}} = 6 \times 10^{10} \times L_{p0} - 0.0147 \quad (32)$$

$$P_{s_{SO_4^{2-}}} = 4 \times 10^{31} \times {L_{p0}}^{3.0496} \quad (33)$$

$$P_{s_{Ca^{2+}}} = 1 \times 10^{11} \times L_{p0} - 0.7388 \quad (34)$$

$$P_{s_{Mg^{2+}}} = 9 \times 10^{30} \times {L_{p0}}^{2.9414} \quad (35)$$

The correlations can be used for calculating σ and P_s of polyamide membranes with a pore size between 0.4 to 0.86 nm and with pure water permeabilities between 5×10^{-12} to 3×10^{-11} m/s/Pa.

The estimated values of transport parameters can be used to calculate the rejection of ions for a particular polyamide NF membrane when seawater is used as feed.

5.8 Power Consumption Analysis

A power consumption analysis of membrane performance for smart water production from seawater and de-oiled PW for both carbonate and sandstone reservoirs were performed to validate the fourth hypothesis.

5.8.1 Power Consumption Analysis with Seawater as Feed

The retentate from NF membrane is rich in divalent ions and suitable for smart water for carbonates. NF and RO in parallel are suitable for smart water production for sandstones. The experiments were conducted at room temperature with an assumed pump efficiency of 80 %. The NF and RO membranes for smart water production with seawater as feed operated at 16 bar and 55 bar, respectively. Experimental results are directly available for full-scale applications. Normal seawater was feed to commercially available NF membranes with a surface area of 2.3 -2.6 m^2.

Pre-filtered seawater at 1 m^3/h was used as feed in crossflow NF membranes, which resulted in two streams with different ionic compositions. The permeate is rich in monovalent ions (TDS 20,800 - 21,000 mg/L) suitable for sandstones after dilution, whereas the retentate is rich in divalent ions such as SO_4^{2-}, Ca^{2+}, and Mg^{2+} and therefore suitable for carbonates. TDS in retentate depends on pore size and charge of the chosen NF membrane, applied pressure, and temperature.

Smart water for sandstone reservoirs should be low in divalent ions with TDS less than 5,000 mg/L. TDS in NF permeate with seawater as feed is 21,000 mg/L and should be diluted with low TDS water for sandstone applications. Thus, an RO membrane is recommended to be used in parallel to dilute the smart water stream. RO retentate, rich in both divalent and monovalent ions is recirculated to the feed tank.

Total power consumed is calculated using Equation 36.

$$Power(W) = \frac{Feed\ flow\ rate\left(\frac{m^3}{s}\right) \times Feed\ pressure\ (Pa)}{Efficiency\ \eta\ (\%)} \qquad (36)$$

Power consumed for smart water production in sandstones is higher than smart water in carbonates due to higher operating pressure for RO when compared with NF. With an energy recovery factor of 50 % for RO, 50 % of the required energy for the feed pump is recovered from the retentate stream. The RO membrane used for power consumption calculations assumed 8 % permeate recovery i.e., the ratio of permeate flow rate to feed flow rate. The RO permeate flow rate can be increased by selecting an alternative RO membrane with higher recovery.

Figure 31 presents a schematic for smart water production in carbonate and sandstone reservoirs showing flow rates and TDS concentrations. Power consumed per cubic meter of smart water produced for carbonates was 0.70 kWh/m^3 and 5.21 kWh/m^3 for sandstones using seawater as feed. The results are discussed in **Paper I**.

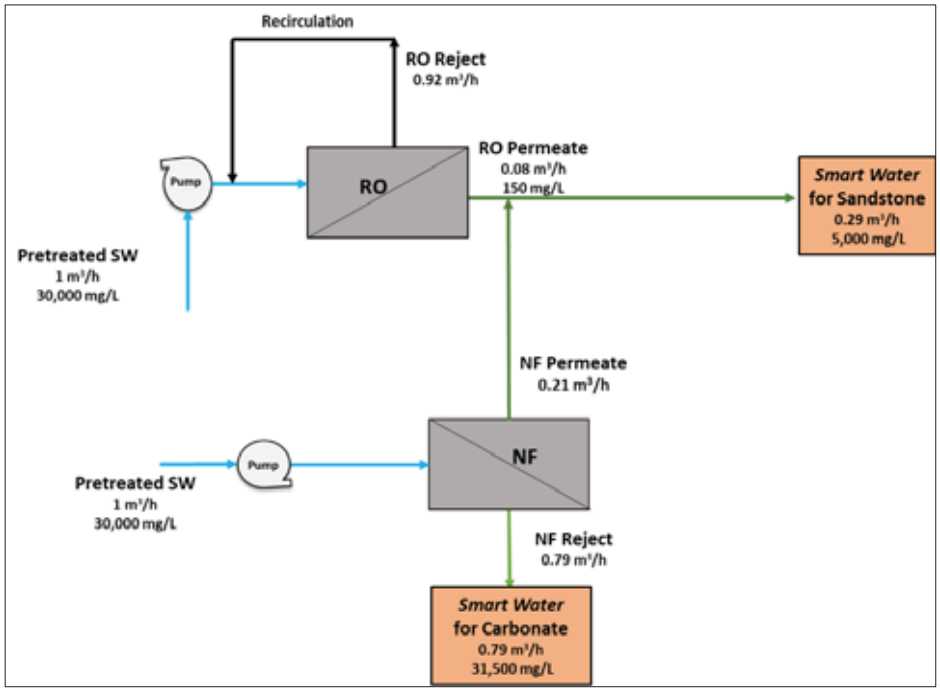

Figure 31. Schematic for smart water production from seawater

5.8.2 Power Consumption Analysis with PW as Feed

Reuse of PW for smart water production is salinity dependant. PW with TDS of 90,000 mg/L was assumed in this research for calculations. A TDS of 90,000 mg/L must be diluted before used as feed for NF. Feed pressures of 9 bar and 55 bar were used for NF and RO membranes, respectively. A diluted PW feed of 40,000 mg/L was used for power calculations. Utilizing retentate as smart water for carbonates has a benefit in reducing concentrate disposal issues.

The power consumption calculations for reusing PW in carbonates and the reason for selecting NF membranes for diluting the high TDS of PW is examined in **Paper II**. The comparison was performed with four different options for producing low TDS water. The options were fresh water from land, NF permeate, RO permeate and distillation.

Figure 32 shows a model for smart water production from PW for both sandstone and carbonate reservoirs. The model presents calculations for a single NF and RO unit. To achieve the required smart water flow rate for injection, multiple membrane stages should be used.

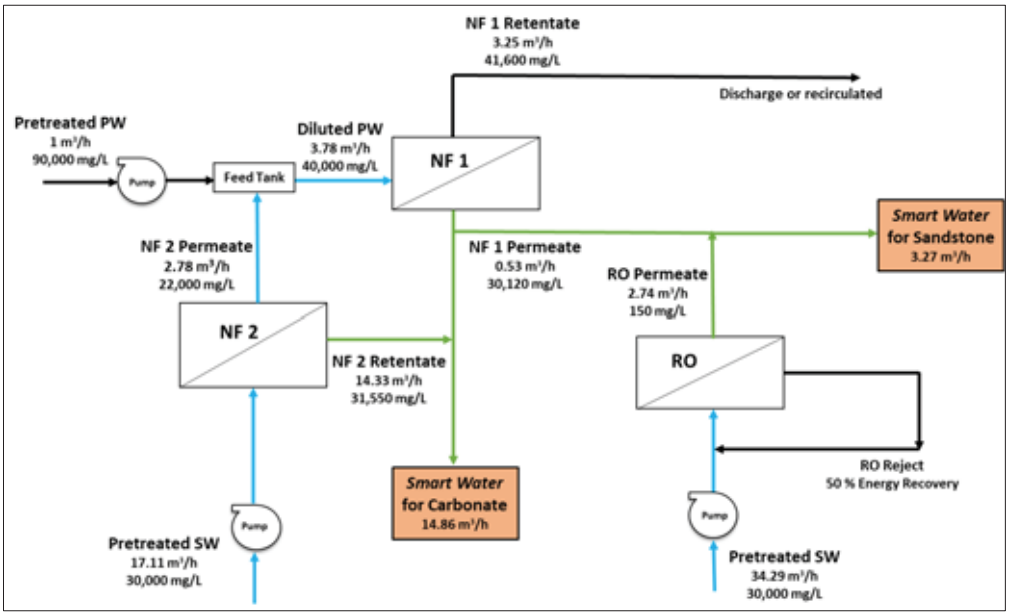

Figure 32. Schematic for smart water production from PW for carbonate and sandstone reservoirs

Smart water TDS of 5,000 mg/L for sandstone reservoirs is produced from permeate from NF and mixed with permeate from RO with seawater as feed. The energy consumption of RO is directly proportional to ion concentrations due to changes in osmotic pressure. This increases the total power consumption for smart water production for sandstone compared to carbonate reservoirs. An energy recovery factor of 50 % was applied to the RO process.

The power consumed for carbonate reservoirs with PW as feed is calculated to 0.88 kWh/m^3 whereas the total power consumed calculated for an NF and RO membrane in parallel for smart water production in

sandstone reservoirs from PW feed is 13.99 kWh/m^3. The power consumed could be lower if the initial TDS of PW is in the range of 40,000 mg/L instead of an initial TDS of 90,000 mg/L. Likewise, increased permeate flow rate could also reduce power consumption. This is possible by selecting NF membranes yielding higher flow rates and with appropriate ion separation efficiency. From the proposed model, it is evident that most of the power is consumed for dilution of feed. Nevertheless, comparing with other desalination techniques, this option is most cost-efficient. One main challenge in PW reuse by membranes is the degree of fouling. Fouling affects the frequency of cleaning and therefore process cost.

The disposal of NF1 retentate is another concern. The retentate is diluted from 90,000 mg/ L to approximately 41,600 mg/L and has an ionic composition similar to seawater. This de-oiled retentate can either be discharged to sea, recirculated to feed tank or reused for pressure support in oil reservoirs.

However, TDS varies with the type of PW. If increased water is produced after secondary injection, PW will nearly have equal concentration to that of injected seawater and makes PW reuse feasible. However, if more concentrated PW is produced, PWRI after required treatment to sub-surface is practicable.

6 Concluding Remarks

This research concluded that smart water for EOR in carbonate and sandstone reservoirs can be produced from seawater and PW by nanofiltration membranes. The ease of operation, lower energy consumption, and small amounts of chemical additives make it attractive and considered environmentally friendly and sustainable.

6.1 Conclusions

With reference to the four hypotheses proposed for the research, the following conclusions are derived.

1. Membranes are practical and feasible from an economic and environmental point of view for smart water production from seawater and de-oiled produced water for both carbonate and sandstone reservoirs. The hypothesis is validated with results presented in **Paper I and Paper II** and is valid under the following conditions:
    - NF membrane experiments with prefiltered seawater with TDS ranging from 30,000 to 34,500 ppm operated at 25 °C with a transmembrane pressure between 9 and 18 bar can produce required smart water for both carbonate and sandstone reservoirs. RO permeate should be added to NF permeate to meet low salinity requirements for sandstones.
    - For PW with TDS above 40,000 ppm, dilution with low TDS water is required for producing smart water using NF membranes.

    2. NF membranes can handle PW with traces of oil and varying pH during smart water production. This hypothesis is validated with results presented in **Paper II** and **Paper III**. No membrane fouling was observed during short term experiments with feed

containing traces of oil. However, fouling can be initiated during long term performance.

PW with feed containing varying pH showed variations in flux and ion rejection. The results confirmed the application of NF membranes for PW treatment confirming hypothesis 1 and 2.

3. A predictive model for selection of NF membranes for smart water production with a minimum number of variables is presented. Correlations were developed to determine the reflection coefficient and solute permeability of individual ions through polyamide NF membranes with a pure water permeability between 5×10^{-12} to 3×10^{-11} m s^{-1} Pa^{-1} validating hypothesis 3.

A power consumption analysis is performed when seawater and de-oiled PW was used as membrane feed for both carbonate and sandstone reservoirs. It was confirmed that membranes can produce economically feasible smart water, thus validating hypothesis 4.

The following key findings were obtained during this research.

1) Flux and ion retention increased with an increase in applied pressure indicating no fouling of membranes during the experiments.
2) Experiments confirm that membrane pore size and charge are the main factors determining ion rejection.
3) Negative rejection of monovalent ions (Na^{+}) was observed when the concentration of divalent ions (Mg^{2+}) was increased in the feed to maintain charge electroneutrality. This phenomenon was observed only at lower pressures and the rejection values changed to positive with an increase in pressure.
4) Retentate produced at 12 bar had an overall TDS of 30,000 mg/L with a flow rate of 1050 L/h. The NF retentate with seawater as feed is used for carbonates and thus eliminates concentrate

disposal issues compared to alternative desalination technologies such as distillation and reverse osmosis.

5) The NF permeate is used as smart water for sandstones. At 12 bar, NF permeate had a flow rate of 90 L/h with an overall TDS of 21,000 mg/L at pH 8. For sandstones, low salinity is required and should be mixed with low TDS water.
6) Increased divalent ion concentrations for carbonates resulted from spiking chemicals to NF membrane feed. Results confirmed that adding divalent ions in the feed is more beneficial than adding it in retentate.
7) No fouling was initiated during short-term membrane separation with synthetic PW with traces of organic compounds. Sr^{2+} and Ba^{2+} concentrations were efficiently reduced, which could prevent scaling when PW was used as membrane feed.
8) Experiments with three different membranes (ESNA 2540, NF 270 2540 and HYDRACoRe50 2540) with varying feed pH confirmed the occurrence of protonation and deprotonation of membrane functional groups, which lead to pore expansion resulting in increased flux. At very low pH, pore shrinkage occurred resulting in decreased flux.
9) Variations in pore sizes with pH with respect to Mg^{2+} was calculated using Spiegler-Kedem and SHP models. The results confirmed that the pore radius r_p of ESNA decreased from 0.87 nm to 0.42 nm and for NF 270, r_p decreased from 0.5 to 0.37 nm. For HYDRACoRe, r_p decreased from 0.8 to 0.7 nm.
10) Flux was higher at basic pH values. Highest flux was observed for ESNA indicating a larger pore size than NF 270 and HYDRACoRe. Maximum flux was observed at pH 8 for all three membranes confirming that the membranes work best at seawater pH. A sharp decrease in Mg^{2+} rejection was observed at basic pH for ESNA and NF 270. The values changed from 98 % at pH 2.5 to 56 % at pH 10.2 for NF 270.

11) A feed-forward back propagation ANN model for predicting ion rejection was implemented. The model quantitatively predicted rejection of ions without using any membrane properties such as pore radius, membrane charged density or effective membrane thickness. The model considers the effect of varying feed pH and increasing operating pressure for different flux on ion rejection. An overall agreement was obtained for ANN predictions and experimental results for all the three tested NF membranes.
12) It was confirmed that proper selection of input variables and number of neurons with a set of training data help to optimize the ANN prediction of membrane performance. An ANN network with seven neurons in the hidden layer with a tansig transfer function was most suitable for predicting ion rejections in this research. A relatively low mean square error in the range of 0.00011 to 0.00393 for individual ion rejections were calculated.
13) It was confirmed that membrane properties can be manipulated by changing feed pH during smart water production for modifying flux and ion rejection to either type of reservoirs.
14) Smart water production by nanofiltration has two concerns:
    - For smart water with seawater as feed in carbonates, along with high concentrations of divalent ions in the retentate, monovalent ions are also present due to counterion effects.
    - For both reservoirs, approximately 14 % of PW could be reused as smart water due to low membrane recovery from high PW feed TDS (90,000 mg/L). Nevertheless, if more concentrated PW should be treated (TDS higher than 90,000 mg/L), sub-surface PWRI with required pre-treatment is practicable.
15) A power consumption analysis is proposed, along with a schematic for smart water production, with flow rates and compositions for each stream. This provides the end-users a choice of membrane configurations for industrial use.

16) Smart water production in carbonates with seawater as feed showed a power consumption of 0.70 kWh/m^3. For sandstones, the power consumed is higher at 5.21 kWh/m^3. This is due to a combination of NF and RO membranes used to dilute NF permeate to TDS < 5,000 mg/L.
17) The total power consumed by two NF membranes in parallel for smart water production in carbonates from PW feed is calculated to 0.88 kWh/m^3.
18) The total power consumed by NF and RO membranes in parallel for smart water production in sandstones from PW feed is calculated to 13.99 kWh/m^3.
19) The membrane transport parameters, reflection coefficient and solute permeability were determined by fitting Spiegler- Kedem model using flux and rejection values obtained from experiments with six NF membranes. The pore radii of these membranes were estimated with charged ions using a steric hindrance pore model.
20) The pore radii of membranes were estimated from 0.4 nm to 2.15 nm and the experiments concluded that the membranes had a pore size distribution rather than a single pore radius.
21) Correlations were developed to determine reflection coefficient and solute permeability of ions for polyamide NF membranes to predict ion rejection. The proposed correlations predict rejection, reflection coefficient and solute permeability with close accuracy. The main advantage of these correlations is that they require a few input data that can be easily obtained from simple experiments.
22) The correlations obtained can be used for determining reflection coefficient and solute permeability of polyamide membranes between 5×10^{-12} to 3×10^{-11} m s^{-1} Pa^{-1}, which include membranes with a pore size of 0.4 to 0.86 nm.
23) A sharp change in transport parameters of sulfate was observed when plotted against pure water permeabilities of polyamide membranes. Hence, choosing an NF membrane for smart water

production in carbonates requires much attention when having pure water permeabilities above 2.6×10^{-11} m s^{-1} Pa^{-1} where the SO_4^{2-} rejection will be low.

Membranes are a mature technology in water and wastewater treatment. In the oil and gas industry, however, membrane experience is more limited. Current research is important since it aims at optimizing offshore wastewater management by reusing PW with minimum environmental impact.

The research knowledge, obtained from the experiments and the developed predictive model, confirms that membranes can be used for smart water production from seawater and produced water, thus validating the main objective of the thesis.

6.2 Future Work

- All research activities dealing with smart water production by membranes have been covered in this research. The next required stage is testing the produced brines in the respective cores to evaluate the extent of oil recovery. Further process improvements should be made after core testing.
- The fate of production chemicals present in PW was not included in this research but has to be verified. Experiments analyzing the type of chemicals permeating through NF should be identified for reuse.

References

[1] IEA, "World Energy Outlook," 2017.

[2] E. Donaldson, G. Chilingarian and T. Yen, Enhanced oil recovery, II processes and operations, Elsevier, 1989.

[3] D. Green and G. Willhite, "¨Enhanced Oil Recovery¨ SPE Textbook Series Vol.6," 1998.

[4] F. Craig, The reservoir engineering aspects of waterflooding, H.L.Doherty Memorial Fund of AIME, 1971.

[5] M. Jaafar, N. Mohd and M. Hamid, "Measurement of isoelectric point of sandstone and carbonate rock for monitoring water encroachment," *Journal of Applied Sciences,* no. 14, pp. 3349-3353, 2014.

[6] W. Anderson, "Wettability literature survey- part 2," *Journal of Petroleum Technology,* pp. 1246-1262, 1986.

[7] J. Buckley, "Effective wettability of minerals exposed to crude oil," *Current Opinion in Colloid and Interface Science,* pp. 191-196, 2001.

[8] K. Lee and J. Neff, Produced Water- Environmental risks and advances in mitigation technologies, Springer Science + Business Media, 2011.

[9] F.-R. Ahmadun, A. Pendashteh, L. C. Abdullah, D. R. A. Biak, S. S. Madaeni and Z. Z. Abidin, “Review of technologies for oil and

gas produced water treatment," *Journal of Hazardous Materials,* no. 170, pp. 530-551, 2009.

[10] S. Munirasu, M. A. Haija and F. Banat, "Use of membrane technology for oil field and refinery produced water treatment- A review," *Process Safety and Environmental Protection,* 2016.

[11] Environmental Report, "Environmental Report- Environmental work by the Oil and Gas Industry," Norsk Olje and Gass, 2016.

[12] M. Cheryan, Ultrafiltration and Microfiltration Handbook, CRC Press:Boca Raton, FL, 1998.

[13] M. Mulder, Basic principles of membrane technology, Kluwer Academic Publishers, 1996.

[14] M. Nilsson, G. Tragårdh and K. Ostergren, "The influence of pH, salt and temperature on nanofiltration performance," *Journal of Membrane Science,* pp. 97-106, 2008.

[15] A. Al-Karaghouli and L. Kazmerski, "Energy consumption and water production cost of conventional and renewable - energy - powered desalination processes," *Renewable Sustainable Energy Rev.,* pp. 343-356, 2013.

[16] L. W. Jye and A. F. Ismail, Nanofiltration membranes: Synthesis, Characterization and Applications, CRC Press, Taylor and Francis Group, 2017.

[17] A. Pérez- González, A. Urtiaga, R. Ibáñez and I. Ortiz, "State of the art and review on the treatment technologies of water reverse osmosis concentrates," *Water Research,* 2012.

[18] S. Strand, E. Høgnesen and T. Austad, "Wettability alteration of carbonates- Effects of potential determining ions (Ca2+ and SO42-) and temperature," *Colloids and Surfaces A: Physiochem. Eng. Aspects,,* pp. 1-10, 2006.

[19] T. Austad, "Water-based EOR in carbonate and sandstone: New chemical understanding of the EOR- potential using ¨Smart water¨.," in *Enhanced Oil Recovery Field Case Studies*, Sheng. J, Gulf Professional Publishing: Houston, TX, 2013, pp. 301-335.

[20] T. Austad, A. Rezaeidoust and T. Puntervold, "Chemical mechanism of low salinity water flooding in sandstone reservoirs," *SPE 129767,* 2010.

[21] I. D. Torrijos, T. Puntervold, S. Strand, T. Austad, H. I. Abdullah and K. Olsen, "Experimental study of the response time of the low - salinity enhanced oil recovery during secondary and tertiary low salinity waterflooding," *Energy and Fuels,* no. 30, pp. 4733-4739, 2016.

[22] I. D. P. Torrijos, Enhanced oil recovery from sandstone and carbonates with ¨ Smart Water¨, ISBN: 978-82-7644-708-8: Unversity of Stavanger, 2017.

[23] G. Tang and N. Morrow, "Salinity, temperature, oil composition, and oil recovery by waterflooding," *SPE Reservoir Engineering,* no. 12(4), pp. 269-276, 1997.

[24] N. Morrow and J. Buckley, "Improved oil recovery by low-salinity waterflooding," *Journal of Petroleum Technology,* no. 63(5), 2011.

[25] G. Jerauld, K. Webb, C. Lin and J. Seccombe, "Modelling low-salinity waterflooding, SPE 102239," *SPE Annual Technical*

Conference and Exhibition, San Antonio, Texas, 24-27 September, 2006.

[26] Y. Zhang and N. Morrow, "Comparison of secondary and tertiary recovery with change in injection brine composition for crude oil/sandstone combinations," *SPE 99757 presented at the SPE/DOE Symposium on Improved Oil recovery,* 2006.

[27] I. D. P. Torrijos, T. Puntervold, S. Strand and A. Rezaeidoust, "Optimizing the low salinity water for EOR effects in sandstone reservoirs- Composition vs salinity," in *78th EAGE Conference and Exhibition*, 2016.

[28] S. Fathi, T. Austad and S. Strand, "Water-based enhanced oil recovery (EOR) by ¨Smart Water¨: Optimal ionic composition for EOR in carbonates," *Energy and Fuels,* pp. 5173-5179, 2011.

[29] T. Puntervold, S. Strand, R. Ellouz and T. Austad, "Modified seawater as a smart water fluid in chalk," *Journal of Petroleum Science and Engineering,* no. 133, pp. 440-443, 2015.

[30] P. Zhang and T. Austad, "Wettability and oil recovery from carbonates: Effects of temperature and potential determining ions," *Colloids and Surfaces A: Physiochem and Eng. Aspects,* no. 279, pp. 179-187, 2006.

[31] P. Zhang, M. T. Tweheyo and T. Austad, "Wettability alteration and improved oil recovery by spontaneous imbibition of seawater into chalk: Impact of the potential determining ions Ca2+, Mg2+, and SO42-," *Colloids and Surfaces A. Physicochem. Eng. Aspects,* no. 301, p. 199.208, 2007.

[32] S. Fathi, T. Austad and S. Strand, "Water-based enhanced oil recovery (EOR) by ¨Smart Water¨ in carbonate reservoirs," *SPE*

154570 presented at the SPE EOR Conference at Oil and Gas West Asia, Muscat, Oman, 16-18 August, 2012.

[33] R. W. Baker, Membrane Technology and Applications, John Wiley & Sons, Ltd, 2004.

[34] X.-L. Wang, T. Tsuru, M. Togoh, S.-I. Nakao and S. Kimura, "Evaluation of pore structure and electrical properties of nanofiltration membranes," *Journal of Chemical Engineering of Japan,* 1994.

[35] S. Bandini, J. Drei and D. Vezzani, "The role of pH and concentration on the ion ejection in polyamide nanofiltration membranes," *Journal of Membrane Science,* no. 264, pp. 65-74, 2005.

[36] J. Luo and W. Yinhua, "Effect of pH and salt on nanofiltration- A critical review," *Journal of Membrane Science,* no. 438, pp. 18-28, 2013.

[37] J.-J. Qin, M. H. Oo, H. Lee and B. Coniglio, "Effect of feed pH on permeate pH and ion rejection under acidic conditions in NF process," *Journal of Membrane Science,* no. 232, pp. 153-159, 2004.

[38] J. Luo, L. Ding, Y. Su, ShaopingWei and Y. Wan, "Concentration polarization in concentrated saline solution during desalination of iron dextran by nanofiltration," *Journal of Membrane Science,* no. 363, pp. 170-179, 2010.

[39] A. Siddiqui, S. Lehmann, V. Haaksman, J. Ogier, C. Schellenberg, M. van Loosdrecht, J. Kruithof and J. Vrouwenvelder, "Porosity of spacer-filled channels in spiral - wound membrane systems:

Quantification methods and impact on hydraulic characterization," *Water Research,* no. 119, pp. 304-311, 2017.

[40] N. Hilal, H. Al-Zoubi, N. Darwish, A. Mohammad and M. Abu Arabi, "A comprehensive review of nanofiltration membranes: Treatment, pretreatment, modeling, and atomic force microscopy," *Desalination,* no. 170, pp. 281-308, 2004.

[41] R. Epsztein, E. Shaulsky, N. Dizge, D. M. Warsinger and M. Elimelech, "Role of ionic charge density in Donnan exclusion of monovalent anions by nanofiltration," *Environmental Science and Technology,* pp. 4108-4116, 2018.

[42] W. Bowen, A. Mohammad and N. Hilal, "Characterisation of nanofiltration membranes for predictive purposes/use of salts, uncharged solutes and atomic force microscopy," *Journal of Membrane Science,* no. 126, pp. 91-105, 1997.

[43] F. Donnan, "Theory of membrane equilbria and membrane potentials in the presence of non-dialysing electrolytes. A contribution to physical,chemical physiology," *Journal of Membrane Science,* no. 100, pp. 45-55, 1995.

[44] A. E. Childress and M. Elimelech, "Effect of solution chemistry on the surface charge of polymeric reverse osmosis and nanofiltration membranes," *Journal of Membrane Science,* no. 119, pp. 253-268, 1996.

[45] A. E. Childress and M. Elimelech, "Relating nanofiltration membrane performance to membrane charge (electrokinetic) characteristics," *Environmental Science and Technology,* no. 34, pp. 3710-3716, 2000.

[46] A. E. Yaroshchuk, "Dielectric exclusion of ions from membranes," *Advances in Colloid and Interface Science,* no. 85, pp. 193-230, 2000.

[47] S. Bandini and D. Vezzani, "Nanofiltration modeling: The role of dielectric exclusion in membrane characterization," *Chemical Engineering Science,* no. 58, pp. 3303-3326, 2003.

[48] L. A. Richards, B. S. Richards, B. Corry and A. I. Schafer, "Experimental energy barriers to anions transporting through nanofiltration membranes," *Environmental Science & Technology,* no. 47, pp. 1968-1976, 2013.

[49] B. Tansel, "Significance of thermodynamic and physical characteristics on permeation of ions during membrane separation: Hydrated radius, hydration free energy and viscous effects," *Separation and Purification Technology,* no. 86, pp. 119-126, 2012.

[50] K. Spiegler and K. O., "Thermodynamics of hyperfiltration (reverse osmosis): Criteria for efficient membranes," *Desalination,* vol. 1, pp. 311-326, 1966.

[51] O. Kedem and A. Katchalsky, "Thermodynamical analysis of the permeability of biological membranes to non-electrolytes," *Biochimica et Biophysica Acta,* pp. 229-246, 1958.

[52] C. K. Diwara, S. Lo, M. Rumeau, M. Pontie' and O. Sarr, "A phenomenological mass transfer approach in nanofiltration of halide ions for a selective defluorination of brackish drinking water," *Journal of Membrane Science,* pp. 103-112, 2003.

[53] S. Jain and S. K. Gupta, "Analysis of modified surface force pore model with concentration polarization and comparison with

Spiegler-Kedem model in reverse osmosis systems," *Journal of Membrane Science,* no. 232, pp. 45-61, 2004.

[54] Z. Murthy and S. Gupta, "Estimation of mass transfer coefficient using a combined nonlinear membrane transport and film theory model," *Desalination,* no. 121, pp. 131-137, 1997.

[55] S.-I. Nakao and S. Kimura, "Models of membrane transport phenomena and their applications for ultrafiltration data," *Journal of Chemical Engineering of Japan,* 1982.

[56] R. Bowen and W. Mohammad, "Diafiltration by nanofiltration: Prediction and optimization," *AIChE Journal,* no. 44, pp. 1799-1812, 1998.

[57] A. Hussain, S. Nataraj, M. Abashar, I. Al-Mutaz and T. Aminabhavi, "Prediction of physical properties of nanofiltration membranes using experiment and theoretical models," *Journal of Membrane Science,* pp. 321-336, 2008.

[58] O. Labban, C. Liu, T. H. Chong and J. H. Lienhad, "Fundamentals of low - pressure nanofiltration: Membrane characterization, modeling, and understanding the multi-ionic interactions in water softening," *Journal of Membrane Science,* no. 521, pp. 18-32, 2017.

[59] M. H. Beale, M. T. Hagen and H. Demuth, Neural Networks Toolbox (TM)- Users Guide, The MathWorks, Inc., 2018.

[60] AWWA M46, "Manual of water supply practices- Reverse Osmosis and Nanofiltration," 1999.

[61] Filmtec Membranes, "Dow water solutions- Filmtec membranes product catalogue," [Online]. Available: www.lenntec.com.

[62] N. Hydranautics, "Product information catalogue," [Online]. Available: www.membranes.com.

[63] R. R. Nair, E. Protasova, S. Strand and T. Bilstad, "Membrane performance analysis for smart water production for enhanced oil recovery in carbonate and sandstone reservoirs," *Energy & Fuels,* pp. 4988-4995, 2018.

[64] ASTM D7678-17, "Standard test method for total oil and grease (TOG) and total petroleum hydrocarbons (TPH) in water and wastewater with solvent extraction using mid-air laser spectroscopy," ASTM International, 2017.

[65] J. Schaep and C. Vandecasteele, "Evaluating the charge of nanofiltration membranes," *Journal of Membrane Science,* no. 151, pp. 123-129, 2001.

[66] J. Tanninen, M. Mänttäri and M. Nyström, "Effect of salt mixture on fractionation with NF membranes," *Journal of Membrane Science,* no. 283, pp. 57-64, 2006.

[67] X.-L. Wang, W.-N. Wang and D.-X. Wang, "Experimental investigation on separation performance of nanofiltration membranes for inorganic electrolyte solutions," *Desalination,* pp. 115-122, 2002.

[68] C. Labbez, P. Fievet, A. Vidonne, A. Foissy and J. Pagetti, "Retention of mineral salts by a polyamide nanofiltration membrane," *Separation and Purification Technology,* pp. 47-55, 2003.

[69] G. Hill and J. Holman, Chemistry in Context, Laboratory Manual, 2001.

[70] M. I. Chaudhari and S. B. Rempe, "Strontium and barium in aqueous solution and a potassium channel binding site," *The Journal of Chemical Physics,* no. 148, 2018.

[71] G. Hagmeyer and R. Gimbel, "Modeling the rejection of nanofiltration membranes using zeta potential measurements," *Separation and Purification Technology,* vol. 15, pp. 19-30, 1999.

[72] A. Yaroshchuk, "Negative rejection of ions in pressure - driven membrane processes," *Advanced Colloid Interface Science,* pp. 150-173, 2008.

[73] J. Gilron, N. Gara and O. Kedem, "Experimental analysis of negative salt rejection in nanofiltration membranes," *Journal of Membrane Science,* no. 185, pp. 223-236, 2001.

[74] X. Xu and H. Spenser, "Dye-salt separations by nanofiltration using weak acid polyelectrolyte membranes," *Desalination,* no. 129, 1997.

Appendices

Appendix 1 – Paper I

Paper I

Membrane Performance Analysis for Smart Water Production for Enhanced Oil Recovery in Carbonate and Sandstone Reservoirs

Remya Ravindran Nair, Evgenia Protasova, Skule Strand, Torleiv Bilstad

Energy & Fuels, 2018, 32 (4), pp 4988-4995

DOI: 10.1021/acs.energyfuels.8b00447

Appendix 2 – Paper II

Paper II

Evaluation of Nanofiltration Membrane Process for Smart Water Production in Carbonate Reservoirs from Deoiled Produced Water and Seawater

Remya Ravindran Nair, Evgenia Protasova, Skule Strand, Torleiv Bilstad

SPE Productions and Operations (In press)

Available online at https://doi.org/10.2118/181588-PA

Appendix 3 – Paper III

Paper III

Effect of pH on Produced Water Treatment Using Nanofiltration Membranes: Artificial Neural Network for Performance Assessment and Steric Hindrance Pore Model for Flux Variation Evaluation

Remya Ravindran Nair, Evgenia Protasova, Skule Strand, Torleiv Bilstad

Desalination and Water Treatment (In press)

Appendix 4 – Paper IV

Paper IV

Implementation of Spiegler - Kedem and Steric Hindrance Pore Models for Analyzing Nanofiltration Membrane Performance for Smart Water Production

Remya Ravindran Nair, Evgenia Protasova, Skule Strand, Torleiv Bilstad

Membranes, 2018, 8 (3), 78

DOI:org/10.3390/membranes8030078

membranes

MDPI

Article

Implementation of Spiegler–Kedem and Steric Hindrance Pore Models for Analyzing Nanofiltration Membrane Performance for Smart Water Production

Remya R. Nair [1,*], Evgenia Protasova [1], Skule Strand [2] and Torleiv Bilstad [1]

[1] Department of Chemistry, Bioscience and Environmental Engineering, University of Stavanger, Kjell Arholmsgate 41, 4036 Stavanger, Norway; evgy.pro@gmail.com (E.P.); torleiv.bilstad@uis.no (T.B.)
[2] Department of Energy and Petroleum Engineering, University of Stavanger, Kjell Arholmsgate 41, 4036 Stavanger, Norway; skule.strand@uis.no
* Correspondence: remya.nair@uis.no

Received: 8 August 2018; Accepted: 31 August 2018; Published: 6 September 2018

Abstract: A predictive model correlating the parameters in the mass transfer-based model Spiegler–Kedem to the pure water permeability is presented in this research, which helps to select porous polyamide membranes for enhanced oil recovery (EOR) applications. Using the experimentally obtained values of flux and rejection, the reflection coefficient σ and solute permeability P_s have been estimated as the mass transfer-based model parameters for individual ions in seawater. The reflection coefficient and solute permeability determined were correlated with the pure water permeability of a membrane, which is related to the structural parameters of a membrane. The novelty of this research is the development of a model that consolidates the various complex mechanisms in the mass transfer of ions through the membrane to an empirical correlation for a given feed concentration and membrane type. These correlations were later used to predict ion rejections of any polyamide membrane with a known pure water permeability and flux with seawater as a feed that aids in the selection of suitable nanofiltration (NF) for smart water production.

Keywords: nanofiltration; Spiegler–Kedem model; steric hindrance pore model; ion rejection; reflection coefficient; solute permeability; pure water permeability

1. Introduction

Nanofiltration (NF) membranes are pressure driven and selectively separate ions from mixed electrolyte solutes with low energy requirements compared to other desalination technologies. Smart water can be produced by modifying the ionic composition of seawater [1]. Smart water for EOR in carbonate and sandstone reservoirs require different ionic compositions depending on reservoir properties. Divalent ion-rich brine is required for carbonates, whereas a salinity of less than 5000 ppm is preferred for sandstones [1]. Production of smart water from seawater using membranes and the resulting power consumption was discussed in detail in our previous research [2]. However, selection of suitable membranes for smart water production is an extensive process. Thus, predicting membrane ion rejection limited to a couple of steps will avoid intensive membrane experiments.

Application of mathematical models to predict NF membrane performance for selective ion rejection is important for the optimal design and operation of NF membranes for smart water production. However, most modeling studies to date have considered only very dilute solutions and typically containing two or three types of ions. Modeling of concentrated solutions with multi-feed ions, such as seawater, predicts NF performance realistically with regard to industrial applications.

Spiegler–Kedem is a mass transfer-based model that relates flux to the concentration difference of a solute for a given membrane and solvent properties. The experimental data of flux versus

rejection for individual ions for different membranes is used to validate a model. The model is developed using the estimated equation parameters or transport parameters in the Spiegler–Kedem model and is correlated to the structural parameters of a membrane using a steric hindrance pore model. This approach simplifies membrane performance prediction for a given feed ionic composition and provides a consolidated approach to various interacting phenomena that are difficult to define mathematically for mass transport. For the correlations predicted in this research, the model fitting is carried out for a given feed concentration with a certain membrane type (polyamide) so that active mechanisms for all the membranes are similar and can be easily understood. The proposed correlations can be used for predicting ion rejection, thereby aiding the selection of suitable NF membranes for smart water production administered to both carbonate and sandstone reservoirs.

The principal objective of this research is to develop a predictive model to quantify the selectivity of porous polyamide membranes with high feed concentrations for smart water production. To develop such a model, membrane transport parameters and effective pore size were determined using the Spiegler–Kedem model and a steric-hindrance pore model.

2. Theory

2.1. Nanofiltration Membranes

NF membranes permit preferential transport of ions. Separation processes are differentiated based on membrane pore sizes. NF membranes have pore sizes between 0.1 and 1 nm [3] with a molecular weight cut off (MWCO) of 100–5000 Da [4]. Mass transfer through NF includes convection and solution-diffusion [5]. NF selectively separates divalent and monovalent ions. This is mainly due to the strong dependence on the operating parameters, pressure, and feed concentrations, and on the membrane structural parameters such as pore radius and the ratio of membrane porosity to membrane thickness, $A_k/\Delta x$. The separation mechanisms also depend on the hydrophilic/hydrophobic characteristics of the membrane [6].

The performance of the membranes is generally measured in terms of rejection R and flux J_v. Rejection is a measure of the membrane's ability to reject a solute. Membrane rejection is calculated using Equation (1).

$$R = \left(1 - \frac{C_p}{C_f}\right) \tag{1}$$

where C_p and C_f are the permeate and feed concentrations, respectively.

Flux J_v ($\mathrm{Lm^{-2}\ h^{-1}}$) is calculated using Equation (2)

$$J_v = \frac{V}{t \times A} \tag{2}$$

where V is the volume of the permeate collected in a given time interval t, and A is the membrane area.

2.2. Spiegler–Kedem Model

Transport of solutes through a charged membrane can be described using the principles of non-equilibrium thermodynamics where the membrane is considered a black box. This approach allows the membranes to be characterized in terms of only the reflection coefficient σ and solute permeability P_s. In a two-component system consisting of solute and water with flux J_v, the solute flux J_s is related by three membrane coefficients [7]:

1. The hydraulic permeability L_p.
2. The solute permeability P_s.
3. The reflection coefficient σ.

The relation between J_v and J_s and the membrane coefficients is given by Equations (3) and (4) as introduced by Kedem and Katchalsky [8].

$$J_V = L_p(\Delta P - \sigma\Delta\pi) \tag{3}$$

$$J_s = P_s\Delta C_s + (1-\sigma)J_v\, C_m \tag{4}$$

where $\Delta C_s = C_m - C_p$, and C_m is the solute concentration at the membrane surface. ΔP is the pressure difference between the feed and permeate, and $\Delta\pi$ is the osmotic pressure difference of the two fluids. According to Equation (4), the solute flux is the sum of diffusive and convective terms. Transport of the solute by convection is due to an applied pressure gradient across the membrane. The concentration difference on the membrane side and the permeate results in transport by diffusion.

When a high concentration difference exists between the retentate and the permeate, the Spiegler–Kedem model can be used [5], as in this research. The solute permeability coefficient P_s and reflection coefficient σ can be obtained by fitting experimental values of solute rejection versus flux, according to the Spiegler–Kedem model as represented by Equations (5) and (6).

$$R_{\text{obs}} = \sigma\,\frac{(1-F)}{1-\sigma F} \tag{5}$$

where

$$F = \exp\,(-\frac{1-\sigma}{P_s}J_{v)} \tag{6}$$

F is a dimensionless parameter that depends on the reflection coefficient, solvent flux, and solute permeability coefficient. The reflection coefficient represents the rejection capability of a membrane. No rejection occurs when $\sigma = 0$ and 100% rejection occur when $\sigma = 1$ [9]. Also, σ can be considered to represent the maximum rejection at an infinite volume flux.

Permeability can be defined as the flux of a solute or solvent through the membrane per unit driving force. P_s is the overall solute permeability coefficient.

The Spiegler–Kedem model is based on irreversible thermodynamics to describe transport when the membrane structure and transport mechanism within the membrane is not fully understood [10]. The Spiegler–Kedem model is generally applied when there are no electrostatic interactions between the solute and the membrane such as when the membrane is uncharged or when the solute is neutral. NF membranes are mostly negatively or positively charged. Many authors have used this model with charged NF membranes [6,11] and suggested that σ and P_s depend on the effective membrane charge and concentration of the feed solution. The effect of membrane charge is, however, neglected in this research for analyzing membrane performance at high feed concentrations.

The following assumptions were made while using the Spiegler–Kedem model in this research:

(1) The driving forces are pressure and concentration gradients.
(2) The model predicts the transport of the solute and solvent through the membrane irrespective of the type of solute, charge, solvent, and membrane.
(3) Membrane fouling and membrane sensitivity towards chemicals such as chlorine, effects of temperature, and pH are not considered.

2.3. Steric Hindrance Pore Model (SHP)

Structural parameters of the membranes were estimated using the SHP model developed by Nakao and Kimura [12] for the separation of aqueous solutions of a single organic solute by ultrafiltration membranes and was later successfully used for NF membranes by researchers such as Wang et al. [13]. According to the model, transport of spherical ions through cylindrical pores

hindered by frictional forces and the steric effect are considered. Following this model, the membrane parameters σ and P_s are given as

$$\sigma = 1 - S_F \{1 + (16/9)q^2\} \quad (7)$$

$$P_s = D \times S_D(A_k/\Delta x) \quad (8)$$

where

$$S_D = (1-q)^2 \quad (9)$$

$$S_F = 2(1-q)^2 - (1-q)^4 \quad (10)$$

and

$$q = \frac{r_s}{r_p} \quad (11)$$

where S_D and S_F are the steric hindrance factors for diffusion and convection respectively. D is diffusivity, $A_k/\Delta x$ is the ratio of membrane porosity to membrane thickness, r_s is the Stokes radius of the solute, and r_p is the pore radius. The Stokes radii used for calculations [14,15] are presented in Table 1.

Table 1. Stokes radii of major ions used for calculations [14,15].

Ions	Cl^-	Na^+	SO_4^{2-}	Ca^{2+}	Mg^{2+}
Stokes Radius (nm)	0.121	0.184	0.231	0.310	0.348

The stability of membranes is usually tested to assure the reliability of the experiments. This is mainly performed by measuring the pure water permeability ($L_p = J_v/\Delta P$) of the membranes. The pure water permeability L_p is also expressed by Hagen–Poiseuille in the pore model and is defined as

$$L_P = r_p^2\left(\frac{A_k}{\Delta x}\right)/8\mu \quad (12)$$

where μ is the viscosity.

3. Experimental Methods

Experiments were performed with a lab-scale membrane unit consisting of low-pressure and high-pressure pumps, a pressure valve, a pressure gauge, and two prefilters with 20 µ and 5 µ pore size as pre-treatment units upstream of the NF. One membrane is operated at a time and the retentate and permeate were recirculated to a 100 L feed tank to retain identical feed concentrations. The experiments were performed at room temperature with pure water and seawater. The applied pressure across the membranes ranged from 9 bar to 18 bar. Three trials were performed for each membrane with both pure water and seawater as feed. Pre-filtered seawater used for membrane experiments had total dissolved solids (TDS) of 30,400 mg/L, conductivity of 47.5 mS/cm, and pH at 7.9.

Prior to the experiments, the membranes were washed with pure water to remove any membrane preservatives. Eight different membranes with spiral wound configurations from two manufacturers (Nitto Hydranautics, Oceanside, CA, USA and Dow Filmtec, Oceanside, CA, USA) were used for the experiments and the membrane characteristics are provided in Table 2. NF 270 and SR 90 were from Dow Filmtec while all other six membranes were from Nitto Hydranautics. These commercially available membranes were negatively charged since their surface layers were made of polyamide or sulfonated polysulphone.

Table 2. Membrane characteristics as provided by the suppliers.

Membranes	HYDRACoRe10	HYDRACoRe50	NF 270	SR 90	ESNA	NANO-SW	LFC3	HYDRApro501
Material	Sulphonated Polyethersulfone				Composite Polyamide			
pH range	2–11		3–10		2–10	3–9	2–10.6	2–11
Area (m^2)	2.3		2.6				2.3	

MWCO of HYDRACoRe10 and HYDRACoRe50 are 3000 and 1000 Daltons, respectively.

Individual ion concentrations in the feed, permeate, and retentate was measured using ion chromatography (Dionex^{TM} ICS-5000+ DP, from Thermo Fisher Scientific, Waltham, MA, USA). TDS and conductivity were measured using a TDS meter VWR collection CO3100N and pH by VWR Phenomenal pH 1100 L (both from VWR International Limited, Leicestershire, UK)

All membranes, except for HYDRApro 501, had a maximum operating temperature of 45 °C. For HYDRApro 501, the operating temperature was pressure dependent: 41 bar at 65 °C and 14 bar at 90 °C. Maximum operating pressure for the rest of the membranes ranged from 41–41.6 bar according to the manufacturers.

Pure water permeability (L_p) was experimentally determined by plotting flux J_v versus transmembrane pressure ΔP and is represented by Lm^{-2} h^{-1} bar^{-1}. The slope corresponding to each linear line determined the pure water permeability [10]. The hydraulic properties of the studied membranes were analyzed by measuring water flux as a function of pressure. Membrane water permeability was evaluated after achieving a steady-state condition with stable flux after operating the membranes for about 30 min.

4. Results and Discussion

4.1. Pure Water Permeability

Figure 1 shows the dependency of operating pressure on flux through eight membranes. A linear relation was obtained for water flux as a function of operating pressure. According to Figure 1, the pure water permeability of the membranes decreased in the sequence HYDRACoRE 10 > ESNA > NF 270 > HYDRACoRe 50 > SR 90 > NANO-SW > LFC3 > HYDRApro 501.

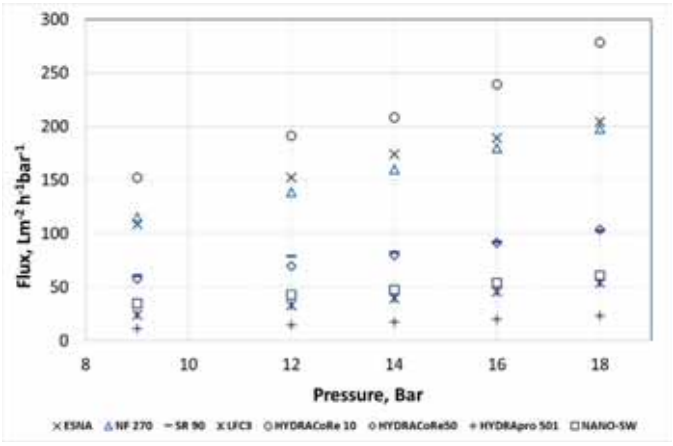

Figure 1. Pure water flux as a function of operating pressure for eight different membranes.

LFC3 is a reverse osmosis membrane while HYDRApro 501 is used specifically for industrial applications with difficult feed streams, according to the manufactures. The permeabilities of these two membranes were lowest among the tested membranes. Thus, only pure water permeability

experiments were performed for LFC3 and HYDRApro 501 membranes and these two membranes were not considered for further calculations of membrane transport parameters.

Relatively high flux was obtained for the other six membranes. High fluxes of these NF membranes at low pressure confirmed that NF membranes can be used as in energy saving compared to reverse osmosis membranes. Table 3 shows the water permeability of membranes when pure water and seawater were used as the feed.

Table 3. The permeability of membranes with different feed solutions.

Membranes	Pure Water (L m^{-2} h^{-1} bar^{-1})	Seawater (L m^{-2} h^{-1} bar^{-1})
HYDRACoRe 10	13.56	9.5
ESNA	10.52	7.9
NF 270	9.38	6.1
HYDRACoRe 50	5.15	3.8
SR 90	4.46	3.3
NANO-SW	3.27	1.9
LFC3	2.85	-
HYDRApro 501	1.32	-

L_p of the tested membranes did not vary throughout the experiments. Hence, the membranes could be considered stable during the experimental period.

The effect of feed concentrations on the membrane flux was evident from the difference in water permeability between the two solutions in Table 3. Pure water permeability was highest through HYDRACoRe10, suggesting more open pores compared to the other tested membranes.

4.2. Calculation of σ, P_s, and r_p Based on the Spiegler–Kedem and SHP Models

Experimental results for rejection and flux during permeation experiments with seawater were calculated using Equations (1) and (2). First, the transport parameters σ and P_s for each ion were estimated using a nonlinear least squares method by fitting the Spiegler–Kedem model by plotting rejection versus flux for six membranes. Coefficients selected were with above 95% confidence bounds. Second, the pore radius based on individual ion rejection data for every membrane was determined from its membrane parameter σ based on the steric hindrance pore model (SHP) using Equations (7), (10), and (11). The value for r_p (determined as = r_s/q) were calculated using the Stokes radius of the solute (r_s) as presented in Table 1.

Membrane parameters were estimated by fitting rejection versus flux using the Spiegler–Kedem equation. Figure 2 shows the dependency of the real rejection on volume flux for Na^+ for NANO-SW. The data points present the rejection values from the experiment and the solid line shows the values calculated using the Spiegler–Kedem equation with the best-fitted σ and P_s. Figure 2 shows that the theoretical curves are in close agreement with experimental values.

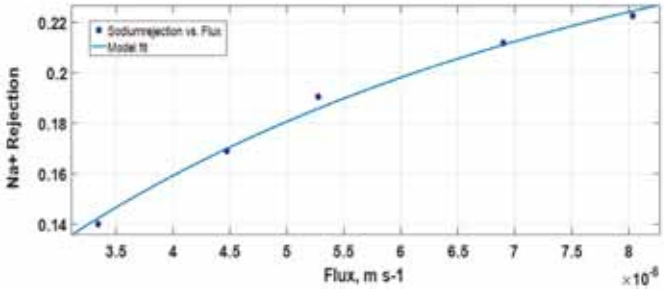

Figure 2. Rejection versus flux (m s^{-1}) for Na^+ for NANO-SW.

The effective membrane pore radius for each ion was calculated from the transport parameters σ and P_s based on the SHP model when seawater was used as the feed and is presented in Table 4.

Table 4. Calculated σ, P_s, and average r_p for ions for all tested membranes.

Membranes	Ions	σ (—)	P_s (m s^{-1})	q	r_p (nm)
ESNA	Cl^-	0.14	3.023×10^{-5}	0.30	0.41
	Na^+	0.14	1.701×10^{-5}	0.29	0.63
	SO_4^{2-}	0.66	6.211×10^{-6}	0.69	0.34
	Ca^{2+}	0.29	1.953×10^{-5}	0.44	0.71
	Mg^{2+}	0.24	1.26×10^{-5}	0.40	0.86
NF 270	Cl^-	0.18	2.105×10^{-5}	0.34	0.35
	Na^+	0.19	1.521×10^{-6}	0.35	0.52
	SO_4^{2-}	0.97	5.341×10^{-7}	0.93	0.25
	Ca^{2+}	0.41	1.879×10^{-5}	0.53	0.58
	Mg^{2+}	0.45	6.154×10^{-6}	0.56	0.62
SR 90	Cl^-	0.36	4.241×10^{-6}	0.50	0.24
	Na^+	0.25	7.313×10^{-6}	0.41	0.45
	SO_4^{2-}	0.99	4.859×10^{-7}	0.96	0.24
	Ca^{2+}	0.82	1.474×10^{-6}	0.79	0.39
	Mg^{2+}	0.92	3.276×10^{-7}	0.85	0.41
HYDRACoRe10	Cl^-	−0.01	-4.844×10^{-7}	-	-
	Na^+	0.03	3.115×10^{-5}	0.13	1.42
	SO_4^{2-}	0.16	1.728×10^{-5}	0.32	0.73
	Ca^{2+}	0.15	7.254×10^{-5}	0.31	0.99
	Mg^{2+}	0.05	5.447×10^{-5}	0.16	2.15
HYDRACoRe50	Cl^-	0.17	1.329×10^{-5}	0.33	0.37
	Na^+	0.24	1.538×10^{-5}	0.40	0.46
	SO_4^{2-}	0.67	3.849×10^{-6}	0.70	0.33
	Ca^{2+}	0.32	5.928×10^{-6}	0.47	0.67
	Mg^{2+}	0.38	1.417×10^{-5}	0.51	0.68
NANO-SW	Cl^-	0.37	9.045×10^{-7}	0.50	0.24
	Na^+	0.29	4.439×10^{-6}	0.44	0.42
	SO_4^{2-}	0.99	3.298×10^{-8}	0.96	0.24
	Ca^{2+}	0.88	2.171×10^{-6}	0.84	0.37
	Mg^{2+}	0.93	3.471×10^{-7}	0.88	0.40

Table 4 shows that reflection coefficients and solute permeability vary for each ion. The pore radii of these membranes were calculated using the Stokes radius of each ion. It was earlier reported by Luo and Wan [16] that the r_p of NF 270 is 0.43 nm. The pore size of NF 270 was previously determined using atomic force microscopy by Hilal et al. [17] and suggested to be between 0.47–0.99 nm with a mean of 0.71 nm. An average pore size of 0.47 nm was determined for NF 270 using the SHP model in this research. The calculated pore size of NF 270 was in the same range as recorded by several researchers confirming the validity of the calculations. The results show that for these membranes, a pore size distribution was more likely than a fixed pore size, and the identification of an effective pore radius does not indicate the presence of geometrically defined pores in NF membranes.

According to Table 4, polyamide membranes showed better rejection for divalent ions since the reflection coefficient was high for divalent ions compared to monovalent ions. According to the obtained results, the Spiegler–Kedem model was able to fit the experimental data of flux versus rejection for all ions and for all membranes except for HYDRACoRe 10. For HYDRACoRe 10, negative Cl^- reflection coefficients were obtained for all performed trials with the model. This could be due to the very low rejection of Cl^- or probably a negative rejection of Cl^- even though it was not observed during experiments. Negative rejection implies that the system has more Cl^- in the permeate compared

to the feed. Negative rejection of an ion occurs when a higher concentration of that ion is present in the smaller permeate volume relative to the larger feed volume. Negative rejection is observed mostly at low operating pressures [18]. The results show that HYDRACoRe 10 membrane has a larger pore size than the usual NF range which explains the poor ion separation of HYDRACoRe 10.

Table 4 shows that membranes with larger pore sizes had lower reflection coefficients. In other words, membranes with higher pure water permeability had lower individual ion reflection coefficients. A relative pore size comparison was performed with Mg^{2+} since it is a divalent cation with the highest Stokes radius compared to other ions tested for pore radius calculations, along with the fact that Mg^{2+} is attracted by the negatively charged membrane (unlike $SO_4{}^{2-}$) and would therefore permeate the membrane easily if the pore size was appropriately large for the ion. Hence, with respect to Mg^{2+}, the pore size of the tested membranes was in the sequence HYDRACoRe 10 > ESNA > HYDRACoRe 50 > NF 270 > SR 90 > NANO-SW.

However, the high feed concentrations and the ionic interactions that occurred among unaccounted ions and major ions in seawater, along with the interactions between ions and the membrane, added to the overall complexity in separation mechanisms of NF membranes. This provides a challenge to any model based on high feed concentrations.

4.3. Selection of NF Membranes for Smart Water Production Using a Predictive Model

The ionic composition required for smart water depends mainly on the type of reservoir. For carbonate reservoirs, an NF membrane with a high rejection of divalent ions and low monovalent ion rejection should be selected. For sandstone reservoirs, low salinity is preferred. Thus, a membrane with moderate flux will be suitable, which results in low divalent ion permeation.

According to Equation (12), pure water permeability is a parameter that combines the structural properties of the membrane and is used as a critical parameter that determines the ion rejection of a membrane. The only other property that influences water permeability is the feed viscosity, as shown in Equation (12). During the experiments, the structural parameters remained the same provided temperature and pH of the feed are controlled. Several researchers [19,20] have established that temperature and pH affect the pore size and change the flux. In this research, the difference in viscosity between pure water and seawater was neglected when L_p was used for correlating the reflection coefficient and solute permeability of membranes.

Thus, according to Equation (12), pure water permeability was directly related to the structural parameters such as effective membrane pore radius, and to $A_k/\Delta x$ (ratio of membrane porosity to membrane thickness). It can be inferred that the transport parameters of a solute are related to the structural properties of a specific membrane, as shown in Equations (7)–(11). Knowing the transport parameters, it is possible to predict the rejection (R_{obs}) of a membrane using the Spiegler–Kedem model.

4.3.1. Relating L_p with σ and P_s

L_p versus σ and P_s of individual ions were plotted to find a relation between pure water permeability, reflection coefficient, and P_s. Transport parameters were calculated for four polyamide membranes, ESNA, NF 270, SR 90, and NANO-SW with varying L_p. These four membranes were chosen since:

(1) Table 4 shows that HYDRACoRe 10 had poor ion separation. HYDRACoRe 50, made of sulfonated polyethersulfone, was not used to have comparable membrane materials for the model.
(2) The L_p chosen for the plot to create the model was in the range required for smart water production. Pure water permeability higher than that of ESNA would have resulted in very low divalent ion rejection. Choosing a membrane with lower permeability than NANO-SW meant a tighter membrane leading to higher rejection for any flux and low recovery thereby increasing power consumption.

Figure 3a shows the pure water permeability of polyamide NF membranes versus σ and Figure 3b presents L_p versus solute permeability P_s of chloride for each membrane.

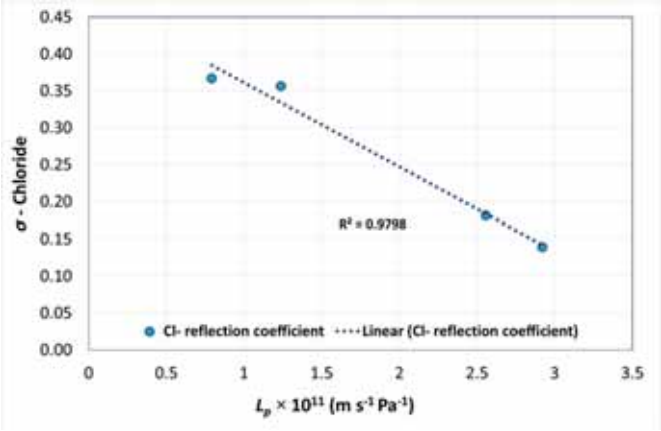

(a)

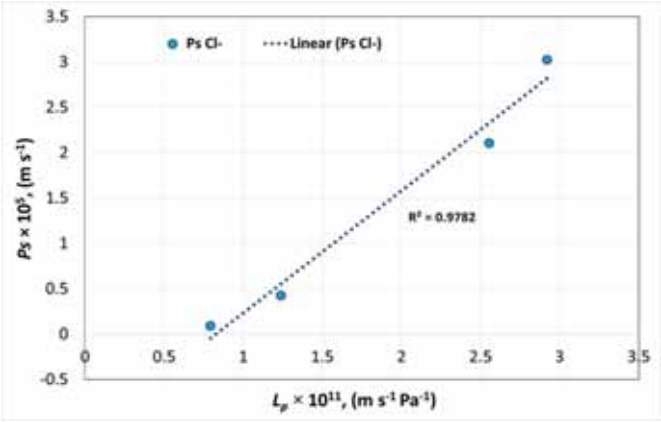

(b)

Figure 3. Pure water permeability versus (**a**) reflection coefficient and (**b**) solute permeability of chloride.

Figure 3a shows that with an increase in water permeability, the reflection coefficient of ions decreased whereas Figure 3b shows that the solute permeability increased. This confirmed that when the effective membrane pore radius increases, permeability increases, resulting in lower ion rejection.

Similarly, Figures 4a and 4b represents the pure water permeability of NF membranes versus σ and P_s of sodium for each membrane, respectively.

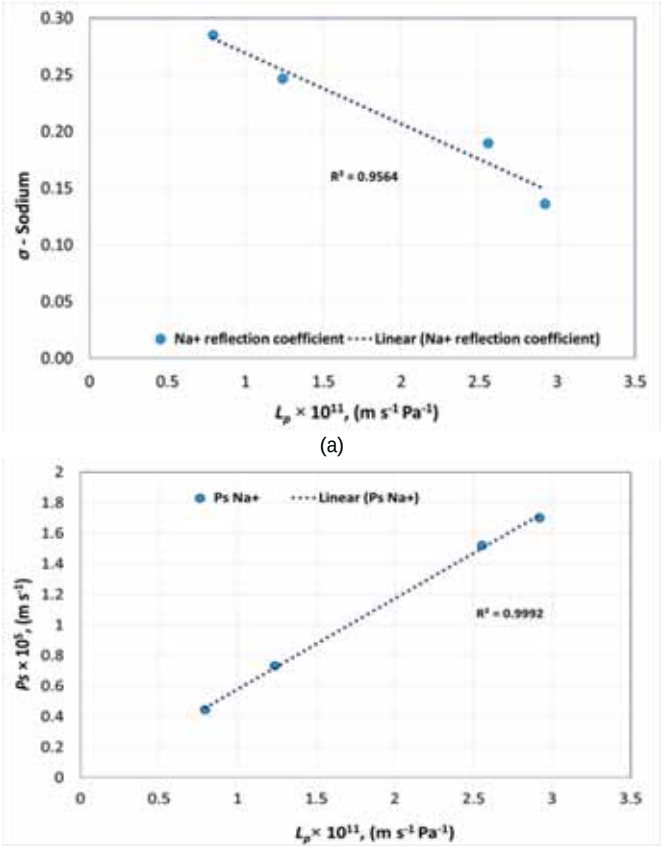

Figure 4. Pure water permeability versus (**a**) reflection coefficient and (**b**) solute permeability of sodium.

Figure 5a presents the pure water permeability of membranes versus σ and Figure 5b presents L_p versus P_s of sulfate for each membrane.

According to Figure 5a, the sulfate reflection coefficient shows a sharp decline with a small change in water permeability. This was mainly because of divalent anion on the negatively charged membrane surface. In Figure 5b showing pure water permeability versus P_s, the sulfate permeability remains unchanged for a range of permeabilities until approximately 2.6×10^{-11} m s^{-1} Pa^{-1}. After this value, a sharp increase was observed similar to the sharp decline in reflection coefficient of sulfate. A deviation in the reflection coefficient and solute permeability of SO_4^{2-} can be explained in relation to the thermodynamic properties of the ion. Ion permeation through a membrane is affected by the hydrated size and hydration free energy of the ions. During membrane transport, the transmembrane pressure creates shear stress that results in ions with low hydration energy being able to easily permeate through the membrane whereas ions with higher hydration energy and hydrated radius will be rejected by the membrane. SO_4^{2-} is a divalent anion with a hydration free energy of -1145 KJ/mol and a hydrated radius of 0.379 nm [21]. When the negatively charged ion is in contact with a negatively charged membrane surface, ion repulsion occurs, resulting in a higher rejection. Similarly, to maintain electroneutrality on both sides of the membrane, anions with a lower hydration energy and hydrated radius permeate through the membrane. Hence, Cl^- will be preferentially permeated compared to

SO_4^{2-} due to a lower hydration energy of −340 KJ/mol and hydrated radius of 0.324 nm. In Figure 5a, for ESNA, the reflection coefficient for SO_4^{2-} was lower at 0.66, whereas for the other three membranes, the SO_4^{2-} reflection coefficient was greater than 0.95. This can be explained with regard to the r_p calculated relative to Mg^{2+} as presented in Table 4. The pore radius r_p calculated was 0.86 nm, thus SO_4^{2-} permeated more for ESNA due to the steric effect resulting in lower σ and higher P_s compared to the other three membranes with a pore size close to 0.4 nm that is in close proximity to the SO_4^{2-} hydrated radius. Hence, a combination of steric effect and divalent anion-membrane repulsion prompted SO_4^{2-} rejection in NANO-SW, SR 90, and NF 270.

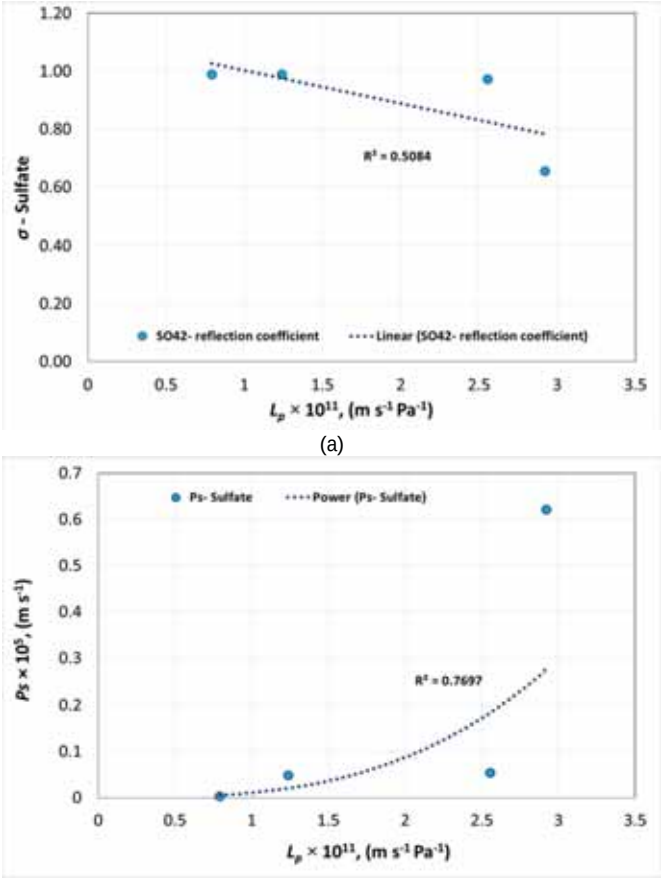

Figure 5. Pure water permeability versus (**a**) reflection coefficient and (**b**) solute permeability of sulfate.

Figure 6a,b shows the pure water permeability of membranes versus σ and P_s of calcium for each membrane, respectively.

According to Figure 6a, the reflection coefficient decreased gradually with increasing permeability. However, a small variation in calcium permeability was observed at lower permeabilities as shown in Figure 6b.

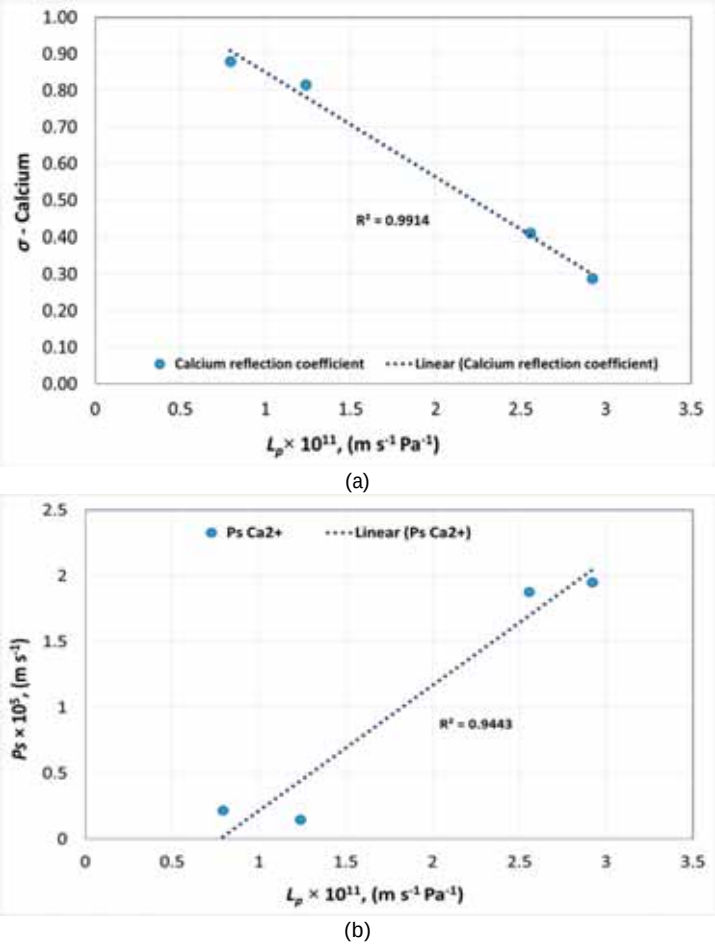

Figure 6. Pure water permeability versus (**a**) reflection coefficient and (**b**) solute permeability of calcium.

Figure 7a,b shows the pure water permeability of membranes versus σ and P_s of magnesium for each membrane, respectively.

According to Figure 7a, the reflection coefficient of Mg^{2+} deviated slightly from linear behavior for membranes with low pure water permeability. Mg^{2+} is a divalent cation with a hydration energy of −1922 KJ/mol with a hydrated radius of 0.470 nm [21]. According to Figure 7a,b, when pure water permeability decreased with respect to pore radius, the reflection coefficient of Mg^{2+} increased, confirming the higher rejection and lower permeation of Mg^{2+}. The deviation from linear behavior was observed for membranes (NANO-SW and SR 90) with a calculated $r_p \approx 0.4$ nm with respect to Mg^{2+}, where r_p is close to its hydrated radius.

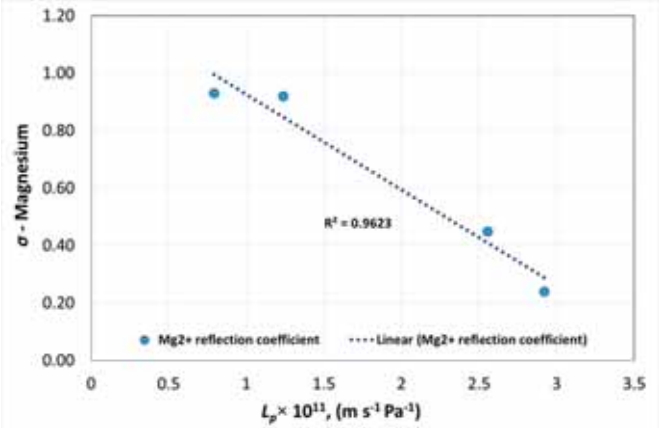

(a)

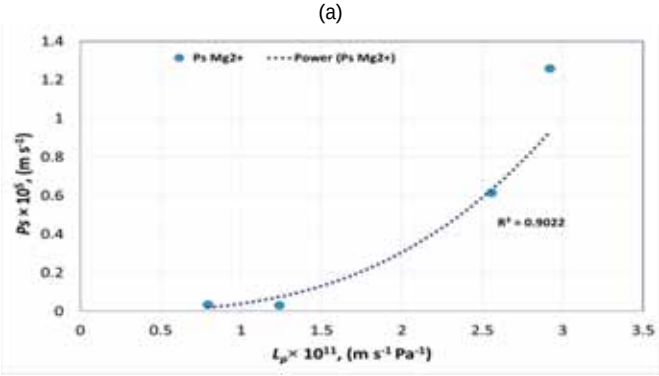

(b)

Figure 7. Pure water permeability versus (**a**) reflection coefficient and (**b**) solute permeability of magnesium.

4.3.2. Correlations for the Determination of σ and P_s of a Polyamide Membranes

The correlation developed was considered valid if the feed is seawater with no change in ionic concentration and viscosity for all tested polyamide membranes.

The following equations were obtained from Figures 3–7, to determine σ and P_s of each ion with a given pure water permeability L_{p0}.

$$\sigma_{Cl^-} = -1 \times 10^{10} \times L_{p0} + 0.4749 \quad (13)$$

$$\sigma_{Na^+} = -6 \times 10^{9} \times L_{p0} + 0.3318 \quad (14)$$

$$\sigma_{SO_4^{2-}} = -1 \times 10^{10} \times L_{p0} + 1.118 \quad (15)$$

$$\sigma_{Ca^{2+}} = -3 \times 10^{10} \times L_{p0} + 1.1354 \quad (16)$$

$$\sigma_{Mg^{2+}} = -3 \times 10^{10} \times L_{p0} + 1.2559 \quad (17)$$

$$P_{s_{Cl^-}} = 1 \times 10^{11} \times L_{p0} - 1.1144 \quad (18)$$

$$P_{s_{Na^+}} = 6 \times 10^{10} \times L_{p0} - 0.0147 \quad (19)$$

$$P_{s_{SO_4^{2-}}} = 4 \times 10^{31} \times {L_{p0}}^{3.0496} \quad (20)$$

$$P_{s_{Ca^{2+}}} = 1 \times 10^{11} \times L_{p0} - 0.7388 \quad (21)$$

$$P_{s_{Mg^{2+}}} = 9 \times 10^{30} \times {L_{p0}}^{2.9414} \quad (22)$$

As previously explained, the correlations represented by Equations (13)–(22) are applicable only for seawater with similar TDS and ionic composition. For a change in feed, the coefficients need to be established through experimental data. Equations (13)–(22) can be used for determining σ and P_s of polyamide membranes with pure water permeabilities between 5×10^{-12} to 3×10^{-11} m s^{-1} Pa^{-1}, which include membranes with a pore size of 0.4 to 0.86 nm, according to Table 4.

The following steps were performed to run the model for predicting transport parameters and rejection.

(1) Using Equations (13)–(22), the model was run to predict $\sigma_{\text{theoretical}}$ and $P_{s,\text{theoretical}}$ for two NF membranes with pure water permeabilities as in Table 5.
(2) Flux for the above-mentioned NF membranes with seawater as feed was calculated using Equation (2). A random flux value at 12 bar was chosen for the model.
(3) The values for $\sigma_{\text{theoretical}}$ and $P_{s,\text{theoretical}}$, and flux at 12 bar was substituted into Equations (5) and (6) to calculate the theoretical rejection ($R_{\text{theoretical}}$).
(4) To validate the calculated equations, ion rejection by the two chosen NF membranes was experimentally determined ($R_{\text{experimental}}$) using Equation (1) for individual ions in seawater. These rejection values were plotted against the respective membrane flux values, and transport parameters were determined by fitting the values using the Spiegler–Kedem equation. Hence, $\sigma_{\text{experimental}}$ and $P_{s,\text{experimental}}$ were determined.

Table 5 shows the results obtained based on the model and on experiments performed by two chosen NF membranes.

Table 5. Comparison of experimental and theoretical values from the Spiegler–Kedem equation.

Pure Water Permeability, m s^{-1} Pa^{-1}	Flux at 12 bar, m s^{-1}	Ions	$\sigma_{\text{theoretical}}$	$\sigma_{\text{experimental}}$	$P_{s,\text{theoretical}}$, m s^{-1}	$P_{s,\text{experimental}}$, m s^{-1}	$R_{\text{theoretical}}$	$R_{\text{experimental}}$
2.56×10^{-11}	2.06×10^{-5}	Cl^-	0.22	0.18	1.44×10^{-5}	2.11×10^{-5}	0.16	0.11
		Na^+	0.18	0.19	1.52×10^{-5}	1.52×10^{-5}	0.13	0.14
		SO_4^{2-}	0.83	0.97	1.99×10^{-6}	5.34×10^{-7}	0.79	0.96
		Ca^{2+}	0.37	0.41	1.82×10^{-5}	1.88×10^{-5}	0.23	0.24
		Mg^{2+}	0.44	0.45	6.27×10^{-6}	6.15×10^{-6}	0.42	0.41
1.24×10^{-11}	8.90×10^{-6}	Cl^-	0.35	0.36	1.23×10^{-6}	4.24×10^{-6}	0.35	0.29
		Na^+	0.26	0.25	7.28×10^{-6}	7.31×10^{-6}	0.17	0.16
		SO_4^{2-}	0.99	0.99	2.18×10^{-7}	4.86×10^{-7}	0.97	1.00
		Ca^{2+}	0.76	0.82	4.99×10^{-6}	1.47×10^{-6}	0.53	0.75
		Mg^{2+}	0.89	0.92	7.44×10^{-7}	3.28×10^{-7}	0.85	0.96

Table 5 shows a close correlation between the model and experimental values of σ, P_s, and rejection of all ions except for Ca^{2+} for the membrane with lower pure water permeability. This validates the robustness of the model. Table 5 indicates that rejection for the divalent anion SO_4^{2-} was highest for all tested membranes indicating the negative surface of the NF membranes. Focusing on the rejection of divalent cations, Mg^{2+} was rejected more than Ca^{2+} due to its larger Stokes radius as shown in Table 1.

The individual ion selectivity is a key parameter for selecting appropriate membrane for smart water production. In this research, the Spiegler–Kedem model was used for determining individual ion transport through the membrane rather than overall solute transport, which has been extensively studied previously. The study is relevant for end users to select proper NF membranes for producing smart water without extensive membrane experiments.

5. Conclusions

Membrane transport parameters were determined by fitting the Spiegler–Kedem equation using flux and rejection values obtained from experiments using six NF membranes. The theoretical rejection

values obtained by fitting the Spiegler–Kedem equation showed good correlations with experimental values for NF membranes with a similar membrane material. It was evident that it was difficult to increase the membrane water flux without losing ion selectivity and membrane flux was directly related to the effective membrane pore radius. The flux was higher for membranes with $r_p > 0.7$ nm. However, membrane ion rejection decreased with higher r_p. The hypothetical pore radii of six membranes were evaluated from permeation experiments with charged ions using a steric hindrance pore model. The pore radii of membranes were estimated from 0.4 nm to 2.15 nm. The experiments concluded that the membranes had a pore size distribution rather than a single pore radius. A sharp change in σ and P_s of sulfate were observed when plotted against pure water permeabilities of polyamide membranes. Hence, choosing an NF membrane for smart water production in carbonates requires much attention when having pure water permeabilities above 2.6×10^{-11} m s^{-1} Pa^{-1} where the SO_4^{2-} rejection will be low. The suggested method helps to predict NF rejection for smart water production from seawater and for feeds with a high concentration and multi-ionic solutions as in softening and desalination.

Supplementary Materials: The following are available online at http://www.mdpi.com/2077-0375/8/3/78/s1, Figure S1: Rejection versus flux for Na^+ for ESNA fitted using Spiegler–Kedem model, Figure S2: Rejection versus flux for Na^+ for HYDRACoRe10 fitted using Spiegler–Kedem model, Figure S3: Rejection versus flux for Na^+ for HYDRACoRe50, Figure S4: Rejection versus flux for Na^+ for NF270, Figure S5: Rejection versus flux for Na^+ for SR 90, Figure S6: Rejection versus flux for Na^+ for NANO SW, Figure S7: Rejection versus flux for Na^+ for all NF membranes.

Author Contributions: Conceptualization, R.N. and T.B.; Methodology, R.N.; Software, R.N.; Validation, R.N., E.P., S.S. and T.B.; Formal Analysis, R.N.; Investigation, R.N.; Resources, R.N., E.P.; Data Curation, R.N.; Writing-Original Draft Preparation, R.N.; Writing-Review & Editing, E.P., S.S., T.B.; Visualization, R.N.; Supervision, S.S., T.B.; Project Administration, T.B.; Funding Acquisition, T.B.

Funding: This research did not receive any specific grant from funding agencies in the public, commercial, or not-for-profit sectors.

Acknowledgments: The authors acknowledge the Research Council of Norway and the industry partners, ConocoPhillips Skandinavia AS, Aker BP ASA, Eni Norge AS, Total E&P Norge AS, Equinor ASA, Neptune Energy Norge AS, Lundin Norway AS, Halliburton AS, Schlumberger Norge AS, Wintershall Norge AS, and DEA Norge AS of The National IOR Centre of Norway for support.

Conflicts of Interest: The authors declare no conflict of interest.

References

1. Austad, T. Water-based EOR in Carbonate and Sandstone: New Chemical Understanding of the EOR-Potential using "Smart water". In *Enhanced Oil Recovery Field Case Studies*; Sheng, J., Ed.; Gulf Professional Publishing: Houston, TX, USA, 2013; pp. 301–335.
2. Nair, R.R.; Protasova, E.; Strand, S.; Bilstad, T. Membrane performance analysis for smart water production for enhanced oil recovery in carbonate and sandstone reservoirs. *Energy Fuels* **2018**, *32*, 4988–4995. [CrossRef]
3. Cheryan, M. *Ultrafiltration and Microfiltration Handbook*; CRC Pres: Boca Raton, FL, USA, 1998.
4. Oatley-Radcliffe, D.; Walters, M.; Ainscough, T.J.; Williams, P.M.; Mohammad, A.W.; Hilal, N. Nanofiltration membranes and processes: A review of research trends over the past decade. *J. Water Process. Eng.* **2017**, *19*, 164–171. [CrossRef]
5. Hilal, N.; Al-Zoubi, H.; Mohammad, A.; Darwish, N. Nanofiltration of highly concentrated salt solutions up to seawater salinity. *Desalination* **2005**, *184*, 315–326. [CrossRef]
6. Gilron, J.; Gara, N.; Kedem, O. Experimental analysis of negative salt rejection in nanofiltration membranes. *J. Membr. Sci.* **2001**, *185*, 223–236. [CrossRef]
7. Spiegler, K.; Kedem, O. Thermodynamics of hyperfiltration (reverse osmosis): Criteria for efficient membranes. *Desalination* **1966**, *1*, 311–326. [CrossRef]
8. Kedem, O.; Katchalsky, A. Permeability of composite membranes: Part 1. Electric current, volume flow and flow of solutes through membranes. *Trans. Faraday Soc.* **1963**, *59*, 1918–1953. [CrossRef]
9. Murthy, Z.; Gupta, S.K. Estimation of mass transfer coefficient using a combined nonlinear membrane transport and film theory model. *Desalination* **1997**, *109*, 39–49. [CrossRef]

10. Jye, L.W.; Ismail, A.F. *Nanofiltration Membranes—Synthesis, Characterization and Applications*; CRC Press, Taylor & Francis Group: Boca Raton, FL, USA, 2017.
11. Diwara, C.K.; Lo, S.; Rumeau, M.; Pontie, M.; Sarr, O. A phenomenological mass transfer approach in nanofiltration of halide ions for a selective defluorination of brackish drinking water. *J. Membr. Sci.* **2003**, *219*, 103–112. [CrossRef]
12. Nakao, S.I.; Kimura, S. Models of membrane transport phenomena and their applications for ultrafiltration data. *J. Chem. Eng. Jpn.* **1982**, *15*, 200–205. [CrossRef]
13. Wang, X.L.; Tsuru, T.; Togoh, M.; Nakao, S.I.; Kimura, S. Evaluation of pore structure and electrical properties of nanofiltration membranes. *J. Chem. Eng. Jpn.* **1994**, *28*, 186–192. [CrossRef]
14. Bowen, R.; Mohammad, W.A. Diafiltration by Nanofiltration: Prediction and Optimization. *AIChe J.* **1998**, *44*, 1799–1812. [CrossRef]
15. Hussain, A.; Nataraj, S.; Abashar, M.; Al-Mutaz, I.; Aminabhavi, T. Prediction of physical properties of nanofiltration membranes using experiment and theoretical models. *J. Membr. Sci.* **2008**, *310*, 321–336. [CrossRef]
16. Luo, J.; Wan, Y. Effect of highly concentrated salt on retention of organic solutes by nanofiltration polymeric membranes. *J. Membr. Sci.* **2011**, *372*, 145–153. [CrossRef]
17. Hilal, N.; Al-Zoubi, H.; Darwish, N.; Mohammad, A. Characterisation of nanofiltration membranes using atomic force microscopy. *Desalination* **2005**, *177*, 187–199. [CrossRef]
18. Yaroshchuk, A. Negative rejection of ions in pressure-driven membrane processes. *Adv. Colloid Interface Sci.* **2008**, *139*, 150–173. [CrossRef] [PubMed]
19. Nilsson, M.; Tragårdh, G.; Ostergren, K. The influence of pH, salt and temperature of nanofiltration performance. *J. Membr. Sci.* **2008**, *312*, 97–106. [CrossRef]
20. Deshmukh, S.S.; Childress, A. Zeta potential of commercial RO membranes: Influence of source water type and chemistry. *Desalination* **2001**, *140*, 87–95. [CrossRef]
21. Tansel, B. Significance of thermodynamic and physical characteristics on permeation of ions during membrane separation: Hydrated radius, hydration free energy and viscous effects. *Sep. Purif. Technol.* **2012**, *86*, 119–126. [CrossRef]